UNIVERSITAT POLITÈCNICA DE VALÈNCIA

Escuela Técnica Superior de Ingeniería del Diseño

UNIVERSITAT POLITÈCNICA DE VALÈNCIA

School of Design Engineering

Wind tunnel investigations on performances and aerodynamics of a wind turbine

Master's Thesis

Master's Degree in Aeronautical Engineering

AUTHOR: Sánchez García, Víctor Manuel

Tutor: Quintero Igeño, Pedro Manuel

External cotutor: ROMANO, GIOVANNI PAOLO

ACADEMIC YEAR: 2021/2022

UNIVERSITAT POLITÈCNICA DE VALÈNCIA

Escuela Técnica Superior de Ingeniería del Diseño

Wind tunnel investigations on performances and aerodynamics of a wind turbine

Máster Universitario en Ingeniería Aeronáutica

MSc Thesis

Author:
Victor Manuel Sanchez Garcia
Tutor:
Giovanni Paolo Romano
Co-Tutor:
Pedro Manuel Quintero Igeño

July 2022

Wind tunnel investigations on performances and aerodynamics of a wind turbine

SAPIENZA
UNIVERSITÀ DI ROMA

Sapienza Università di Roma

Faculty of Civil and Industrial Engineering

Laurea Magistrale in Ingegneria Aeronautica

Author:
Victor Manuel Sanchez Garcia

Tutor:
Giovanni Paolo Romano
Mechanical and Aerospace Engineering Department

Co-Tutor:
Pedro Manuel Quintero Igeño
Departamento de Máquinas y Motores Térmicos

Universitat Politècnica de València

Escuela Técnica Superior de Ingeniería del Diseño

Grado en Ingeniería Aeroespacial

UNIVERSITAT POLITÈCNICA DE VALÈNCIA

ROMA, July 2022

Una volta che abbiate conosciuto il volo,
camminerete sulla terra guardando il cielo,
perché là siete stati e là desidererete tornare.

Leonardo da Vinci

Abstract

Keywords

Aerodynamics, wind turbine, wind-tunnel, electrical performance, PIV, "RoDaVi"

Sommario [IT]

Questo documento si occupa dello studio di una turbina eolica di nuova concezione progettata per entrare nel mercato eolico urbano a bassa potenza. Il progetto iniziale appartiene alla start-up "AirCrafted" che opera nel campo delle energie rinnovabili e dell'industria aeronautica.

La turbina eolica è caratterizzata da un asse verticale basato ed è chiamata "RoDaVi", acronimo di rotore Da Vinci, perché il suo design si basa sull'ottimizzazione delle prime idee dell'inventore.

Per quanto riguarda i risultati, nella tesi viene effettuata un'analisi preliminare con modelli in scala 1:10 della turbina con una bilancia dinamometrica per conoscere i parametri aerodinamici della turbina e l'influenza delle diverse configurazioni in galleria del vento (velocità, angolo di attacco, spessore, ...).

Successivamente, con una turbina in scala 1:3, viene effettuata un'analisi delle prestazioni elettriche della turbina per diverse angolazioni e velocità di flusso. La dimensione scelta è dovuta alle limitazioni della galleria del vento. La turbina è collegata ad un generatore sincrono a magneti permanenti, che a sua volta è collegato ad un impianto elettrico che simulerebbe una vera carica della batteria. Diverse misurazioni vengono effettuate con vari motori dei principali parametri elettrici utilizzando sensori come un torsiometro e un wattmetro.

L'ultima analisi viene eseguita con tecnologia PIV. Un laser, una fotocamera ad alta potenza e un generatore di microbolle vengono utilizzati per studiare il campo fluido (velocità e vorticità).

Abstract [EN]

This document deals with the study of a newly designed wind turbine intended for entering the low power urban wind market. The initial design belongs to the start-up "AirCrafted" that works in the field of renewable energy and the aviation industry.

The wind turbine is characterized by a vertical axis, and is called "RoDaVi", an acronym for Da Vinci rotor, because its design is based on the optimization of the inventor's early ideas.

Regarding results, in the thesis a preliminary analysis is carried out with 1:10 scale models of the turbine in a dynamometric balance to know the aerodynamic parameters of the turbine and the influence of the different configurations and designs in the wind tunnel (speed, angle of attack, thickness, ...).

Later, with a 1:3 scale turbine, an analysis of the electrical performance of the turbine for different angles and flow speeds is carried out. The size selected is due to the limitations of the wind tunnel. The turbine is connected to a permanent magnet synchronous generator, which in turn is connected to an electrical system that would simulate a real battery charge. Different measurements are made with various motors of the main electrical parameters using sensors such as a torque meter and a wattmeter.

The last analysis is performed with PIV technology. A laser, a high power photo camera and a micro bubble generator are used to study the fluid field (velocities and vorticity).

Resumen [ES]

El presente documento se ocupa del estudio de una turbina eólica de nuevo diseño pensada para ingresar en el mercado eólico urbano de poca potencia. El diseño inicial pertenece a la start-up "AirCrafted" que trabaja en el ámbito de energía renovables e industria de la aviación.

La turbina eólica se caracteriza por ser de eje vertical, y recibe el nombre de "RoDaVi", acrónimo de Rotor de Da Vinci, porque su diseño se basa en la optimización de las primeras ideas del inventor.

En cuanto a resultados, en la tesis se realiza un análisis preliminar con modelos a escala 1:10 de la turbina en una balanza dinamometrica para conocer los parámetros aerodinámicos de la turbina y la influencia de las diferentes configuraciones y diseños en el túnel de viento (velocidad, ángulo de ataque, grosor, ...).

Más adelante se realiza con una turbina de escala 1:3, un análisis de las prestaciones eléctricas de la turbina para diferentes ángulos y velocidades de flujo. El tamaño seleccionado se debe a las limitaciones del túnel de viento. La turbina se encuentra conectada a un generador síncrono de imanes permanentes, que a su vez se conecta a un sistema eléctrico que simularía una carga de batería real. Se realizan diferentes mediciones con varios motores de los parámetros eléctricos principales utilizando sensores como un torsiometro y un vatímetro.

El último análisis se realiza con la tecnología PIV. Se utilizan un láser, una foto cámara de alta potencia y generador de micro burbujas para estudiar el campo fluido (velocidades y vorticidad).

Resum [CA]

Aquest document s'ocupa de l'estudi d'una turbina eòlica de nou disseny pensada per ingressar al mercat eòlic urbà de poca potència. El disseny inicial pertany a la start-up AirCrafted que treballa en l'àmbit d'energia renovables i indústria de l'aviació.

La turbina eòlica es caracteritza per ser d'eix vertical, i rep el nom de RoDaVi, acrònim de rotor de Da Vinci, perquè el seu disseny es basa en l'optimització de les primeres idees de l'inventor.

Quant a resultats, a la tesi es realitza una anàlisi preliminar amb models a escala 1:10 de la turbina en una balança dinamometrica per conèixer els paràmetres aerodinàmics de la turbina i la influència de les diferents configuracions i dissenys al túnel de vent (velocitat, angle d'atac, gruix,...).

Més endavant es fa amb una turbina d'escala 1:3, una anàlisi de les prestacions elèctriques de la turbina per a diferents angles i velocitats de flux. El tamany seleccionat es deu a les limitacions del túnel de vent. La turbina es troba connectada a un generador síncron d'imants permanents, que a més es connecta a un sistema elèctric que simularia una càrrega de bateria real. Es realitzen diferents mesuraments amb diversos motors dels paràmetres elèctrics principals utilitzant sensors com un torsiòmetre i un vatímetre.

L'última anàlisi es realitza amb la tecnologia PIV. Es fan servir un làser, una foto càmera d'alta potència i un generador de micro bombolles per estudiar el camp fluid (velocitats i vorticitat).

Contents

List of Figures

1 PROJECT STATEMENT

1.1 Introduction

The implementation of wind turbines in urban environments for micro power generation is a resource with high sustainable potential that can contribute positively to a country's renewable goals. Today, this type of micro-generation in cities has only few examples of adaptation. However, the technology can work well if installed in appropriate locations; moreover, it is a new energy production alternative for residential and commercial consumers.

The adaptation of wind turbines in the urban environment for power generation is similar to that of photovoltaics. For this type of energy there are already specific regulations for the adaptation of urban rooftops and their implementation in new buildings for energy generation. However, this is not the case for wind energy due to the lack of prototypes adapted to buildings. The "RoDaVi" design was created to address this need.

The main objective of this research work is to study the energetic performance of the innovative "RoDaVi" wind turbine, using scaled prototypes, starting from discover its aerodynamic behaviour, then characterising electrical performance, and finally observe the fluid field induced by the fluid-structure interaction.

The geometrical characteristics of this turbine make it versatile in flow conditions where other types of turbines are not suitable. So, this new turbine is able to work, with high efficiency, also in those conditions where the wind direction is not orthogonal to the turbine axis, as at the top of building in urban environment

Various tools are used for the different studies. A dynamometric balance for the aerodynamic calculation, an electrical system with different sensors for the electrical calculation, and the PIV technology for the fluid field study.

1.2 Motivation and structure of the study

As it is said before, this study arises from the need to create a prototype that contributes to the generation of electricity in urban environments. For this purpose, different studies about the feasibility of the performance of prototype will be carried out.

In the first part of the project, chapter 2, it will be discussed what kind of similar renewable energies can be found today and what their contribution to society is. Among them, wind energy will be highlighted, discovering its capabilities and explaining the different types

of turbines used for its generation. In addition, the design of the "RoDaVi" engine and its operating principle will be explained.

In chapter 3 or *Methodology*, the useful parameters for the study will be defined. Furthermore, the physical and theoretical procedure on which the study is based will be explained in order to understand how energy is produced.

In the following chapter, all the installations and technologies used in the project will be presented. From how the turbine is supported to the instrumentation used to measure.

The most important installation is the wind tunnel. Here the aerodynamic parameters will be measured using a dynamometric balance, and high frequency measurements will be carried out thanks to an Arduino programmed for this purpose.

In order to estimate the real power that a wind turbine of this type could provide, an electrical set-up is used. The dimensions of this set-up are similar to the one that would be used in the real installation. It consists of various elements that characterise it, such as a three-phase magnetic flux motor, a three-phase flux rectifier diode bridge, a rheostat or variable resistance, and various sensors such as a torque meter and a wattmeter.

Finally, the characteristics of the laser, the high power photocamera, and the bubble generator used in the PIV analysis to study the flow field will be presented.

The results of the studies carried out with the above elements will be presented in chapter 5, which is subdivided into 3 sections. In the first section, an aerodynamic analysis will be carried out using the dynamometric balance on a model 10 times smaller than the real one.

Then, the main study of the work will be presented. A 1:3 scale turbine will be used to characterise the electrical parameters of the problem. The aim is to obtain adequate power values for its applicability in the micro power turbine sector.

The third and last study will be a Particle Image Velocimetry (PIV) study to obtain a view of the flow field, observe how the structure influences the velocity and the creation of vortices.

Finally, chapter 6 will present the conclusions derived from the studies carried out.

1.2.1 Objectives

Once the structure and motivation of the work has been presented, the objectives to be achieved are discussed. Possible future improvements or future projects will also be discussed.

- To understand the importance of renewable energies in today's society and their benefits.
- To give visibility to the need for new designs and implementations of wind energy because of its simplicity.
- Design of a vertical axis wind turbine for use in an urban environment.
- To know how the different types of wind turbines work.
- To know how wind energy is transformed into electricity.

- Implementing and transforming an innovative idea into a real application
- Work in a laboratory environment using the available elements.
- Troubleshoot in real time problems affecting the working environment.
- To know the electrical characteristics of the wind turbine, and quantify them.
- Correct processing of the data acquired.
- Make comparisons between different configurations and situations in order to find an optimal one.
- Learn about PIV technology and its application in flow visualisation.
- Identify the areas with the highest vorticity generated in the fluid field.

2 THEORETICAL BACKGROUND

2.1 Sustainable sources of energy

In the energy sector, energy sources are classified as renewable if they are **not subject to depletion**, or if they are able to regenerate at least at the same rate at which they are used. The International Energy Agency recognises solar, wind, geothermal, geomass, biomass and hydroelectric energy as renewable.

In view of the increase in energy consumption and the planet's resources, it is inevitable that these renewable energy sources will gain strength to the detriment of conventional ones that damage the environment. So, producing more and more renewable energy and moving away from conventional sources is a need shared by all countries in the world.

In the governmental framework, countries and organisations, such as the European Union, are setting targets for decarbonisation and reduction of CO2 emissions for the coming years (there are active plans for 2030 and 2050) [1]. This is why renewable energies must be promoted to achieve this ecological transition. In figure 2.1 the evolution of the growth of these energy sources over the years can be seen in terawatt-hour (TWh).

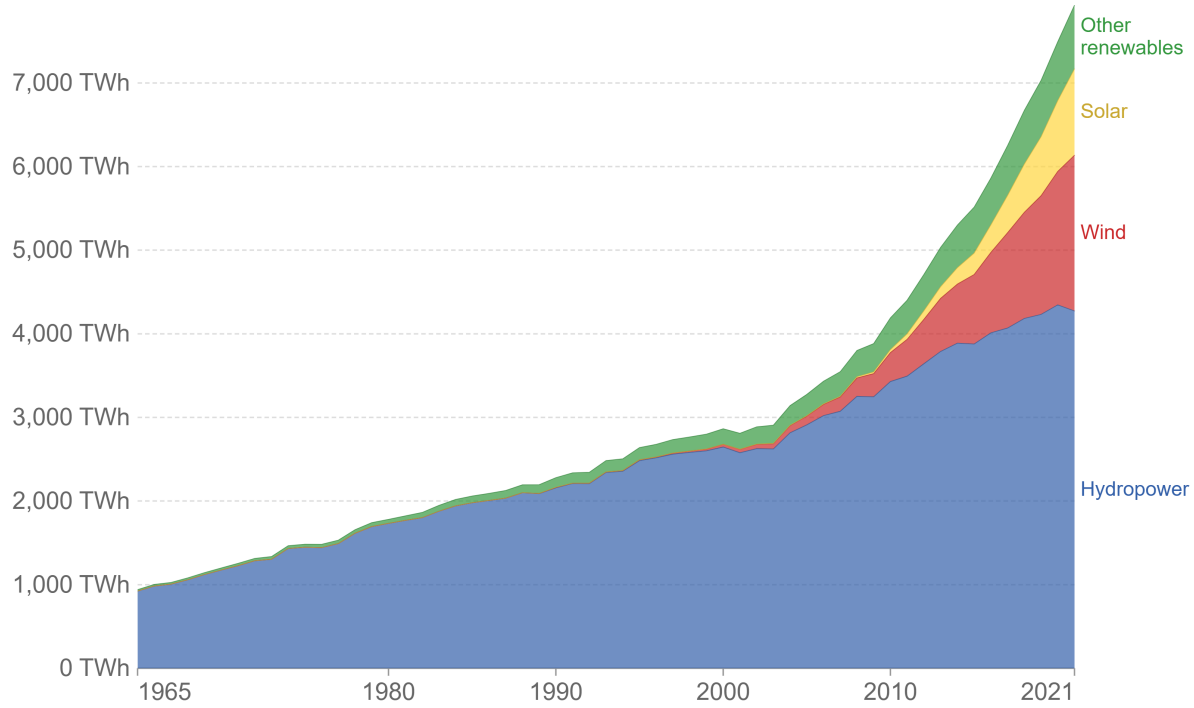

Figure 2.1: Renewable energy generation in world over years [2]

The use of these clean energies contributes to **slowing down climate change**: they do not emit greenhouse gases in the energy generation process. They are also inexhaustible, unlike traditional sources, whose reserves are finite.

One of their greatest advantages is that they **reduce energy dependence**. The need to import fossil fuels makes them dependent on the economic and political situation of the supplier country, which can compromise the security of energy supply. Currently, there are conflicts between countries that make more expensive and difficult to supply energy to other nations that depend on them. On the other hand, by opting for renewable energies, everywhere on the planet there is some kind of renewable resource - wind, sun, water, organic matter - that can be exploited to produce energy in a sustainable way.

All these advantages and the need to implement them in the short term have made them **increasingly competitive** today. The main renewable technologies, such as wind and solar photovoltaic, are drastically reducing their costs, so that they are already fully competitive with conventional technologies at a growing number of sites. Economies of scale and innovation are already making renewables the most environmentally and economically sustainable solution for moving the world.

2.2 Wind energy

Wind energy is the most widespread renewable energy currently available, which uses the power of the wind in a simple way. It currently accounts for almost 25% of renewable energy generation, just behind hydropower energy (figure 2.1). Although it still only accounts for 2% of the world's electricity production, this technique makes it one of the cleanest forms of energy production in existence.

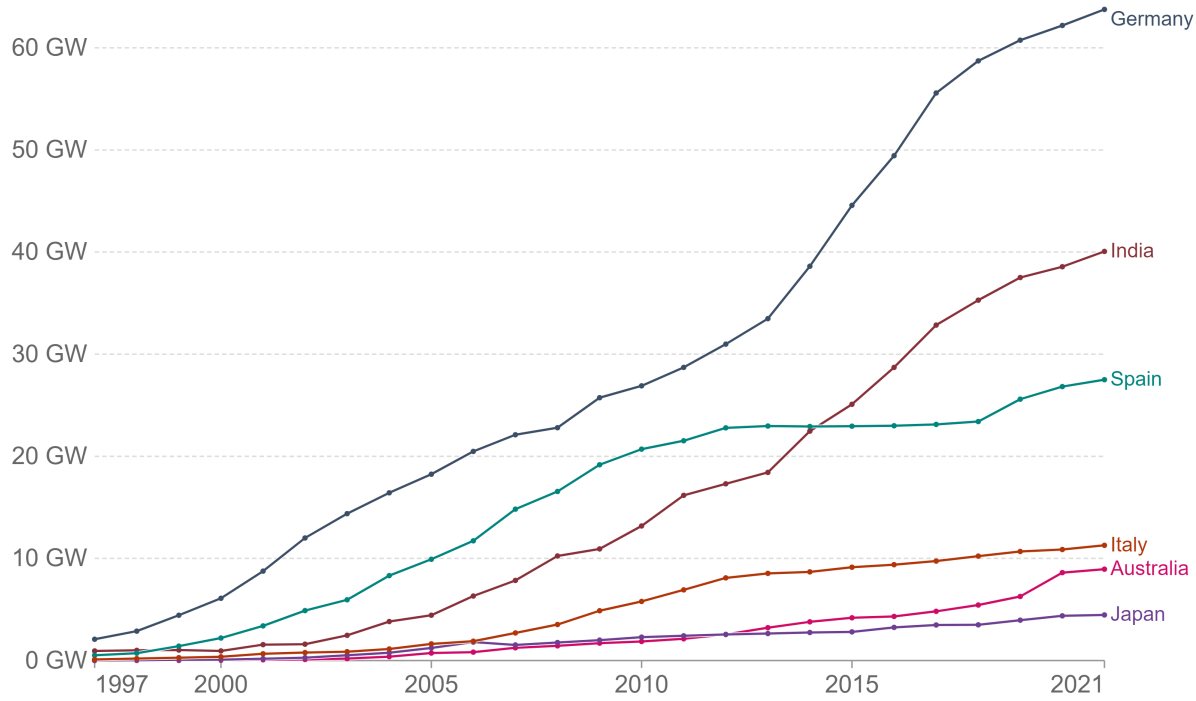

Figure 2.2: Installed wind energy capacity [3]

In addition, wind energy is a local energy, available almost everywhere in the world, which

contributes to reducing energy imports and creating economic wealth and employment locally.

Figure 2.2 shows the cumulative installed wind power capacity, measured in gigawatts (GW), for different countries over the years. It shows that over time, wind energy has been a major issue for developed countries, especially in the first five years of the 21st century. Countries such as Germany and India are currently continuing to have an enormous growth in installed wind energy capacity in order to try to become independent of the fossil energy that they buy from third countries.

Currently, a wind farm with just a few wind turbines (dozens) is capable of producing millions of kilowatt-hours per year. This is enough to power thousands of homes with just one medium-sized wind farm. And this avoids the release of millions of tons of CO2 into the atmosphere and thus contributes to sustainable development.

It may seem that large infrastructures and investments are needed to be able to implement this type of energy, but the reality is that they are not. Apart from the large wind farms that are used to produce this energy on a mass scale, we should not leave behind the local electricity installations, which are used to produce energy for private individuals.

Thanks to these systems it is possible to electrify houses, traffic signs, weather stations, etc. However, it seems to be common to see them in rural areas, but why not in a city?. "RoDaVi" was born as a solution to this need, so that this type of energy wasted in big cities is not missed and has a local impact on the generation of electricity in buildings.

2.3 Types of wind turbines

In the literature, there are different classifications of modern turbines, the most common based on the direction of the rotation axis; but also based on the aerodynamic working principle of the rotor (drag-based or lift based) and the nominal power generated (low, medium or high power).

According to their direction of the rotation axis, basically, the wind turbines are of two types namely **horizontal axis wind turbines**, such as traditional farm windmills used for pumping water and the **vertical axis wind turbines**, such as the egg beater-style Darrieus model, named after its French inventor [4].

Most large modern wind turbines are horizontal-axis turbines. In horizontal-axis turbines, the axis of rotation is horizontal with respect to ground (and roughly parallel to the wind stream) while in vertical-axis turbines, the axis of rotation is vertical with respect to ground (and roughly perpendicular to the wind stream).

2.3.1 Horizontal Axis (HAWT)

Horizontal axis wind turbines, also shortened to HAWT, are the common style that typically think of when someone imagine a wind turbine. A HAWT has a similar design to a windmill, it has blades that look like a propeller that spin on the horizontal axis.

Horizontal axis wind turbines are the most commonly used turbines due to their strength and efficiency dealing with high wind speeds. The base of the towers have to be extremely strong, allowing the rotor shaft to be installed at the top of the tower which allows the

turbine to be exposed to stronger winds. With the blades of the turbine being perpendicular to the wind, the rotation of the blades can generate more power compared to the vertical axis wind turbine. However, the construction of this type of turbine requires a heavy support for the tower to support the weight of the blades, gearbox and generator as well as utilizing a sizable crane to lift the components to the top of the tower.

In a situation where the wind is blowing downwards, the turbine structure may suffer from metal fatigue which could lead to a structural failure. This is resolved by designing the turbines with an upwind design. Additional yaw control is needed for the horizontal axis wind turbines in order to track the direction of the wind, to prevent damaging the turbine. Different types of HAWT are presented in figure 2.3.

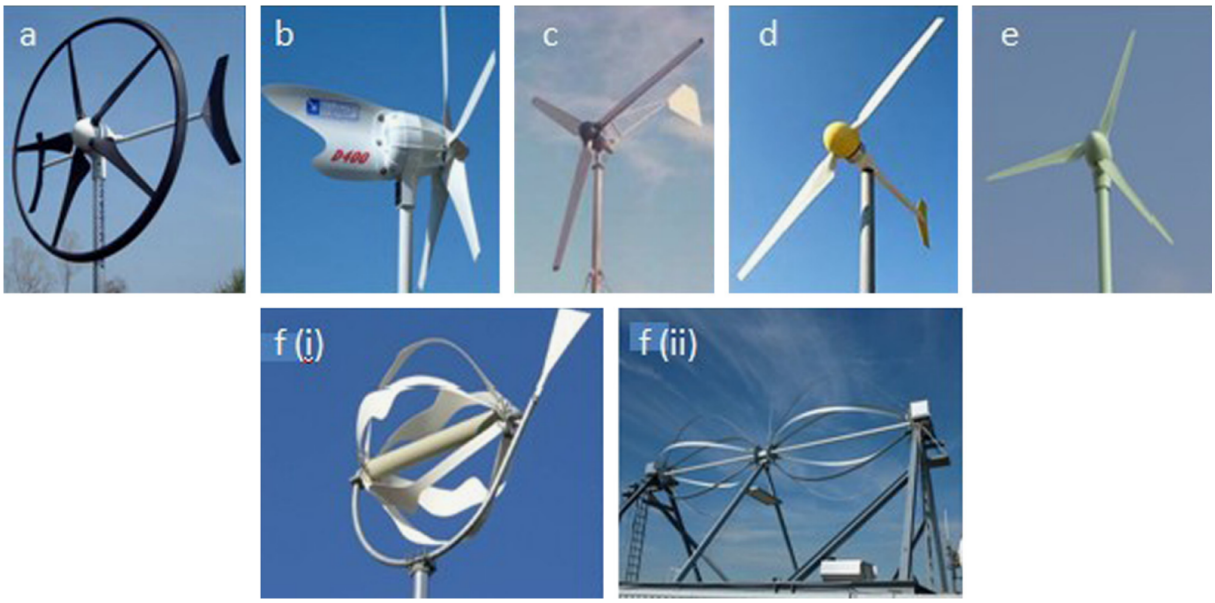

Figure 2.3: Examples of HAWTs. (a) Swift wind turbine, (b) Eclectic wind turbines, (c) Fortis Montana wind turbine, (d) Scirocco wind turbines, (e) Tulipo wind turbine, and (f) the Savonius horizontal type, (i) Energy Ball and (ii) WindWall [5]

HAWT advantages

- The tall tower base allows access to stronger wind in sites with wind shear.
- High efficiency. They can transform 40 to 50% of received wind power into electricity [6]. Since the blades always move perpendicularly to the wind, receiving power through the whole rotation. In contrast, all vertical axis wind turbines, and most proposed airborne wind turbine designs, involve various types of reciprocating actions, requiring airfoil surfaces to backtrack against the wind for part of the cycle.

HAWT disadvantages

- Massive tower construction is required to support the heavy blades, gearbox, and generator.
- Components of a horizontal axis wind turbine (gearbox, rotor shaft and brake assembly) being lifted into position.
- Disrupting the appearance of the landscape due to their height.

- Downwind variants suffer from fatigue and structural failure caused by turbulence when a blade passes through the tower's wind shadow (for this reason, the majority of HAWTs use an upwind design, with the rotor facing the wind in front of the tower).
- Require an additional yaw control mechanism to turn the blades orientated to the wind.
- Require a braking or yawing device in high winds to stop the turbine from spinning and destroying or damaging itself.

2.3.2 Vertical Axis (VAWT)

Vertical axis wind turbines, as shortened to VAWTs, have the main rotor shaft arranged vertically. The main advantage of this arrangement is that the wind turbine does not need to be pointed into the wind. This is an advantage on sites where the wind direction is highly variable or has turbulent winds.

VAWT are less affected by frequent wind direction changes as compared to the horizontal axis wind turbines due to the blades being rotated on the rotor shaft perpendicular to the ground. With the blades and shaft installed in this way, the turbine does not need to rotate to track wind direction. [7] With a vertical axis, the generator and other primary components can be placed near the ground, so the tower does not need to support it, also makes maintenance easier

An advantage of being mounted at ground level is that maintenance of the turbine is easier and can be installed at locations such as rooftops. Disadvantages to this turbine installation is that the efficiency is lower due to air drag and the lower wind speeds compared to the higher wind speeds encountered at higher elevations. A Savonius vertical axis wind turbine has an average efficiency of 10 to 17%, while the Darrieus vertical axis wind turbine reaches 30 to 40% [6].

Air flow near the ground and other objects can create turbulent flow, which can introduce issues of vibration, including noise and bearing wear which may increase the maintenance or shorten its service life. However, when a turbine is mounted on a rooftop, the building generally redirects wind over the roof and this can double the wind speed at the turbine. If the height of the rooftop mounted turbine tower is approximately 50% of the building height, this is near the optimum for maximum wind energy and minimum wind turbulence.

Also, they can rotate really fast without having any risk to wildlife or human habitats as these blades have round edges. They can be placed on the roof of your buildings or houses because the centrifugal force is balanced perfectly here and as a result, the blades can not fly off and make casualties like the conventional ones.

VAWT advantages

- No yaw mechanisms is needed.
- Can be located nearer the ground, making it easier to maintain the moving parts.
- VAWTs have lower wind startup speeds than the typical the HAWTs.
- May be built at locations where taller structures are not possible

- Close to the ground can take advantage of locations where rooftops, hilltops, ridgelines, and passes funnel the wind and increase wind velocity.

VAWT disadvantages

- Most VAWTs have a average decreased efficiency from a common HAWT, mainly because of the additional drag that they have as their blades rotate into the wind. Versions that reduce drag produce more energy, especially those that funnel wind into the collector area.
- Because VAWTs are not commonly deployed they appear novel to those not familiar with the wind industry. This has often made them the subject of wild claims and investment scams over the last 50 years.

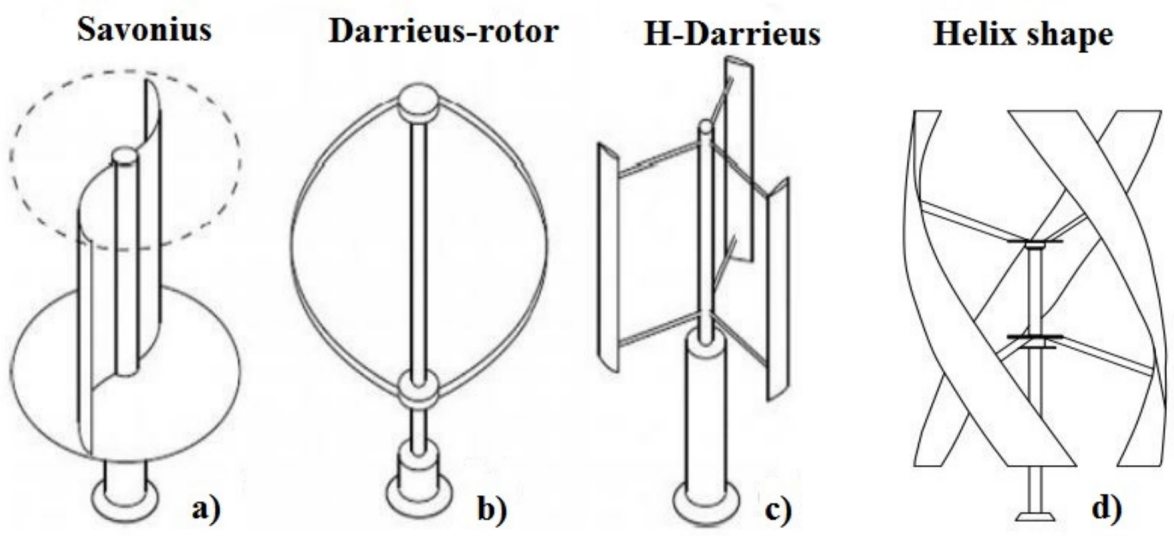

Figure 2.4: Examples of VAWTs [8].

2.3.3 VAWT subtypes

Darrieus

Darrieus wind turbines are commonly called "Eggbeater" turbines, because they look like a giant eggbeater. They have good efficiency, could reach 30 to 40%, but produce large torque ripple and cyclic stress on the tower, which contributes to poor reliability. The torque ripple is the difference in maximum and minimum torque over one complete revolution.

Also, they generally require some external power source (normally an additional Savonius rotor) to start turning, because the starting torque is very low. The torque ripple is reduced by using three or more blades which results in a higher solidity for the rotor. Solidity is measured by blade area over the rotor area.

Savonius

A Savonius is a drag type turbine, they are commonly used in cases of high reliability in many things such as ventilation and anemometers. Because they are a drag type turbine

they are less efficient than the common HAWT. Savonius are excellent in areas of turbulent wind and self starting. Their average efficiency is between 10 to 17%.

The wind initially pushes the concave part of a half-cylinder and causes the rotation of the entire axis, so that while the initial half-cylinder sees how the fluid flow slowly decrease, the opposite half-cylinder sees the flow increasing. The process is repeated giving rise to a continuous rotation.

2.4 "RoDaVi" Rotor

2.4.1 Design

The "RoDaVi" vertical axis wind turbine has been developed and patented by the start-up Aircrafted whose creator is Mr. Francesco Minio Paluello, an aerodynamic engineer.

The "RoDaVi" is structurally similar in shape to Leonardo da Vinci's machine, consisting of a vertically developing spiral surface, which in geometry is called a conical helicoid.

Leonardo's original model has a fixed circular base inscribed in a movable crown wheel, itself connected to a vertical drive shaft. A helical structure tapering upwards is mounted on the shaft, connected by braces to the rotating crown of the base.

From this model came the idea of creating an innovative turbine, with a shape never before patented, that would take advantage of the flow to "curl up" in the air and capture the wind's energy without the need for a starter motor. It is a vertical axis turbine with a central shaft that differs from Leonardo's machine by the aerodynamic shape of the two wing profiles splined along the shaft, and offset by 180°.

This spiral curved airfoil has a thickness and double curvature, with a pitch between the propellers of 6° and belongs to the GM 15 Gilbert Morris type [9], which allows lift generation and drag reduction.

The GM15 profile, despite having an intermediate CL coefficient, has a good compromise to keep the drag coefficient low and obtain a good efficiency.

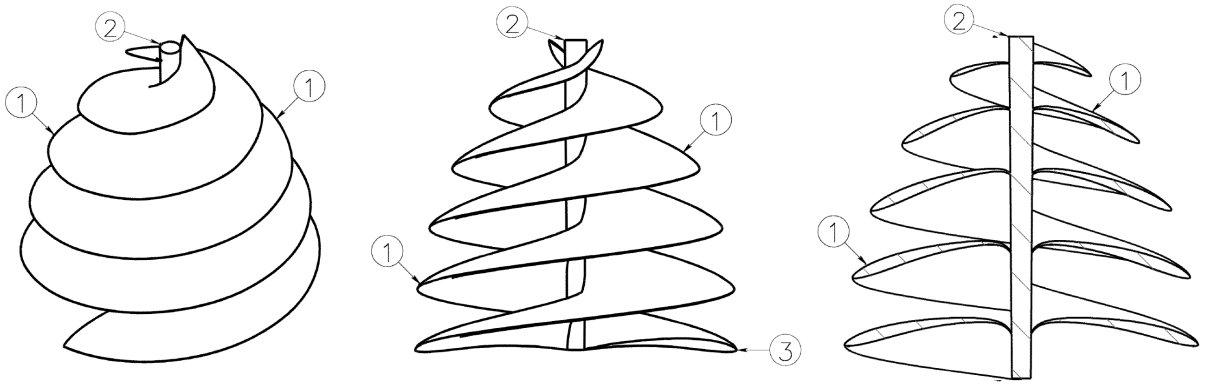

Figure 2.5: RoDaVi design

Figure 2.5 describes the 3 main elements of the turbine. (3) shows the GM15 airfoil used, (1) shows the two helical threads that make up the turbine, and finally (2) shows the shaft to which they are attached.

The shaft is also an important component. Not only does it not only have the expected function of supporting the propeller and moving the rotor away from the ground. It also plays a role in the aerodynamics of the machine, modifying the air flow through the windings in order to obtain the desired characteristics.

The shaft also favours the compression of the air at the base of the turbine, which favours the continuous upward rotational movement of the propeller, so that even at low speeds, the turbine is driven autonomously without the aid of a starter engine.

2.4.2 Prototype variations and their usefulness

Model 1:10 scale

The original model of the turbine had a height of 1.2m and a maximum diameter of 1.1m. It was originally intended to be marketed for installation in an urban micro wind farm for domestic use.

For the first analysis, a turbine 10 times smaller in size is required. This scale model was built by the Aircraft start-up team in polycarbonate using a 3D printer.

The propeller requires the assembly of a steel rod inside the shaft. A high-strength glue for metals and thermoplastics, Lord 460, was used to ensure high reliability, so that the movement of the turbine is integral with the rod support.

Two turbines of this size and construction have been reproduced, characterised by two

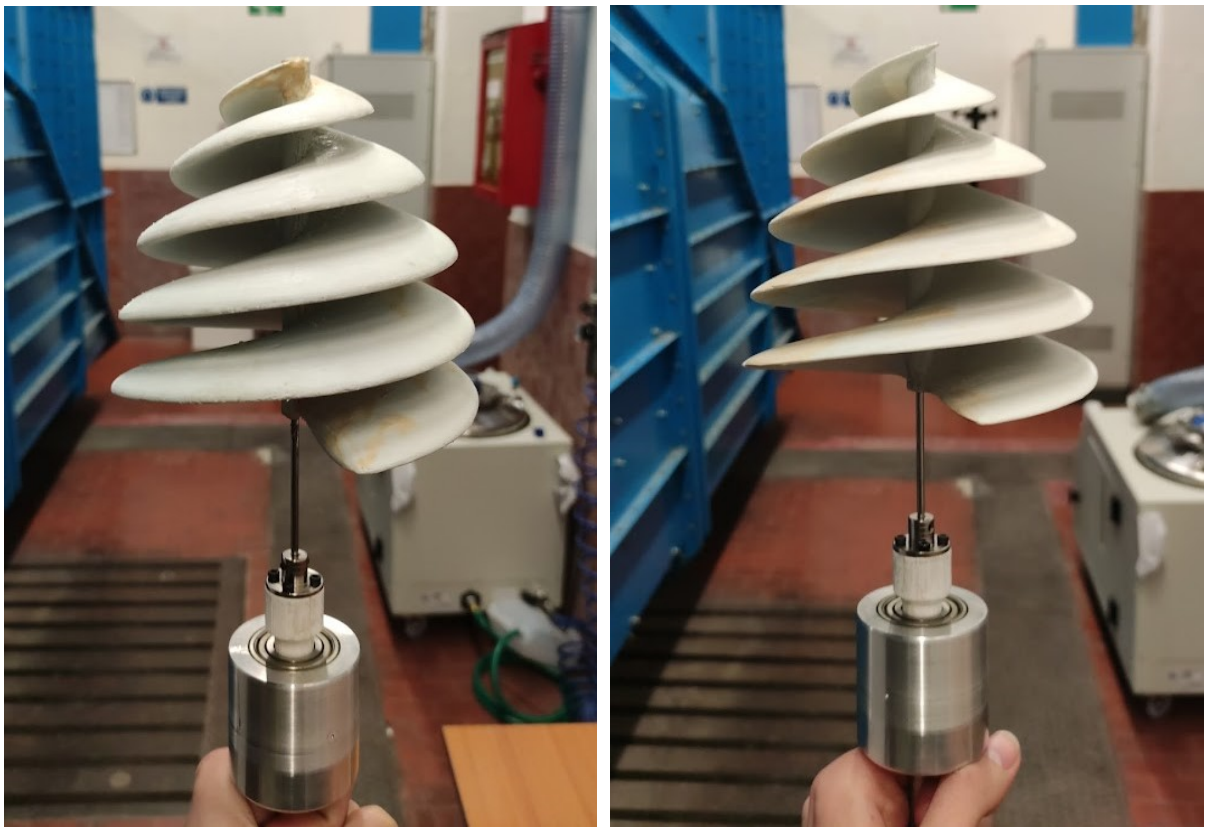

(a) Thick turbine **(b)** Thin turbine

Figure 2.6: RoDaVi turbines 1:10 scale model

different thicknesses, one thinner and one thicker, which makes the turbine a little more heavier, and with a bulky channel shape.

The thinner model was studied at the INSA National Institute in Rennes, underwent CFD simulations and some wind tunnel tests. The studies carried out showed that the results of the numerical analysis did not meet expectations. In particular, the CFD study simulating the fluid-structure interaction did not lead to interesting conclusions and the modelling in software involved considerable difficulties [10].

One of the tests carried out consisted of trying to couple the model to an electric generator to create a circuit using a rheostat, and extrapolate the electrical performance as a function of wind speed. Commissioning was difficult due to the small size of the turbine and the search for a suitable electric motor for the situation. This led to an unsatisfactory analysis of the model, with the conclusion that it is necessary to carry out the study with the prototype turbine, or at least one that is close to reality in size.

Nevertheless, despite these tests, thanks to the collaboration between Aircraft and the University of Rome La Sapienza, it was possible to redesign the measurement configuration and improve the initial experimentation.

For this reason, the two wind turbine models were subjected to separate measurements in the wind tunnel, with the dynamometric balance, to identify the forces acting on them when subjected to flows of different intensity.

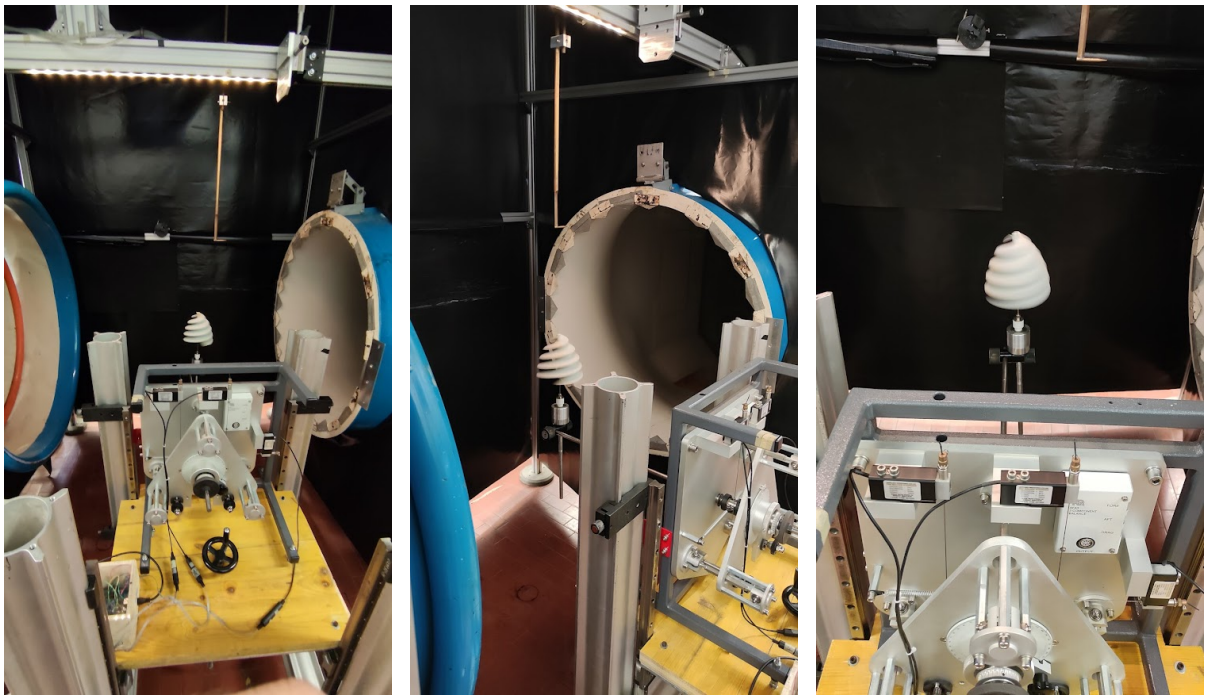

Figure 2.7: Balance set-up with 1:10 scale turbine for preliminary analysis.

These tests served initially to become familiar with the instrumentation and to begin to highlight the initial behaviour of the turbines according to the different settings and positions, and to understand the best configurations for subsequent measurements with the larger models.

The preliminary tests evaluated the resistance of the mini-propellers to any variation in

air flow, so that the wind speed limits could be established within which to act in order to carry out the tests while preserving the integrity of the structures.

Model 1:3 scale

The 1:3 scale model was developed out of the above mentioned need to test the real turbine, in particular the electrical analysis. From the previous tests it became clear that it was impossible to analyse correctly the electrical behaviour of this system on a miniature model and then extrapolate it to reality. So, this adaptation was necessary to overcome the limitations posed by previous studies, mainly due to a non-optimal structure-instrumentation coupling.

This turbine was built specifically to adapt Eng. Paluello's project to the real dimensions of the wind tunnel at Sapienza. Since the tunnel has a diameter of 0.9m, it was decided to build a model with the characteristic size of 40 cm and a height of 43 cm so that, by means of a suitable support, its section would be perfectly centred in the tunnel, and be hit uniformly by the laminar flow, without being affected by wall effects.

The turbine was built step by step, assembling parts produced with the 3D printer in the laboratory, in polymeric material. The assembly of the profiles, the union around the shaft was done manually with a bicomponent putty and a professional high-grip glue, widely used and appreciated in the aeronautical field (for its characteristic of providing adhesion not only between the most common materials, but especially metallic surfaces). On the other hand, ABS plastic material, which is generally used for 3D printing, is a material that basically does not weigh down the structure but at the same time offers excellent wind resistance.

Figure 2.8: Model 1:3 scale turbine

The central shaft, where the propellers are keyed, is hollow internally along its entire length, as it houses the solid iron shaft, which rotates in solidarity with the rotor. It is

held securely to the shaft by means of screws and bolts inserted both at the top and bottom of the turbine base, to prevent the turbine from slipping downwards. To avoid vibrations during rotation, and friction between the rod and the turbine support, cylindrical bearings type SKF 32004 were built for the occasion, and an anchoring system using elastic ropes.

The base on which the turbine is mounted, and the elements that make up this structure, will be presented in the section 2.4.2.

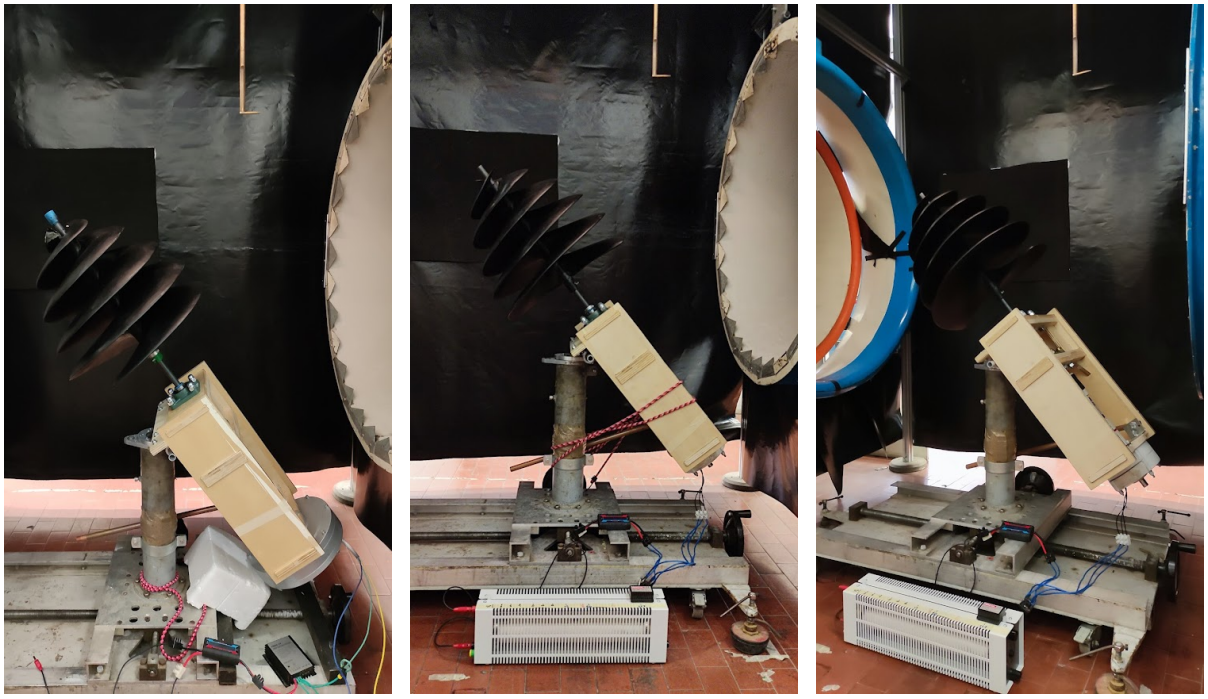

Figure 2.9: Set-up of 1:3 scale model for several configurations

In addition to the electrical circuit variables, this structure will also have geometrical variables. As can be seen in figure 2.9, in the experiments carried out with this structure, the angle at which the flow impinges on the turbine will be varied.

As mentioned before, in this type of HAWT turbine, the flow can be directed in any direction for its operation. However, it is of crucial importance to know which orientation is optimal to maximise its performance.

Also the speed at which the flow hits the turbine is an important variable, so this speed will be varied with the wind tunnel and its influence on the electricity production will be studied.

3 METHODOLOGY

3.1 Working principle and parameters of a wind turbine

According to the laws of fluid mechanics, the wind is a medium that carries kinetic energy and is subject to a variable pressure. Gradients in the atmospheric pressure field, i.e. pressure differences, generate air mass flows.

These wind flows contain kinetic energy that can be absorbed by wind turbines to generate electricity. The kinetic energy of any mass, whether solid, liquid or gaseous, can be expressed as the equation 3.1, where m is the mass and v is the velocity of the moving mass. In this case, the mass is a fluid (air) so the mass flow is defined as equation 3.2, being ρ the fluid density and A the the area through which air flows.

$$E_K = 1/2 \cdot m \cdot v^2 \tag{3.1}$$

$$\dot{m} = \rho \cdot A \cdot v \tag{3.2}$$

Since the time derivative of the energy is the power, taking a constant wind speed v, the power that could be delivered by the wind can be calculated according to the equation 3.3. This P_wind is considered the power available in the wind.

$$P_{wind} = \dot{E_K} = 1/2 \cdot \dot{m} \cdot v^2 = 1/2 \cdot \rho \cdot A \cdot v^3 \tag{3.3}$$

It can be deduced from this equation that, the larger the area through which the wind flows and its velocity, the greater the extractable power of the air.

It should be noted that, although power grows proportionally to the area A, which depends on the type and design of the wind turbine, this power is proportional to the area A. of the wind turbine, this power is proportional to the cube of the wind speed, This is, therefore, the most important variable for energy production. For is therefore crucial in wind energy installations to choose suitable sites where the wind speed is the most wind speed is as high as possible.

Wind turbines extract energy by slowing down the wind. For a wind turbine to be 100% efficient it would need to stop 100% of the wind – but then the rotor would have to be a solid disk and it would not turn and no kinetic energy would be converted. So, not all of the wind's kinetic energy can be fully absorbed by a wind turbine rotor

On the other extreme, if you had a wind turbine with just one rotor blade, most of the wind passing through the area swept by the turbine blade would miss the blade completely and so the kinetic energy would be kept by the wind.

For this reason that there is an optimal ratio between wind speed entering and leaving a wind turbine, namely, the inlet wind speed (v_1) of the wind at the rotor must be three times the output wind speed (v_2) to maximize the power absorbed in the wind turbine. This fact was demonstrated by Albert Betz in 1919, as will be seen in the next section.

3.1.1 Betz Limit [11]

Albert Betz was a german physicist who in 1919 concluded that no wind turbine can convert more than 16/27 (59.3%) of the kinetic energy of the wind into mechanical energy turning a rotor. To this day this is known as the Betz Limit or Betz' Law. This limit has nothing to do with inefficiencies in the generator, but in the very nature of wind turbines themselves.

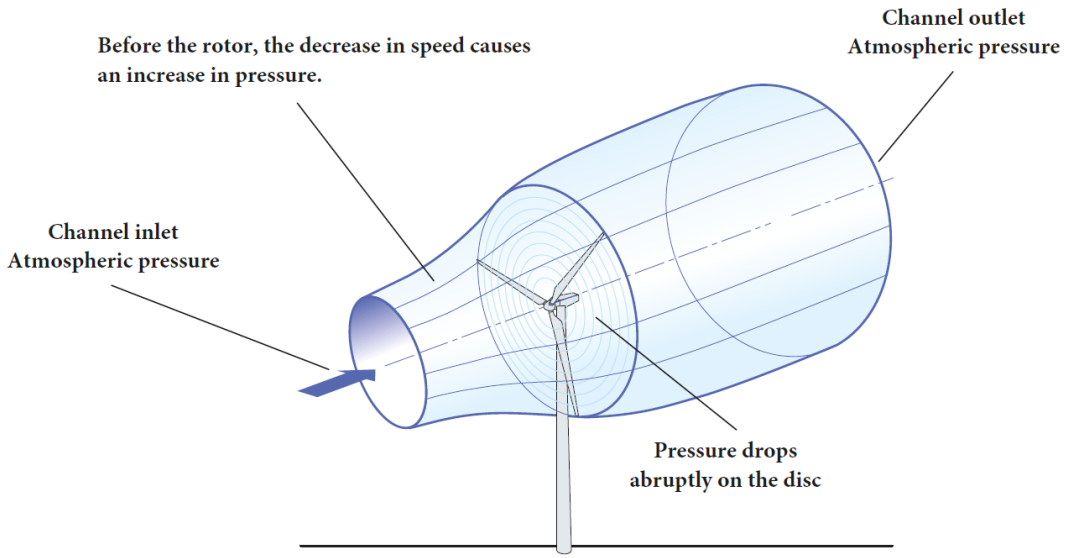

Figure 3.1: Control volume and conditions in Betz model [12]

Betz's theory is based on the following assumptions:

- the set of wind turbine blades is equivalent to a porous disk or rotor of zero thickness (infinite number of blades)
- the air mass flowing through the rotor remains separated from the surrounding mass (figure 3.1);
- the air mass flows only in longitudinal direction.
- the deceleration of the air in the actuating disc is distributed over the entire section of the disc.
- in the sufficiently far upstream and downstream sections the pressure is equal to atmospheric pressure.
- the wind flow does not encounter any obstacles upstream or downstream.

- the wind is stationary and its intensity remains constant with height.
- there are no rotational effects on the air mass.
- the compressibility of the air is neglected (density, ρ, is considered constant)

With this assumptions, Bernoulli's equation is applied to the control volume, considering the discontinuity at the rotor, as equation 3.4. And rotor pressure variation can be expressed as equation 3.5, with the nomenclature of the figure 3.2.

$$\begin{cases} p_1 + \rho \cdot \frac{v_1^2}{2} = p_3 + \rho \cdot \frac{v}{2} \\ p_4 + \rho \cdot \frac{v^2}{2} = p_2 + \rho \cdot \frac{v^2}{2} \end{cases} \tag{3.4}$$

$$\Delta p = p_3 - p_4 = \rho \cdot \frac{v_1^2 - v_2^2}{2} \tag{3.5}$$

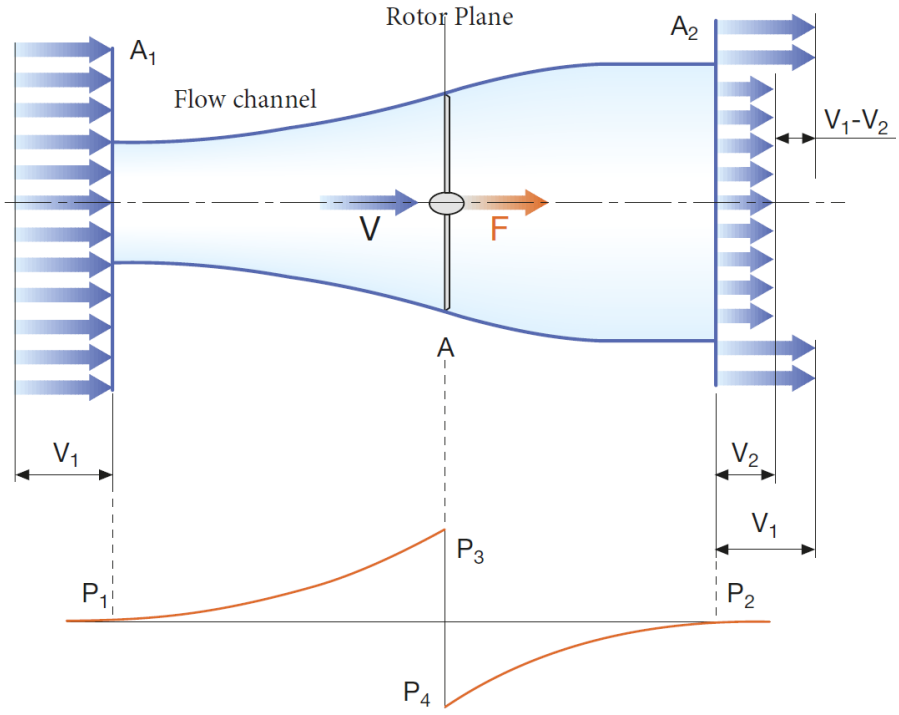

Figure 3.2: Nomenclature and evolution of velocity and pressure in Betz theory [12]

The axial force F in the wind direction on the rotor of section A perpendicular to the flow is given by equation 3.6. And according to the classic mechanics theorem of the linear momentum, this force will be equal to the variation of the quantity of motion of the air stream. And substituting equation 3.2 is obtained equation 3.7

$$F = \Delta p \cdot A = \rho \cdot A \cdot \frac{v_1^2 - v_2^2}{2} \tag{3.6}$$

$$F = F_3 - F_4 = \dot{m} \cdot (v_1 - v_2) = \rho \cdot A \cdot v \cdot (v_1 - v_2) \tag{3.7}$$

By equating both force equations (3.6 and 3.7), the speed at the rotor can be obtained.

$$v = 1/2 \cdot (v_1 + v_2) \tag{3.8}$$

As can be seen, the wind deceleration is split between the upstream and downstream sections of the actuating disc. The *axial induction factor* a is defined as the ratio which represents the decrease in speed at disk.

$$a = \frac{v_1 - v}{v_1} = 1 - \frac{v}{v_1} \tag{3.9}$$

Combining the above equations 3.8 and 3.9, the velocity v in the plane of the rotor and the velocity v_2 at the outlet of the flow channel can be expressed as a function of the axial induction factor a and the velocity at the inlet v_1.

$$\begin{cases} v = v_1 - a \cdot v_1 = (1 - a) \cdot v_1 \\ v_2 = 2 \cdot v - v_1 = 1 \cdot (1 - a) \cdot v_1 - v_1 = (1 - 2a) \cdot v_1 \end{cases} \tag{3.10}$$

The power captured by the blades can be expressed as the product of the force exerted by the wind F and its incident velocity v. Taking into account the velocity definition, as can be seen, the power extracted from the wind is proportional to the mass flow through the rotor and the difference in kinetic energy between the inlet and outlet sections.

And finally the equation can be rearranged and written as a function of a using above velocities relations, as seen in equations 3.11.

$$\begin{cases} P = F \cdot v = (\rho \cdot A \cdot v \cdot (v_1 - v_2)) \cdot v \\ P = \left(\rho \cdot A \cdot \frac{v_1 + v_2}{2}\right) \cdot \left(\frac{v_1^2 + v_2^2}{2}\right) \\ \\ P = 2 \cdot \rho \cdot A \cdot v_1^3 \cdot a \cdot (1 - a)^2 \end{cases} \tag{3.11}$$

In last equation of 3.11, it can be seen that the power depends on several important parameters.

Power varies proportional to the density ρ of the incident air mass, which is why there is a decrease in the power extracted in hot or mountain climates; also proportional to the rotor area A, and this area increases with increasing blade length; with the cube of the input wind speed, which explains the interest in installing wind turbines in places with good wind resources; and finally, with the output wind speed v_2 through the axial induction factor a.

Specifically, there is an optimum value of the output speed v_2, to which the maximum power extraction corresponds.

This value is obtained by deriving P with respect to a and equalling the derivative obtained to zero. It is obtained a second grade solution:

$$\begin{cases} \frac{\partial P}{\partial a} = 2 \cdot \rho \cdot A \cdot v_1^3 \cdot (3 \cdot a^2 - 4 \cdot a + 1) \\ \\ \frac{\partial P}{\partial a} = 0; \quad \Rightarrow \quad 3 \cdot a^2 - 4 \cdot a + 1 = 0 \end{cases} \tag{3.12}$$

Solving this 2nd degree equation yields two possible values for a possible values of a:

- 1, which does not make sense, since would imply a negative exit velocity;
- **1/3**, which corresponds to an output velocity of one third of the input velocity.

So, maximum is obtained at this situation, and for $\mathbf{a = 1/3}$, the maximum power extracted from the wind will be expressed in equation 3.13.

$$P_{max} = \frac{8}{27} \cdot \rho \cdot A \cdot v_1^3 \tag{3.13}$$

Power coefficient C_p

The power coefficient Cp(a) (or efficiency coefficient) is defined as the ratio between the power extracted and the power available from the wind.

$$C_p = \frac{P}{P_{available}} = \frac{2 \cdot \rho \cdot A \cdot v_1^3 \cdot a \cdot (1-a)^2}{1/2 \cdot \rho \cdot A \cdot v^3} = 4 \cdot a \cdot (1-a)^2 \tag{3.14}$$

Taking $\mathbf{a = 1/3}$ provides the theoretical maximum $C_{P,max}$ expressed in the equation 3.15, which is commonly known as the "Betz Limit" and which expresses the following fundamental concept: "The maximum theoretical power extractable from an airstream with an ideal wind turbine cannot exceed 59% of the available incident wind power".

$$C_{p,max.} = \frac{16}{27} \approx 0.59 \tag{3.15}$$

Consequently, no turbine will be able to exceed this value, and will in any case be smaller than it due to dissipative phenomena. In practice, three effects decrease the maximum achievable power coefficient: the rotation of the wake behind the rotor, the finite number of blades and the non-zero aerodynamic drag.

Since the power output of a wind turbine as a function of the power coefficient Cp and the available wind power is given by equation 3.16.

$$P = C_p \cdot \frac{1}{2} \cdot \rho \cdot A \cdot v_1^3 \tag{3.16}$$

The electrical power generated can be calculated from the equation 3.17, where η_{mec} is the overall mechanical efficiency of the whole drive train, from the rotor through the multiplier to the electrical generator, and η_{elec} is the efficiency of the electrical generator.

$$P_{elec} = \eta_{elec} \cdot \eta_{mec} \cdot P \tag{3.17}$$

Tip Speed Ratio (TSR) λ

The specific speed (TSR, Tip Speed Ratio (TSR), denoted by λ, is defined as the ratio between the tangential velocity at the tip of the blade (v_t) and the wind speed at the inlet of the flow tube the wind speed at the inlet of the flow channel (v_1).

$$\lambda = \frac{v_t}{v_1} = \frac{\Omega \cdot R}{v_1} \tag{3.18}$$

For a given rotor, the ratio λ-Cp depends on the pitch angle of the blade. Keeping the pitch angle constant, the following considerations can be made:

- there is a single value of TSR for which the conversion efficiency is maximum (C_p, max) and which depends on the blade type;
- when changing the wind speed v_1, if the TSR is to be kept constant and equal to the value for which $C_{p,max}$ is obtained, the rotational speed of the blades must also be changed;
- for low TSR values there is a reduction in lift and an increase in drag until the stall condition is reached;
- for high TSR values you have a reduction of both lift and drag, in what is known as the "runaway" condition;
- the optimum TSR depends on the number n of blades and the smaller the number of blades, the faster they must rotate to extract the maximum power from the wind (TSR increases);
- The shape of the TSR vs Cp curve depends on the type of wind turbine (figure 3.3).

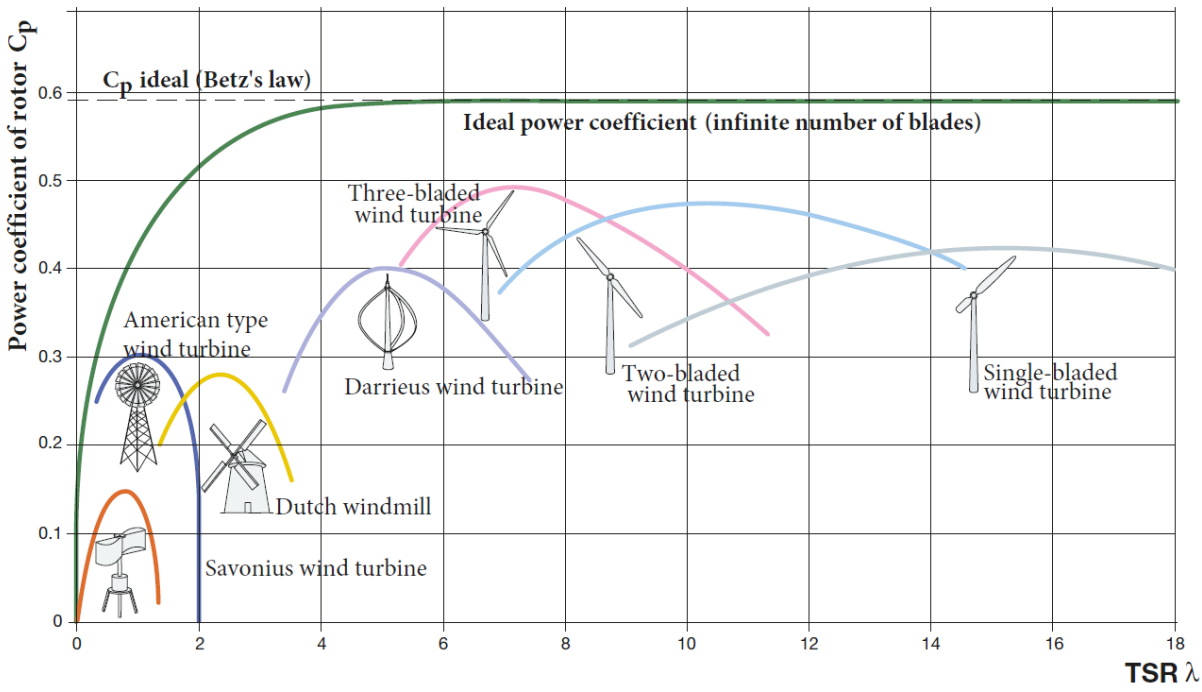

Figure 3.3: Cp vs TSR for different wind turbines designs [12]

Fast wind turbines are defined as those with a high optimal TSR, while *slow wind turbines* are defined as those with a low optimal TSR.

Table 3.1 gives the typical values of angular tip speed for different types of wind turbines with a wind speed of $7^{m}/_{s}$. The values are calculated using their optimal TSR obtained from figure 3.13. As can be deduced from the values in table 3.1, horizontal axis wind turbines are fast, as they have a high tip speed, even with a low angular velocity, since the radius of the rotor is generally much larger than that of vertical axis turbines.

Wind turbine type	**Optimal TSR** λ	**Tip Velocity** $v_t\,[^{m}/_{s}]$	**Rotor radius** $[m]$	**Ang. velocity** $\Omega\,[rpm]$
VAWT Savonius	1	7	1	67
VAWT Darrieus	5	35	1.5	223
HAWT bipala	10	70	28	24
HAWT tripala	7	49	45	10

Table 3.1: Typical values of different designs [12].

In order to maximise the energy produced annually with the operation of the wind turbine, the power coefficient C_p should be kept at its maximum value as long as possible, even if the wind speed varies.

3.2 Aerodynamic fundamentals

3.2.1 Blade Element Momentum Theory (BEM)

A blade is essentially a wing on which two air flows act which depend on: the wind flowing through the flow channel with velocity $\vec{v_1}$ parallel to the wind turbine axis; and the rotation of the blade itself which creates a drag velocity component $\vec{v_t}$ perpendicular to the previous velocity.

Assuming v_1 equal over the entire cross-section of the flow tube, at a distance r from the rotor axis, v_t is given by equation 3.19, where $\vec{\Omega}$ is the angular velocity of rotation of the rotor [rad/s].

$$\vec{v_t} = -\vec{\Omega} \cdot r \tag{3.19}$$

Therefore, the total velocity of the air flow licking the blade (in the reference system integrated in the blade itself) is given by the vector sum of two components.

$$\vec{v} = \vec{v_1} + \vec{v_t} \tag{3.20}$$

$$v = \sqrt{v_1^2 + v_t^2} = \sqrt{v_1^2 + (\Omega \cdot r)^2} \tag{3.21}$$

As can be seen, the velocity of the air flow incident on the blade increases with the rotational speed of the blade.

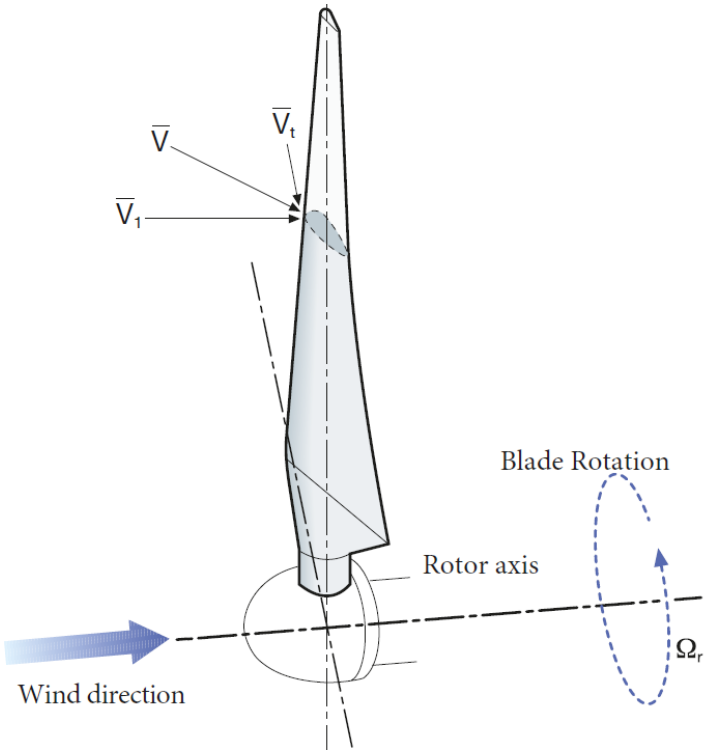

Figure 3.4: Velocity components in a blade

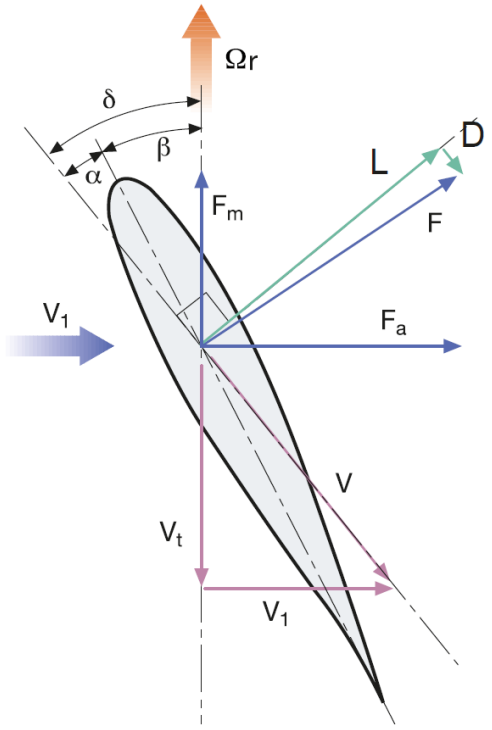

Figure 3.5: Forces in a blade [12]

3.2.2 Lift and Drag forces

The consequence of the resultant airflow (v) on the wing profile of the blade is the creation of two aerodynamic forces which are defined in figure 3.5.

These two are: the lift force L which is perpendicular to the direction of the resultant airflow, and the drag force D parallel to the direction of the resultant airflow.

Different geometrical angles can also be found:

- α, angle of attack or angle, which is the angular difference between the direction of the resulting airflow and the maximum chord of the blade section;
- β,pitch angle, which is the angular difference between the plane of rotation of the blade axis and the maximum chord of the blade section;
- $\delta = \alpha + \beta$ constructive angle

Lift and drag are expressed, respectively, by equations 3.22 and 3.23, where C_L and C_D are the lift and drag coefficients respectively.

$$L = 1/2 \cdot \rho \cdot v^2 \cdot A \cdot C_L \quad \Rightarrow \quad C_L = \frac{L}{1/2 \cdot \rho \cdot v^2 \cdot A} \tag{3.22}$$

$$D = 1/2 \cdot \rho \cdot v^2 \cdot A \cdot C_D \quad \Rightarrow \quad C_D = \frac{D}{1/2 \cdot \rho \cdot v^2 \cdot A} \tag{3.23}$$

3.3 Electricity generation

To convert the mechanical power extracted from the wind into electrical power, an electrical machine acting as a generator must be coupled to the axis of rotation.

There are two basic types of electrical machines: those that generate direct current and those that generate alternating current.

Direct current generators, also known as dynamos, are made up of multiple windings located on the rotor and which are subjected to a static magnetic field produced by permanent magnets or by an electromagnetic inductor. This type of electrical machine needs to switch the electrical circuits that are conducting current at any given moment to ensure constant movement in the same direction.

DC generators can be used in low-power wind turbines where a DC output voltage is required. The reason why they are not used in the generation of higher power is because they have a more complex structure of windings and connections and because they are not very efficient due to the losses that exist due to friction.

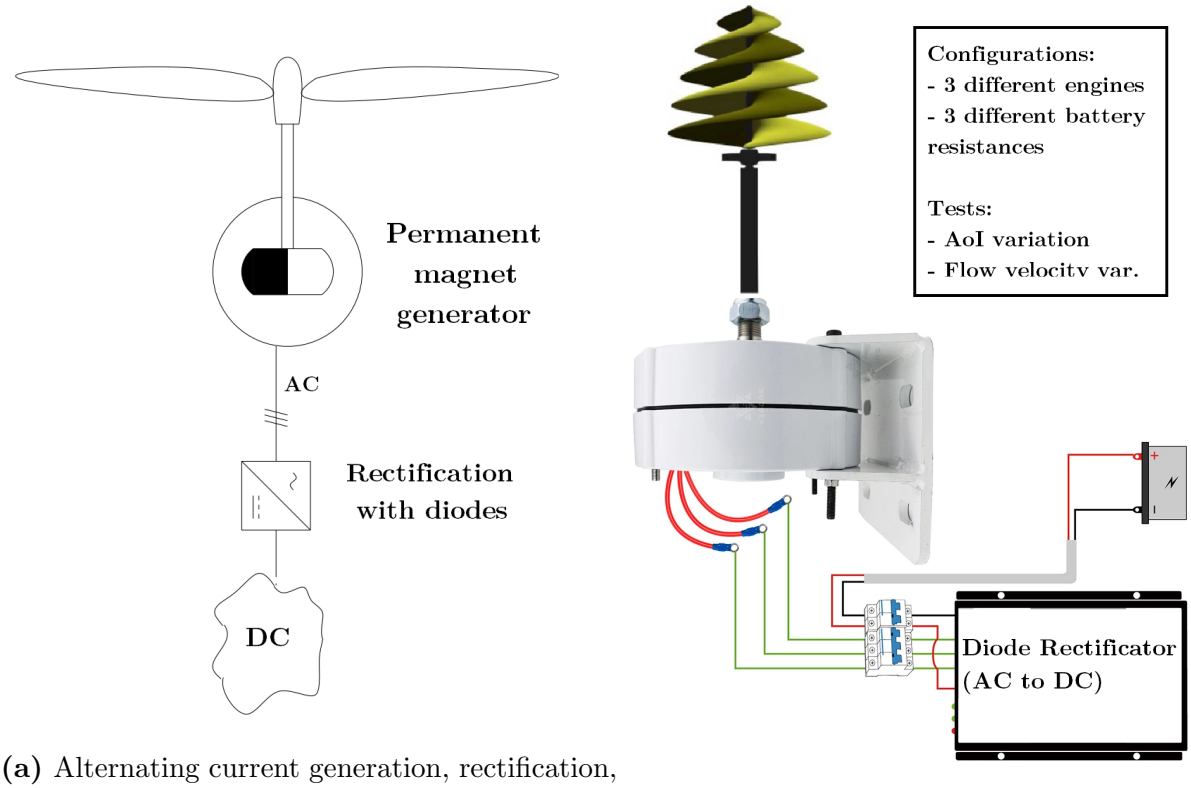

(a) Alternating current generation, rectification, and conversion to DC for storage.

(b) General scheme of the electric test.

Figure 3.6: Electricity generation diagrams

However, there is another way to obtain direct current without using a DC generator: the generation of alternating current (AC) and its subsequent rectification with diodes. This form of generation is more efficient and involves lower losses and higher efficiency.

And in this case, this method of power generation is selected and the electrical machine used is an alternating current generator of permanent magnets. This selection is due to

the fact that these are the engines that are available in the laboratory. Moreover, it is the most common way to proceed with turbines of this type.

For this particular case, figures 3.6 show two schematic diagrams of the power generation. In fig 3.6a in general schematic form, and the 3.6b particularized to the turbine and generator used.

In both cases the system consists of the same main elements, being this way the simplest form of energy production. With this few elements electrical circuit the generation electricity with wind energy is produced.

However, the tested electric circuit consists of more elements, which are necessary for the data acquisition and the several studies configurations. These elements, which make up the complete circuit, will be introduced in section 4.3. To see the complete electrical installation, please refer to figure 4.5.

Diode rectifier

As it is said above, in this project, it is possible to use an alternating current generator and to transformed it into a direct current thanks to the implementation of and a full-wave rectifier based in diodes. This transformed direct current allows to charge the battery.

The internal operation of the diode current rectifier is shown in figure 3.7. The diode bridge transforms the inlet alternating current $v1$ to direct current $v2$ at the output, ready to charge the batteries.

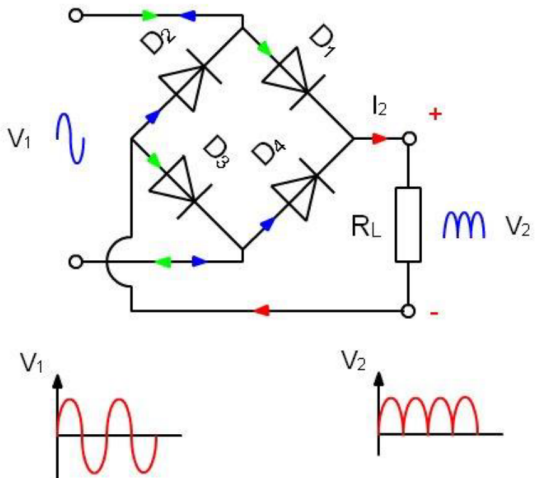

Figure 3.7: Diode rectificator scheme.

As can be seen in the image, it rectifies the sinusoidal wave of alternating current ($v1$) to direct current ($v2$) which is expressed as an average value.

4 EXPERIMENTAL SET UP

4.1 Wind-tunnel

The wind tunnel is a large plant designed to test aerodynamic models, with the function of recreating the flow conditions around the test model as similar as possible to real situations. There are different types of wind tunnels and they are classified according to the velocity field generated and the Mach number produced.

The experimental tests, necessary for the aerodynamic characterisation of the RoDaVi rotor, were carried out in the wind tunnel of the laboratory of the Sapienza Department of Mechanical and Aerospace Engineering (DIMA).

The wind tunnel is of the subsonic closed-loop type. It consists of a duct divided into several parts. Figure 4.1 shows a simple diagram of the real wind tunnel with all its parts shown.

In the "test section", which is the open part, is where the moving fluid acquires the physical characteristics set for the experiment, the model is placed in the study, while the measuring devices are kept strictly outside it.

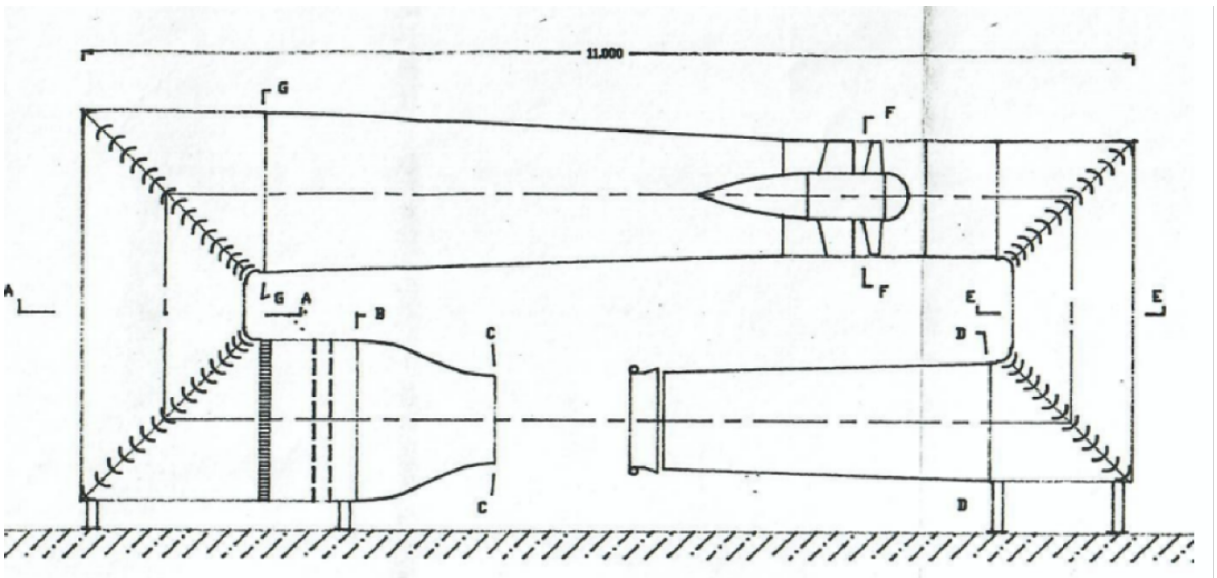

Figure 4.1: DIMA laboratory wind tunnel [13].

The DIMA turbine has overall dimensions of 11 x 4.2 x 1.7 m and a diameter in test section of 0.9 m, an installed power of 50 kW, and can reach a speed of 45 m/s without overloading the engine.

The wind speed is controlled by adjusting the rotational speed (rpm) of a fan by varying the frequency of the motor supply via an inverter.

The advantages of using closed-loop tunnels over open wind tunnels are flow quality, operating costs and low noise level; on the other hand, the disadvantages are construction costs, cleaning and cooling.

4.1.1 Pitot tube

To measure the wind speed, a Pitot tube was used, placed in the test section, immediately after the inlet, in a position that does not interfere with the flow of air that affects on the model under study.

By measuring the fluid pressure at a given point in the pipe, the Pitot tube allows the velocity of the fluid at that point to be estimated. And using the relationship between the velocity and the area through which the fluid flows, also the volumetric flow rate of the fluid can be calculated. It is possible to demonstrate this phenomenon using Bernoulli's Theorem.

The real Pitot tube, together with a simplified schematic of it, is plotted in Figure 4.2.

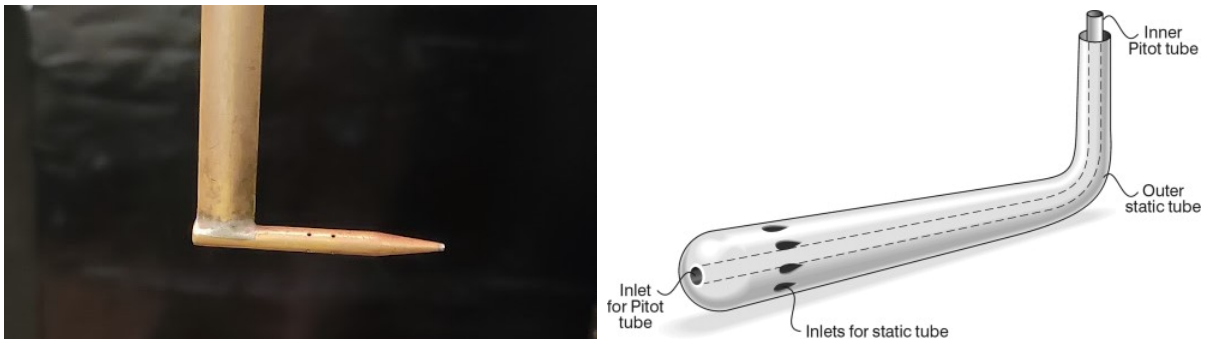

(a) Real Pitot tube **(b)** Scheme Pitot [14]

Figure 4.2: Pitot tube

The Pitot tube is connected, by means of two plastic tubes, to a digital micromanometer, model PCE-HVAC 2, which returns the values of pressure, velocity and ambient temperature.

Its use is fundamental, as it allows the instantaneous values of the wind speed in the tunnel and also the pressure to be known, so that from a simple reading on the display, all the parameters can be kept under control and, if necessary, the number of revolutions of the tunnel engine can be adjusted to obtain the desired conditions. The ambient temperature is useful for determining air flow parameters such as density and viscosity. The air velocity measurement range is from 1 to 80 m/s, with an accuracy of $\pm$ 2.5 % of the measured value.

4.2 Dynamometric balance

To measure the forces acting on the model under study with changing wind speed and inclination, the AFA3 dynamometric balance, produced by TecQuipment was used.

The dynamometric balance is an extremely sensitive instrument that is capable of quantifying the forces and moments acting on a structure connected to it, through the use of three strain gauges. Two allow the lift and pitch moment to be calculated while the third allows calculate directly the drag.

The balance is placed in a framework set-up with a triangular plate when the forces are applied to another fixed plated, both connected by three supporting legs in each triangle vortex. The supporting legs use spherical joins in order to constrain the movement in a plane parallel to the fixed plate (in a horizontal way), having three degree of freedom at the triangular plate, so 3 strain gauges are needed.

This three sensors are the responsible for obtaining the forces in terms of voltage difference. The output from each load cell is taken to a strain gauge amplifier carried on the mounting plate and this value is taken to a display in an electronic voltmeter, or in this case directly to the pc. Lift and drag forces are calculated directly from the load cell outputs making use of the calibration factors that are previously implemented.

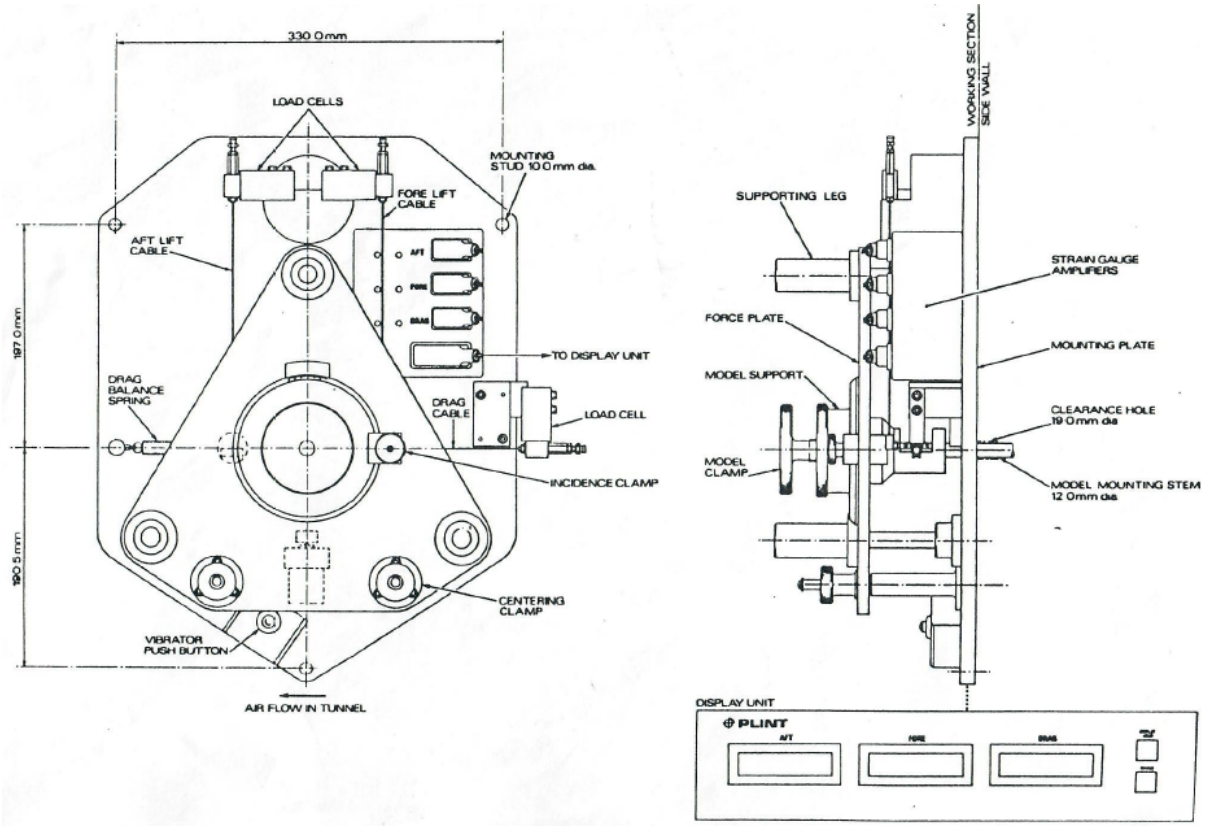

Figure 4.3: Schematic view of elevation and profile of the balance [15]

The balance has been modified with the use of Arduino which has improved the sampling performance, in fact it can reach a sensitivity of 0.01 N and through the usb connection

it is possible to send the acquired data directly to the pc, in the form of a matrix where the first the lift and drag values are calculates.

4.2.1 Data acquisition with Arduino

The acquisition of the signals generated by the components of the balance are processed and collected through the Arduino device. Inside the Arduino there is a specific hardware to be able to quickly export the values of the forces that act on the models attached to the balance. This hardware also allows to take thousands of data records of aerodynamic forces in a matter of seconds.

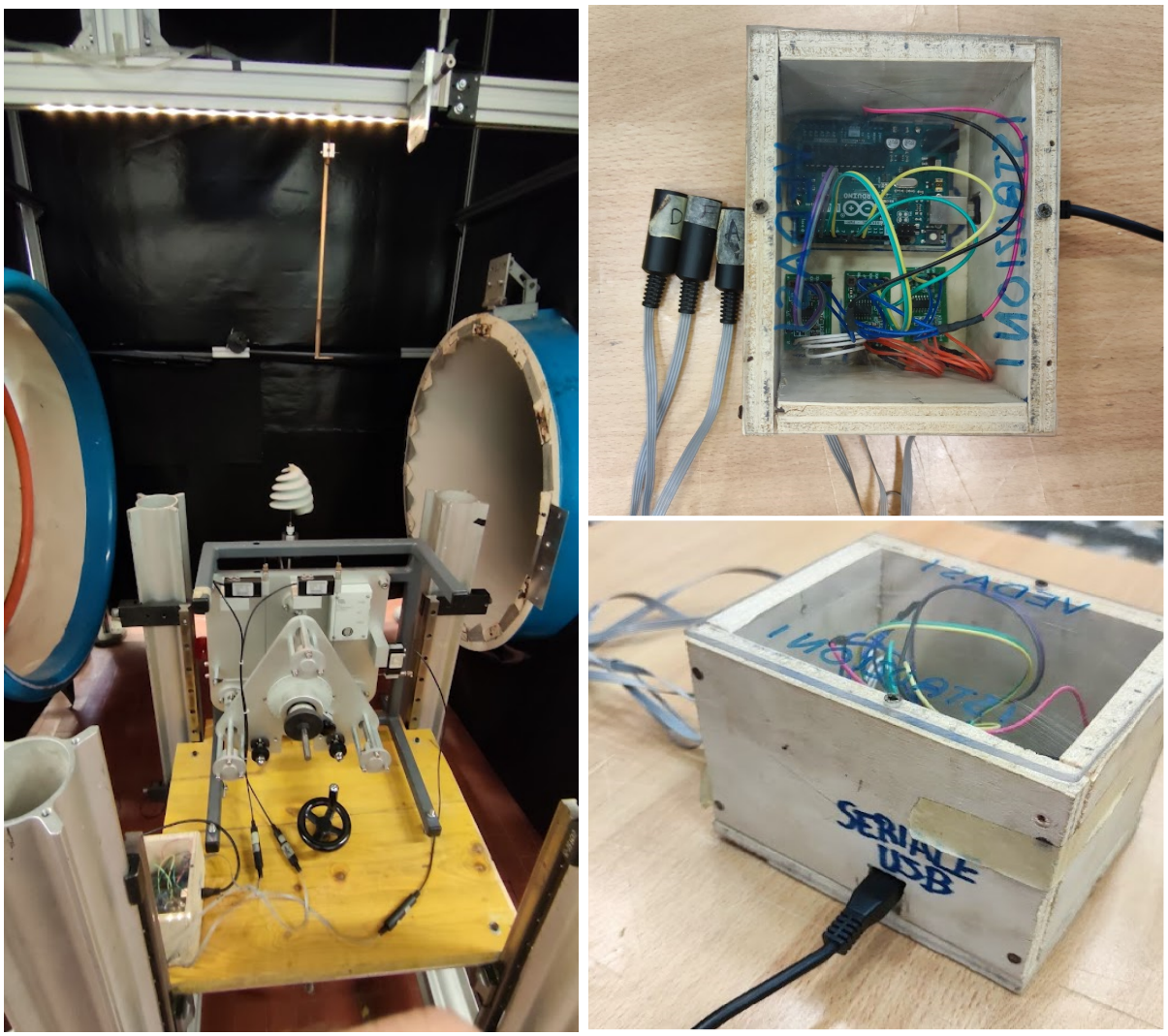

(a) Dynamometric balance **(b)** Arduino system

Figure 4.4: Dynamometric balance set-up

The Arduino hardware interacts with the Matlab, through a code that acquires a number of samples desired at a frequency of 86 Hz. In the case of the turbines, a range of 2000 values measured by the 3 strain gauges chosen has been calculated. Matlab manages the opening and closing of the connection with the Arduino and the storage of data.

The acquisition time can be varied by choosing the number of data acquired, bearing in

mind that, as mentioned above, the acquisition is 86 data per second.

Thus, using Matlab code, the Arduino sends the values of the forces expressed in grams to the pc via a usb serial connection and, therefore, the weights of the entire instrumental set-up are considered.

So not only the forces produced by the turbine to be studied are measured, it is also measured together with the turbine the influence of the accompanying elements, i.e. the arm, the support, and the weighing plate. Thus it is necessary to make measurements also for all cases of the set-up without the turbine. These values at empty configuration are subtracted from the force values obtained with the total system. By doing this, the real data of the forces produced only by the turbine will be obtained, without being disturbed by the forced induced un the necessary elements that assist and support the turbine in the measurement experience.

Once the data has been obtained in Matlab, it is stored in struct form for final processing.

4.3 Electrical installation

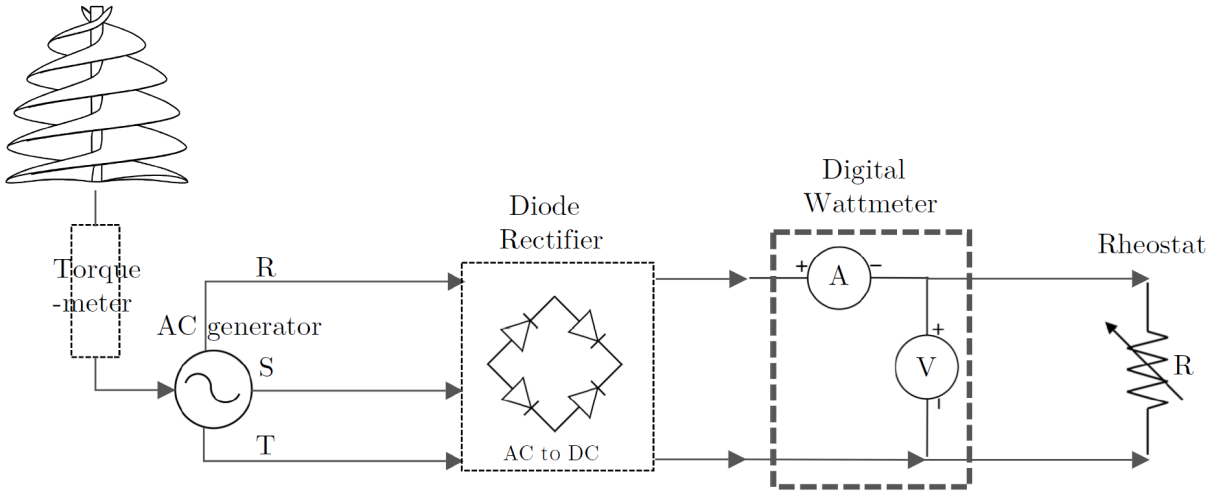

Figure 4.5: Electric diagram of the study

The electrical system is one of the main parts of this study. The principle of power generation with a permanent magnet generator was already presented in section 3.3. The process of transforming alternating current to direct current by means of a diode rectifier system was also explained. In this way the alternating current can be correctly stored in a battery.

This section now presents the main elements that are part of the setup used to measure the mechanical and electrical characteristics of the system. Figure 4.5 shows an electrical diagram with the main components.

The turbine is connected by means of a shaft to a torque meter, which will be in charge of obtaining the mechanical characteristics of its rotation. The turbine shaft is also mechanically connected to a permanent magnet motor. Three different motors with different characteristics and nominal power will be used.

The alternating current produced by the generator is converted to direct current by the diode rectifier. After that a wattmeter is used to measure the electrical parameters of each experiment. Finally, the circuit ends in a rheostat that acts as a battery.

Torque-meter

The torque meter is a device used to analyse the effective mechanical power realised by the engine torque through the measurement of the torque angle and the revolutions of the turbine shaft.

The model used is the *NCTE torque meter Series 2300*, shown in figure 4.6. Next to it is a readout unit, which is used to provide electrical power supply to the torque meter. In addition, there is a specific software from *NCTE*, by means of which, by connecting the computer to the readout unit, the torque meter can be easily calibrated for each measurement, and the thousands of data can be exported for processing.

Figure 4.6: NCTE torque meter Series 2300 and readout unit [16]

Generators characteristics

Three engines with different characteristics will be used for the electrical study. All of them are Permanent Magnet generators and work with alternating current. The working principle of these motors has been seen in section 3.3.

These three motors are commercialised in the segment of small wind turbines due to their good performance. The reason why it has been decided to use this type of models is because they were in the laboratory and it was decided to make a comparison between them.

The three motors are identified in figure 4.7. The first one (4.7a) is a generator of the Chinese brand Shenzhen Global Technology model NE-100W. Its nominal power is 100W. Its main features are no gear, direct drive, low speed rare earth permanent magnet generator, easy to operate, safe and easy to maintain.

Inside there are neodymium iron boron, high grade copper wire winding, power efficient and stable. Also has a special stator and rotor design, start resistance torque is small, and good heat dissipation.

The second generator (4.7b) is a superior model to the first one, the NE-200W model, with a rated power of 200W. Both models are very conventional in turbine applications such as this one.

Finally, the third generator (4.7c), in grey, is an AFPM coreless stator generator with a rated power of 200W. This model is different from the previous ones.

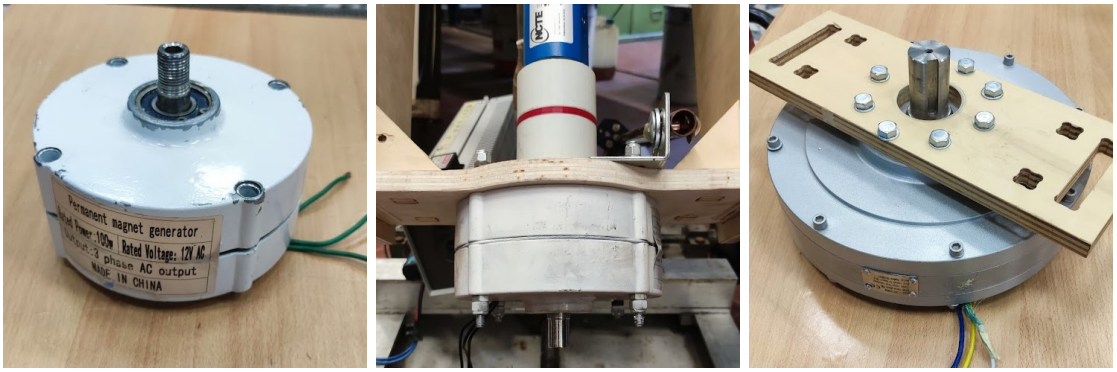

(a) Conventional PM generator of 100W

(b) Conventional PM generator of 200W (mounted)

(c) Coreless stator AFPM generator of 200W

Figure 4.7: Generators used in the experiments.

The nickel structure of an AFPMG is simple, and the winding concept with a stator structure gives the generator a good performance and high efficiency. In addition, it differs from the previous two by some characteristics as no mechanical drive losses, no rotor copper losses due to the permanent magnet excitation and no stator eddy current losses in the ironless (coreless) stator.

Diode rectifier

The diode rectifier is a generic rectifier found on the market. Its operation has been explained above in the basics of electricity generation in section 3.3.

Wattmeter

The device used to measure electrical power is the *ARCELI 150A Watt Meter High Accuracy RC Power Analyzer*. This wattmeter acts as a current, voltage and power meter, and outputs the values on a display. It is shown in figure 4.8.

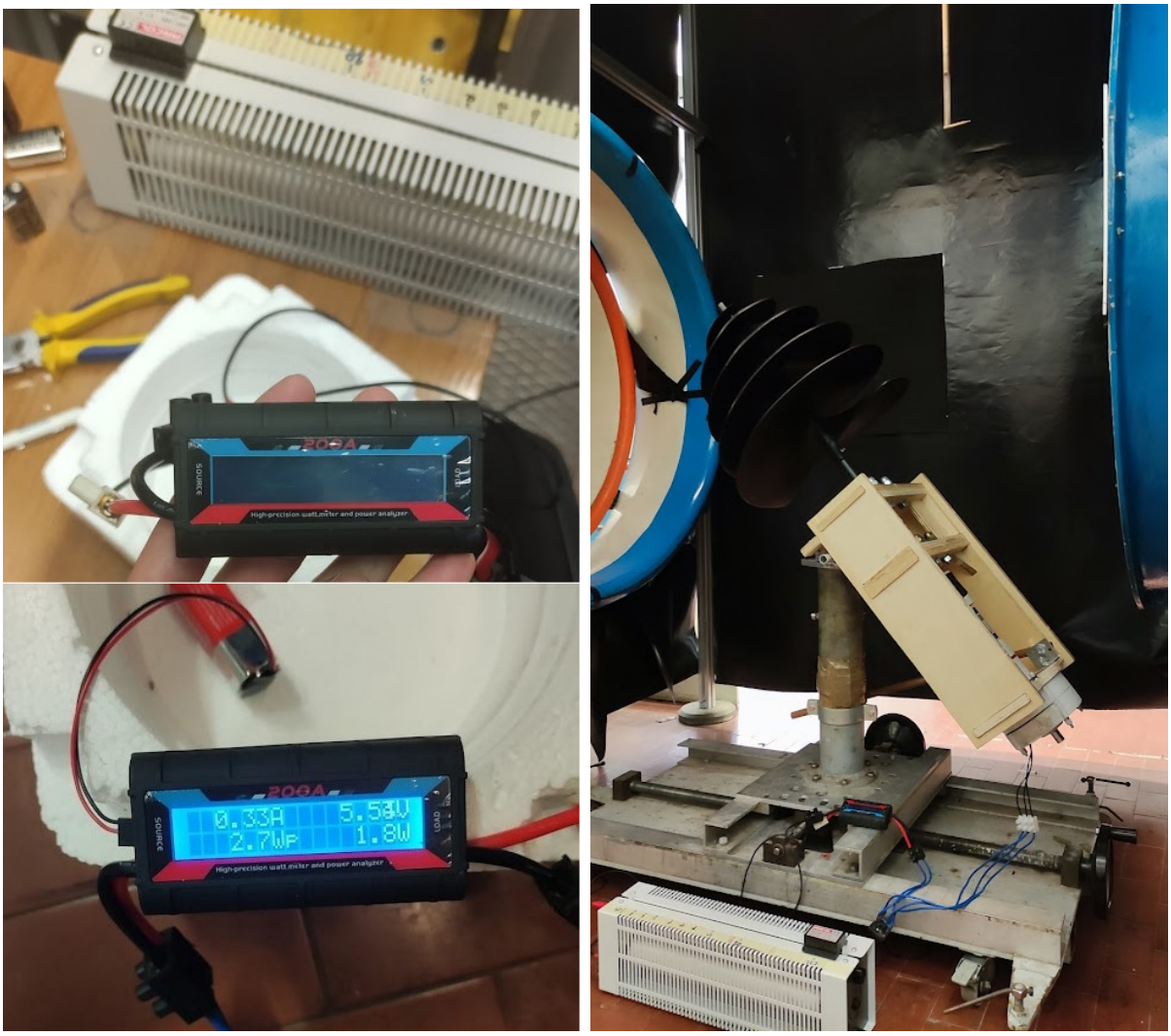

(a) Rheostat on the top and wattmeter **(b)** Set-up with rheostat at bottom

Figure 4.8: Wattmeter and rheostat

Rheostat

The last part of the electrical circuit is composed of a rheostat, replacing a battery. The battery in the real circuit would offer a resistance when being charged. Instead, it is replaced by a rheostat or variable resistor which performs the same function.

In this way the resistance of the circuit can be considered as variable. The way to change the resistance in this rheostat is to modify the length of the internal circuit it has by means of a manually operated slider. The influence of this variation will be studied.

4.4 Particle Image Velocimetry (PIV)

The PIV technique, Particle Image Velocimetry, makes it possible to visualise two-dimensional velocity fields formed around the flow that is traversing a body. The flow must be composed of small tracer particles in order to represent the movement of the fluid. The tracer particles are introduced into the flow directly in the wind tunnel thanks to a bubble generator that allows a continuous generation of bubbles in sufficient quantity to keep them circulating around the model to be analysed.

The particles are produced by a simple mixture of water and liquid soap, and are only a few microns in size, but are visible with the naked eye when they are penetrated by a plane of light generated by a laser beam. It is therefore possible to observe instantaneous velocity fields by acquiring sequential images captured at successive time intervals.

The velocity measurement will be based on the estimation of the particle displacement in a given time interval. The acquisition of particle images is performed with a digital camera capable of producing numerous frames per second, to show the continuous motion of the particles in the plane.

Figure 4.9 shows a general schematic of a PIV system in a wind tunnel, clearly showing the different instruments used and the planes where they act: the laser beam, the camera and the plane or region of irradiated particles.

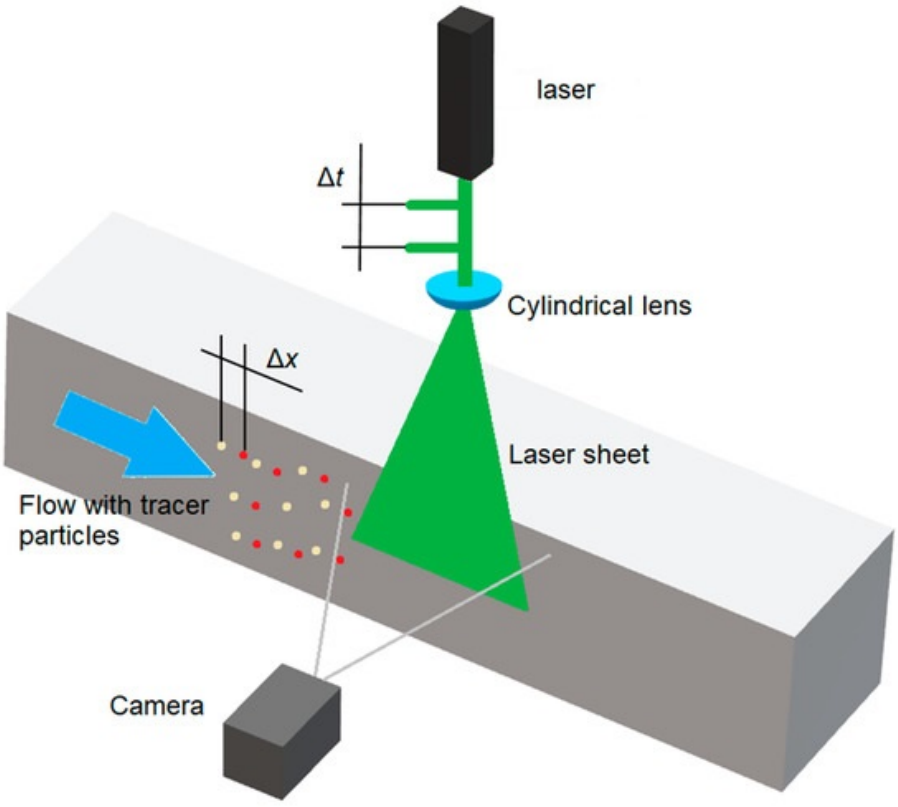

Figure 4.9: Schematic view of PIV vertical plane configuration [17]

4.4.1 Laser

The laser used in the tunnel for experimentation is the *MGL-V-532NM* model, built by the Chinese company *CNI laser*. It is an optical instrument that emits a continuous beam of green light with a wavelength of about 530-560 nm and has an emission power of about 10 W. The laser power can be adjusted by means of touch-screen controls. The laser power is adjustable by means of controls on a touch screen, which can be used to decrease or increase the intensity of the light beam.

For the measurements, the laser was positioned in two different directions, in two different parts of the tunnel. In the first test, it was mounted as shown in figure 4.9, at the top in a central position, to show the vertical plane, that is the velocity field of the particles travelling along the longitudinal path of the tunnel.

In the second test, however, the laser was clamped by means of a plate on an aluminium column perpendicular to the previous beam. Referring to figure 4.9, the laser in this second position was in place of the camera, radiating horizontally across the tunnel cross-section, and vice versa with the camera position.

The light plane cutting the tunnel is 1 mm thick, and has been oriented by turning the laser lens with a small screw, and perfectly aligning the light beam with the tunnel and the camera.

4.4.2 High speed camera and lens

The irradiated particles travel along the laser-generated light plane at wind tunnel speed. Their movement is tracked by the capture frames of the FastCam Mini AX100, a high-speed camera with a maximum resolution of 1024x1024 pixels with maximum frame rates of up to 540,000 fps and a minimum exposure time of 260 ns. It is equipped with a Nikkor lens (AF-S 50mm f/1.4G) whose adjustment is essential for focusing the light plane with the particles. This adjustment is made every time an acquisition is started.

Focusing is necessary because the flow when it hits the camera tends to move the lens from the focus position and loses the clean frame of the bubble mass. This phenomenon appears mainly when the flow velocity is very high and the camera is mounted vertically.

Figure 4.10: FastCam Mini AX100 and Nikkor lens [18]

4.4.3 Bubble generator

The tracers that are introduced into the fluid to study its evolution and thus obtain the velocity field are soap bubbles, which are produced in the *TSI G-1000* micro bubble generator.

The *TSI Bubble Generator BG-1000* generates the ideal seed particles for aerodynamic flow measurements by producing air-filled soap bubbles (15 microns) as tracers for particle image velocimetry and wind tunnel applications.

The mixture of soap and water is produced inside this device, and by means of pressure is introduced through a tube into the setting chamber of the wind tunnel. The particles travel through the convergent nozzle fully integrated with the flow until they reach the test section, where they are illuminated by the laser and ready to be measured.

Figure 4.11: TSI Bubble Generator BG-1000 [19]

5 RESULTS

In this chapter will be presented main results obtained in the wind tunnel. As commented in previous chapters, the results chapter is divided in three sections.

In the first section, a preliminary analysis based on aerodynamic performance of the wind turbine will be carried out using a 1:10 scale model of the original turbine size. This is useful for determine how much of aerodynamic coefficients can be achieved, and to determine the characteristic rotational frequency of the structure.

Further on, a second analysis is undertaken with a 1:3 scale turbine model. This study is based on obtaining the electrical performance of the turbine. The main objective is to determine if there is some configuration in which cost-effective electricity parameters are obtained. In this way, various configurations will be tested to obtain the best configuration. Also a comparison with a turbine of easy construction, already applied to the market for its electrical profitability, such as Savounius, will be conducted.

Finally, last experience will be carried out with some previous configurations in order to see the flow evolution through the turbine, and the main characteristics of the weak that is produced. The PIV laser technology applied to the flow field of the wind tunnel will capture this flow and vorticity evolution. A vertical and a horizontal plane will be measured. A discussion of how flow is perturbed by the structure is of crucial importance for the placement of several turbines and their interaction.

5.1 Preliminary analysis: aerodynamic forces in a 1:10 scale model

This preliminary analysis seek to demonstrate the high aerodynamic performance of "Ro-DaVi" turbine based on the first ideas of Da Vinci's aerial screw. The principal modification on its shapes is the addition of more screw thread, in order to increase the area of contact with the flow, and also to avoid the bulky shape of the original design.

In this original design also the thickness is taken into account. Originally three different thickness models were used, but one was detached from the holder support and was destroyed inside the wind tunnel. So the study will be performed for 2 different models called *thick* (airfoil thickness of 9mm) and *thin* (4.5mm).

Moreover, the reason of using a 1:10 scale model of the original turbine size is due to structural limitations of the dynamometric balance used for measured the forces implied. The magnitude of the forces we would get with the real model and also its weight are not supported by the balance arm.

For both little turbines aerodynamic coefficients can be achieved thanks to the Arduino acquisition system implemented (section 4), and also with a frequency analysis of the data collected the frequency evolution is obtained in order to find out the rotational velocity.

The data is acquired varying the free stream velocity, and also rotating the structure with the balance. It should be recalled that the angle of incidence (AoI) is the angle of traversal rotation of the structure with respect to the floor, being the 0 angle of incidence the configuration with the turbine completely perpendicular to the floor.

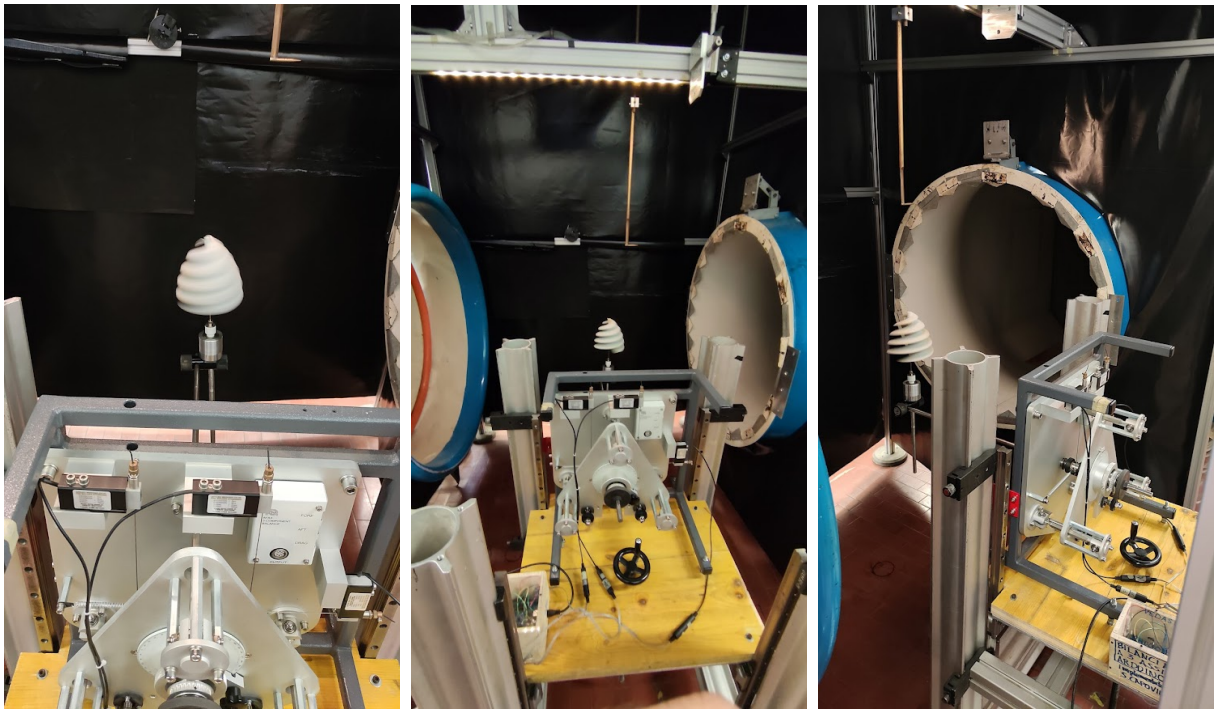

Figure 5.1: Aerodynamic study set-up

It is tested with different angles by changing the *AoI* by 5 degrees (0, 5, 10, 15, 20, 25 degress) for 4 different speeds (10, 12, 14, 16 m/s). The velocity of the flow is increased from the moment the prototype starts to rotate until it is considered to be dangerous due to the fear of detachment of the prototype.This is one of the limitations we will see and will be addressed in further studies.

5.1.1 Force coefficients

The most relevant issue during the process of obtaining the results of this experience with the little turbines was the destruction of two of the three turbines intended to study. This is due to the constructive limitations of the components of the supporting arm explained in section 2.4.2.

The results of one turbine were discarded completely of the study, due to its premature destruction in endurance test phase. Fortunately, the other two turbines were usable for the thickness comparison and aerodynamic study. The second accident happened with the *thin* turbine at 25 degrees of *AoI*, so the parametric study covers until to that angle of inclination.

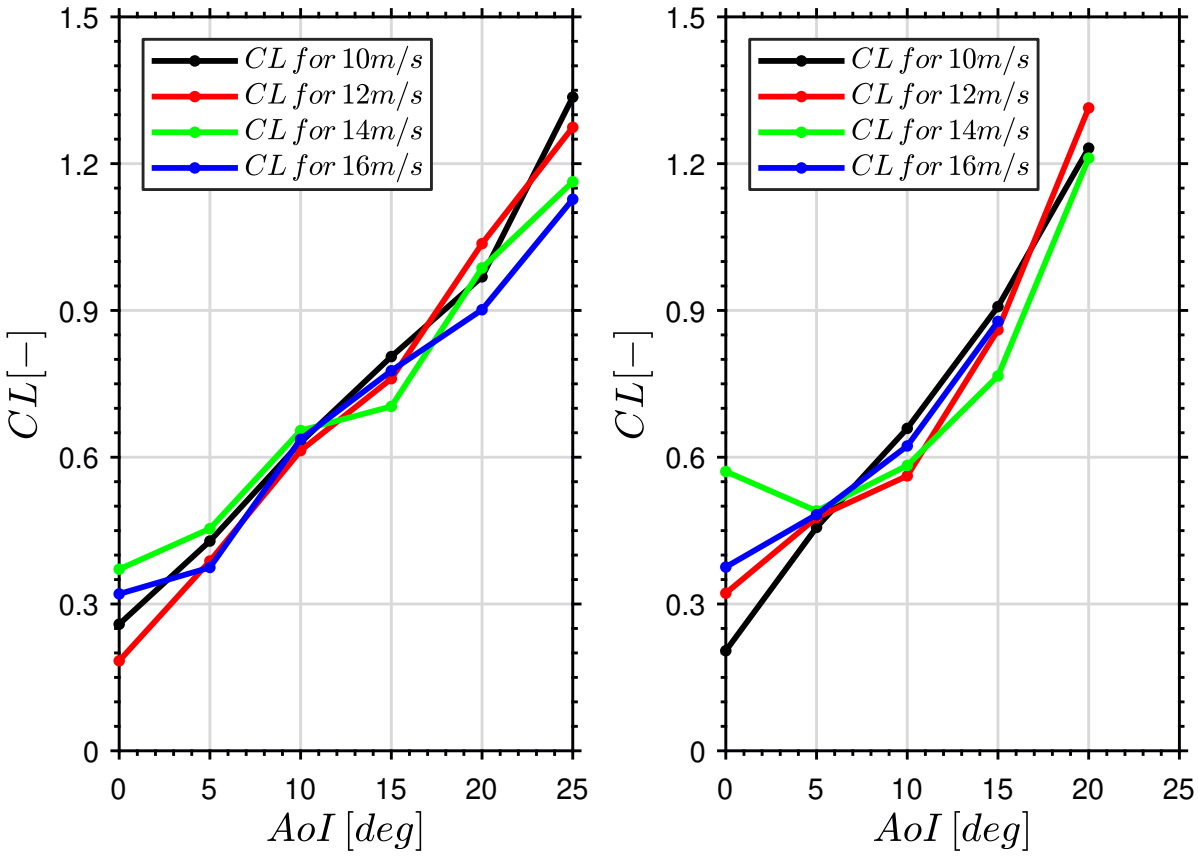

(a) Thick turbine **(b)** Thin turbine

Figure 5.2: Evolution of C_L with the angle of inclination *AoI*

Observing the evolution of C_L can be noted as a general trend a linear increment of the lift coefficient with the growth of the angle of attack for both experiences. There is more than a factor 3 increment from 0° to 25°.

However, this non-dimensional coefficient seems to be practically independent of the velocity, since there is a similar evolution for all the velocities, with a slightly steeper growth slope in low speeds cases.

The behaviour of lift coefficient is similar to an airfoil without reaching stall conditions. In an airfoil there is a linear increment of C_L for low angles of attack (α). Of course this analogy is not exactly true because the 3D flow effects due to the rotation of the turbine should be taken into account, but the comparison will be useful to analyse the aerodynamic behaviour and its similarity to an airfoil.

Thus, this performance of C_L linear increment with the angle of attack is exactly the turbine has with its angle of incidence AoI. Note that both angles are not equal. The turbine has initial angle of attack (α) itself due to its shape with curvature. Nevertheless, the turbine rotates as the flow passes through it, and when it is tilted, this angle of attack varies according to the azimuthal position of the turbine, depending where the free flow is impacting.

So, in other words the angle of attack is irrelevant and a quantitative comparison with an airfoil cannot be extrapolated directly to aerodynamic terms. It is only possible to speak in qualitative terms due to the similarity in both aerodynamic behaviours, reaching even C_L consistent values in the airfoil range.

In any case, this illustrates the need to define this angle of incidence (AoI), instead of using α, as a important variable of study in the model, being always higher than the conventional angle of attack.

Attending to the figure 5.2, where C_L is presented for different angle of attack, it is clear that the lift coefficient of all turbines is increasing linearly with similar slopes for all the velocities of each thickness case.

This similar behaviour is mainly due to the fact that there is no stall and $C_{L_{max}}$ is not achieved yet. As the maximum C_L is not achieved, the turbine, just like in an airfoil, has identical behaviour independently of the free stream velocity in this zone.

This no variation with the velocity is because, the main difference in lift coefficient is the delay of stall when velocity is increased, and therefore higher αs could be achieved, but in this case it is not present this maximum yet. So, for high velocities, stall conditions are supposed to appear at higher angles of attack and as a consequence $C_{L_{max}}$ is increased.

The entrance in stall is retarded for this velocities due to the reattachment of boundary layer for higher velocities, because of the presence of high energy at the flow. For low velocities, energy losses are not compensated at a early angle of attack, so lower incidences can be reached.

This is the reason of the intention of working in turbulent flows (with high velocities) instead of laminar flow, since turbulent flows are more energized and keep the boundary layer until higher angles of attack, obtaining also higher $C_{L_{max}}$ good for aerodynamic performance of the turbine.

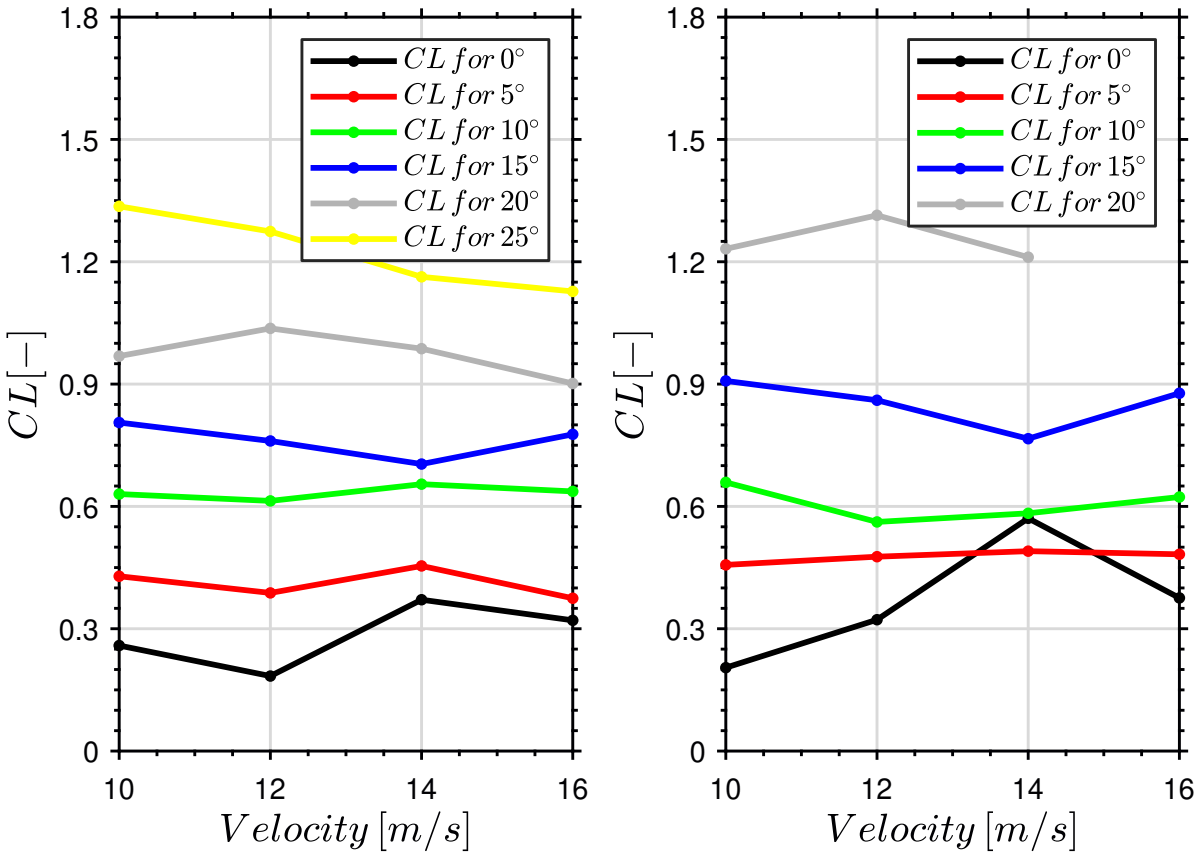

(a) Thick turbine

(b) Thin turbine

Figure 5.3: Evolution of C_L with the free stream velocity

On the other hand, the fact that there is no maximum achieved in the C_L for such high AoI may be due to the re-energization of flow due to the induced twist in the turbine. Perhaps there is no maximum as such due to the angle of attack, and the turbine works with good performance due to this fact. However, as will be seen in subsequent studies, there is a real maximum of performance of the turbine, in which the flow will impact on it without having an adequate behaviour.

A way to clarify that is to re-plot the C_L evolution in function of velocity, which is presented in figure 5.3. Observing the slope of high angles, specially in the thick turbine case, it can be seen that this slope is negative. This means that for larger angles the slope starts to decrease, so it could be said that it is approaching towards the $C_{L_{max}}$.

Attending to the thickness of the prototype used, in figure 5.2 it is seen that results for the thin turbine (5.2b) are slightly higher than the thick ones, having better performance.

This effect is particularly visible for large angles of incidence. This is best illustrated in figure 5.3. From 15-20 degrees the results for the thin turbine are higher than for the thick turbine.

The values obtained for 20 degrees of the thin turbine are even higher than those for 25 degrees of the thick turbine, so the effect of the thickness starts to be considerable for large AoI.

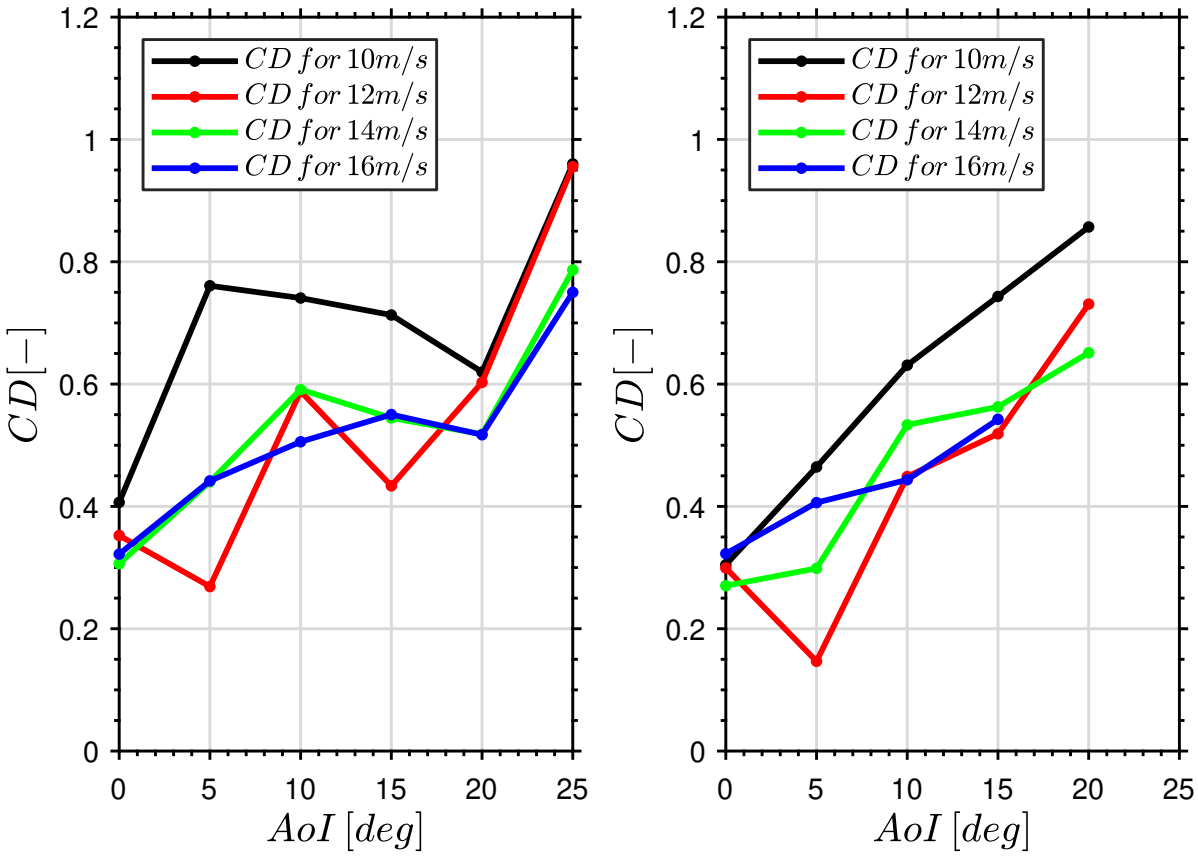

(a) Thick turbine **(b)** Thin turbine

Figure 5.4: Evolution of C_D with the angle of inclination AoI

Despite of this, thick profiles have a moderate transition to stall, in contrast, thin profiles have an abrupt drop in lift, but they achieve a higher $C_{L_{max}}$. This effect also can be seen clearly for C_D in figure 5.4.

As it is said, thickness has a very small effect and it mostly has an effect on drag. The values between both cases are similar again, but the C_D is lower for the thin case. Now the velocity has an effect, and for low speeds it can be seen that a higher drag coefficient is obtained.

Regarding angle of incidence, its evolution is always to increase with AoI, as C_L, until stall is reached, where is expected a sudden increment of drag.

Finally, aerodynamic efficiency is plotted in figure 5.5. Aerodinamic efficiency or AE consist in divide both coefficients: C_L/C_D.

It is observed that the aerodynamic efficiency increases as the angle of attack increases. For the case of the thick turbine (5.5a) a maximum is observed for 20 degrees. This is the configuration that allows optimum system performance with the least resources, as the lift to drag ratio is maximised.

In the case of thin turbine 5.5b, some very high values are observed at the beginning due to low drag. However, the evolution is always increasing with the inclination. For both turbines, similar values are obtained between 0.5 for the lowest speeds and inclinations, and up to 1.8 for the cases of 20 g and 14 m/s, where the optimum is found.

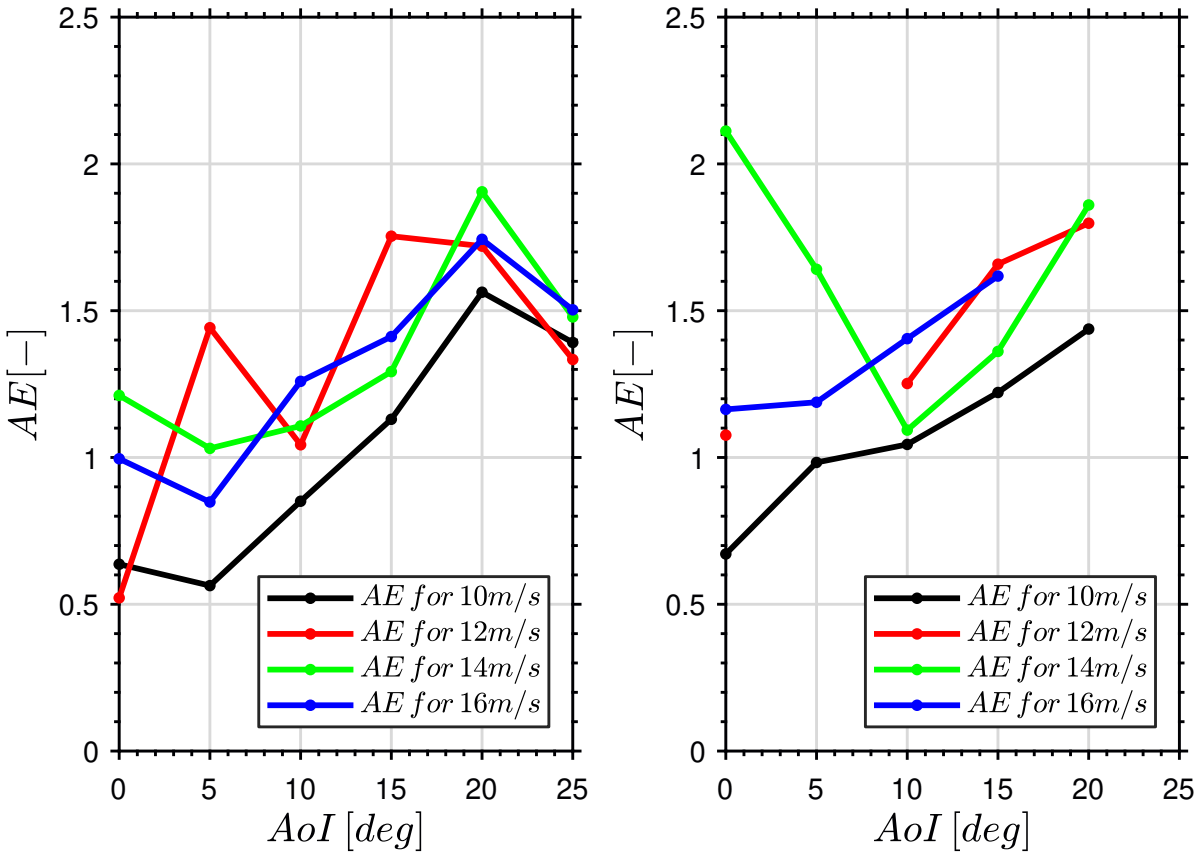

(a) Thick turbine

(b) Thin turbine

Figure 5.5: Evolution of aerodynamic efficiency with the angle of inclination *AoI*

5.1.2 Frequency evolution

The following study shows the evolution of the rotational frequency in the different cases tested. Rotational frequency plays an important role in determining the behaviour of the model, and is directly related to the angular speed (Ω) and the dimensionless Tip Speed Ratio (TSR, λ) parameter.

For now, the interesting part of working with frequency is to study the evolution of the model for a sweep of velocities and angles, and these two parameters (Ω and λ) will be dealt with in later studies.

Frequency has been obtained for each after performing a fast fourier transform of the 2000 data measured in 23.85 seconds (remember that the measuring frequency of the Arduino is 86 Hz as explained in section 4). Drag measurements are selected for the study of frequency decomposition, being very similar to the lift ones.

Once the frequency spectrum is obtained, the upper half, which is a reflection of the lower half, is discarded in order to fulfil the Nyquist theorem. In addition to this, an adequate Gaussian filter is applied in order to neglect the noise induced by the vibration of the structure. In this way the frequency content of each case can be observed.

This frequency spectrum is composed by different peaks clearly visible, which are placed in the frequencies that characterize the rotation. Normally the largest peak is the one that characterises the turning frequency, but it is accompanied by smaller distinguishable peaks that are usually harmonics of this main frequency.

In order to know the main frequency, which dominates the rotation, and the other relevant peaks, the four frequencies with the greatest weight in the spectrum are collected and plotted for each case. These are ordered from highest to lowest content, i.e. the first peak corresponds to the fundamental frequency, followed by its harmonics with the highest content. An example of this is shown in figure 5.6, where the frequency spectrum of the thick case for 5 degrees and 14 m/s is analysed (also in figure 5.7b).

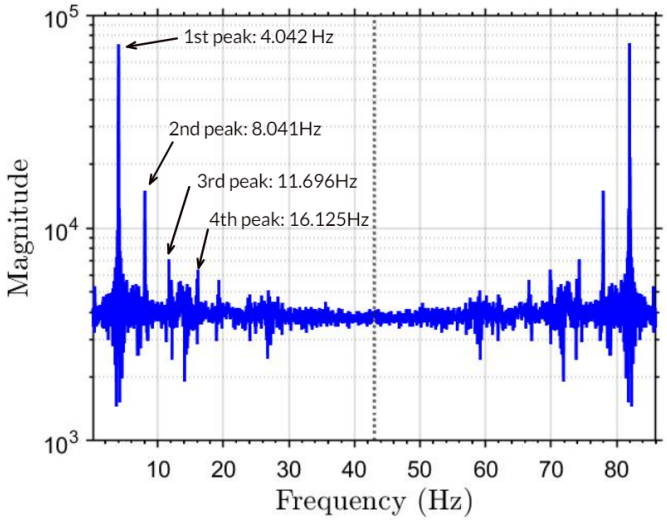

Figure 5.6: Peaks selection and sort method for thick case with 5° and 14 m/s

The results are represented as a function of the free stream velocity angle by angle. The rotation frequency of the thick turbine is plotted in figure 5.7 and thin in figure 5.8.

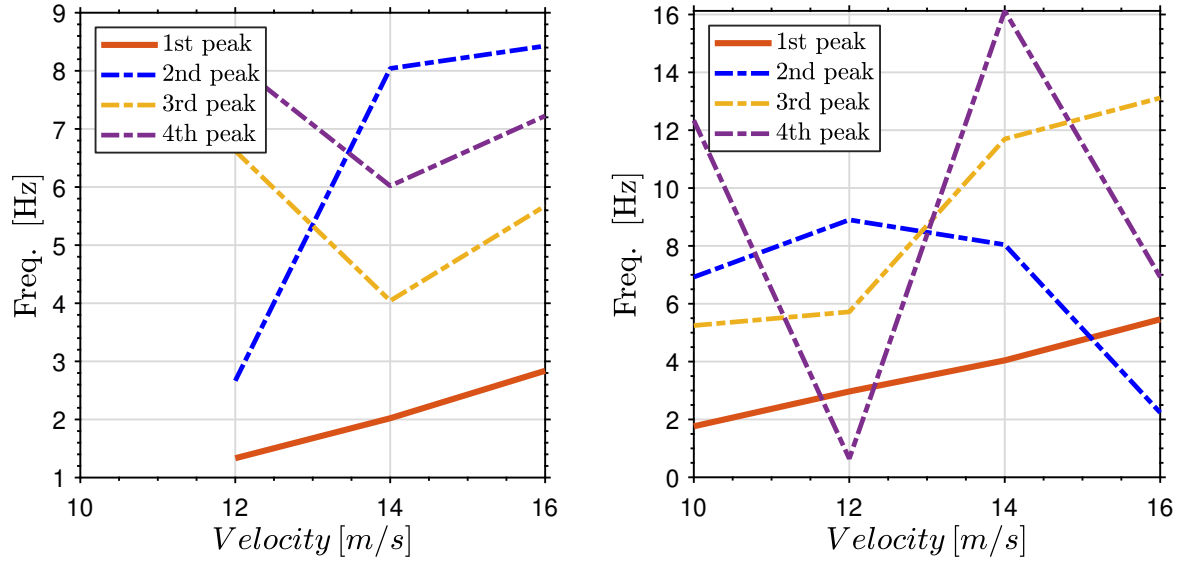

(a) 0 deg

(b) 5 deg

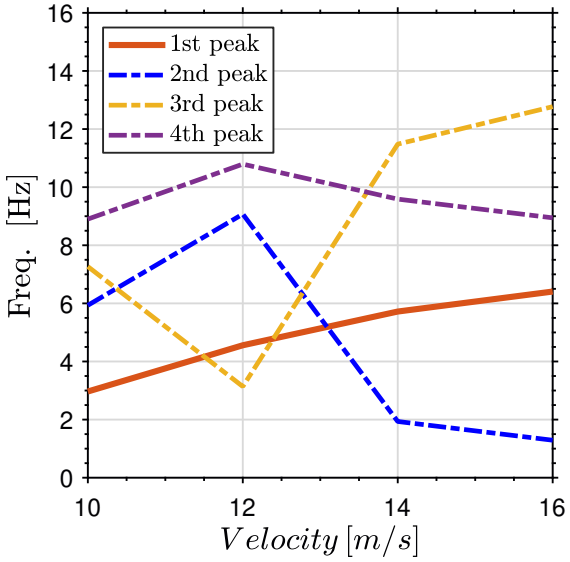

(c) 10 deg

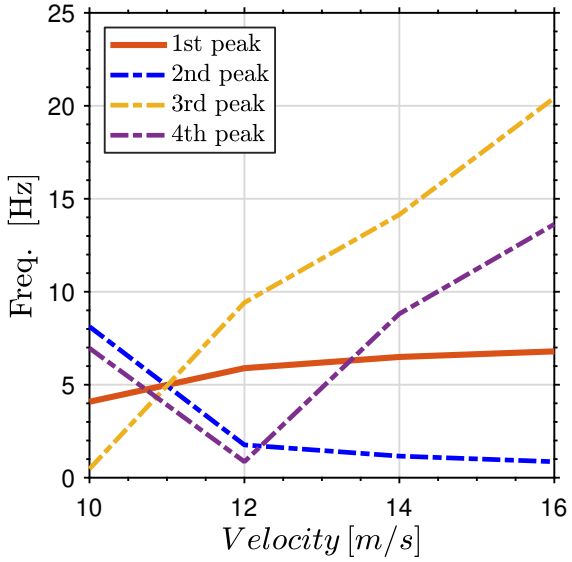

(d) 15 deg

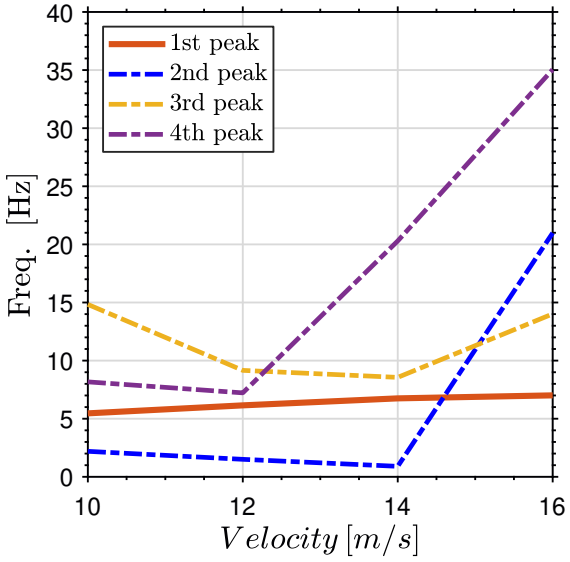

(e) 20 deg

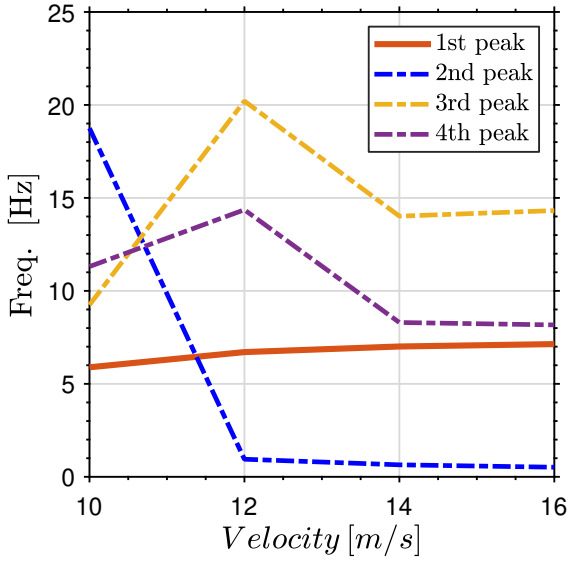

(f) 25 deg

Figure 5.7: Rotation frequency evolution with free stream flow velocity for **thick** turbine

Attending to the results in figures 5.7 and 5.8 could be seen the evolution of frequency in the turbines. As said, the main or fundamental frequency is plotted in a continuous red line and is identified as a *1st peak*. The other 3 discontinuous coloured lines are the different harmonics. As it was explained before, are grouped in terms of frequency content weight, and not by proximity, so there are line crossings.

It is not difficult to imagine that if they were grouped by harmonic families these crosses would not exist, but it has been decided to represent them in this way in order to highlight the greater or lesser importance of each one.

If the lines are observed vertically, in other words, for each flow velocity, the proportionality between one peak and another peak is observed within each case. And, in this way, it is identified that the secondary peaks (2nd, 3rd and 4th) are multiplies of the fundamental frequency (1st), and this is the reason are called harmonics.

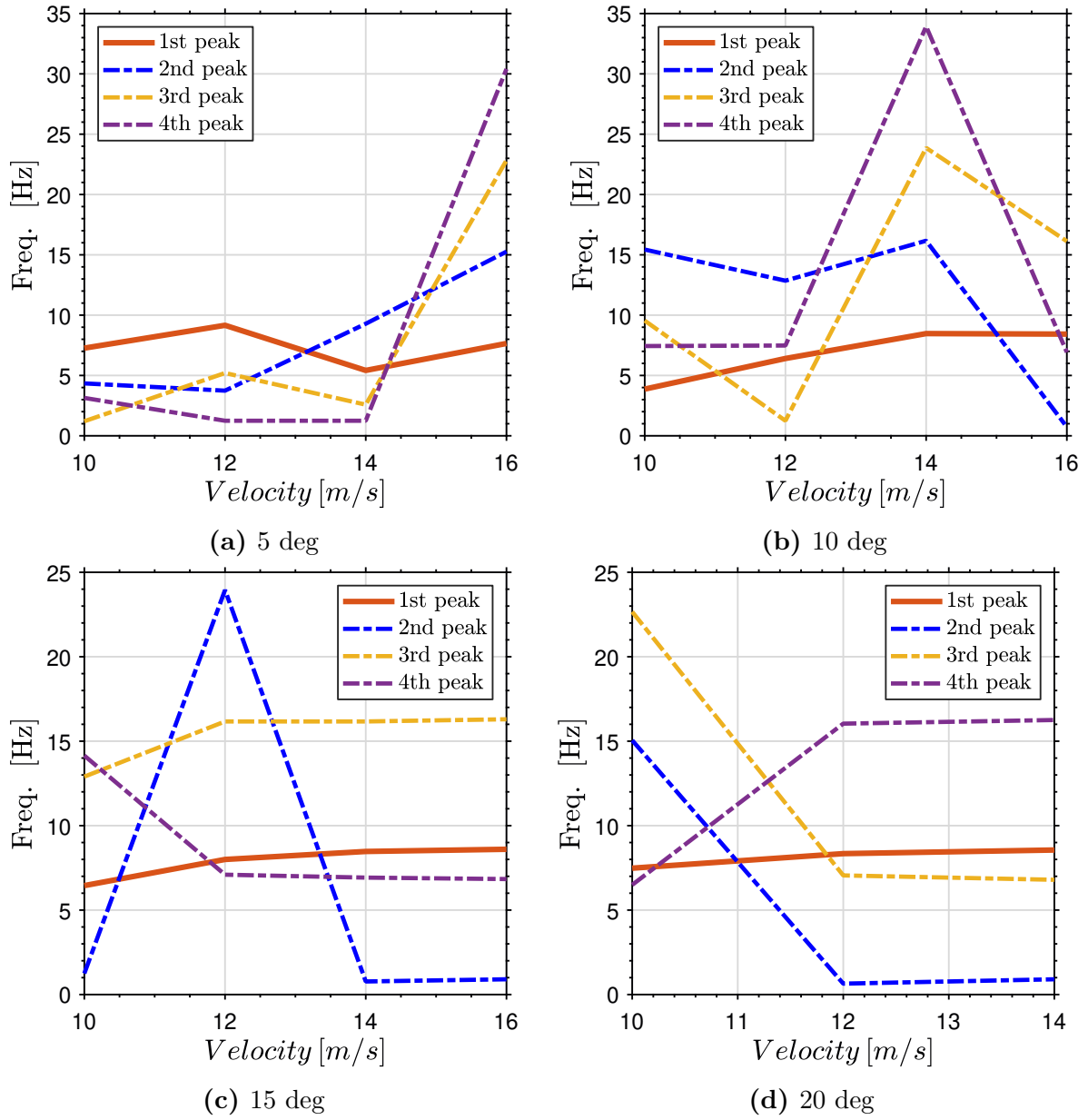

(a) 5 deg **(b)** 10 deg

(c) 15 deg **(d)** 20 deg

Figure 5.8: Rotation frequency evolution with free stream flow velocity for **thin** turbine

This is to be expected, since a system with a periodic motion, in this case the rotation of the turbine, can be kinematically characterised as complex harmonic motion, which is a superposition of simple harmonic motions. In this case, being a periodic motion, the frequencies resulting from the Fourier analysis are all rational multiples of a base frequency (1st peak), as already observed.

Regarding main frequency, the range of operation of both turbines goes from 5 to 9 Hz in a normal operation. The frequency increases with free stream velocity, and also with the angle of incidence. For low velocities this change is higher than for greater ones.

In terms of non-dimensional parameters, this range of frequencies in a 1:10 scale model tubines, will correspond within a range of operation of TSR lower than 1.

The main frequency increases with wind speed and this gives strong support to the hypothesis that this is representing the rotational frequency of the turbine.

The higher main frequencies, or the higher velocities of rotation, are obtained for high angles and flow velocities, so this means that these parameters must be further increased until they reach their limit. However, harmonic frequencies also have a strong influence on the movement and can seriously alter the system, and must also be taken into account.

The harmonics for are maximum for the configurations of 20° for the thick case, and 15° of thin turbine. From these degrees, harmonics below the main frequency start to become important.

Thus there begins to be an evolution of decreasing frequency with speed, indicating that the tendency of the movement of the structure is approaching near its maximum, starting to decrease its rotational speed.

5.1.3 Conclusions of preliminary study

This study has made it possible both to understand the limitations and needs of the problem to be studied and to begin to discover its aerodynamic behaviour.

In this way it can be considered as a preliminary analysis to consider whether the use of this novel type of turbine is aerodynamically feasible.

New characteristic parameters such as AoI have been defined, and the presence of three-dimensional effects in the flow due to the rotation of the prototype has been verified,

In addition, further precautionary safety measures are necessary to avoid the destruction of the prototype. Therefore, for the use of larger prototypes, it will be necessary to design more robust and adequate supports to withstand higher speeds and AoI.

As qualitative comparison of the C_L and C_D, the turbine performance in the angles of incidence measured leads to the conclusion that it is working before stall conditions. So, this means that it would be interesting to keep increasing the angle of inclination to see when this loss of performance occurs. This will be performed in the next studies, for this and more parameters.

This is also visible in the frequency evolution. Unfortunately, it has not been possible to carry out this preliminary study due to the aforementioned structural limitations of the support arm. However, these higher AoIs and velocities will be treated in subsequent

studies on electrical behaviour. The importance of the following studies will be greater, so this preliminary study fulfils the function of finding the needs of the main studies.

5.2 Electrical and mechanical analysis

In this section, the electrical study of the turbine at 1:3 scale will be carried out. Having seen the aerodynamic characteristics of this type of structure in facing a free stream flow, the feasibility of its main task, which is to produce electricity, will now be studied.

For this purpose, as mentioned above, a turbine model adapted to the dimensions of the laboratory's wind tunnel will be used. This 1:3 scale model has a shaft on which it rotates. The shaft is a solid metal bar and is mounted on a wooden support set on top of a metal platform with wheels used to introduce elements into the wind tunnel.

The wooden support is shaped like a rectangular box and its dimensions are similar to those of the real installation. It would contain the systems for transforming mechanical energy into electrical energy that a wind turbine has. Now, in addition to them, it also has the sensors that will acquire the data necessary for the analysis.

This support has different security stops and safety systems to prevent the model from being thrown off by the generation of lift. In addition, by means of bearings, it allows the structure to rotate freely.

A torque meter shall be connected to this shaft inside the wooden structure. Its purpose is to measure the torque generated by the rotation of the turbine. It will also measure the angular speed at which the prototype rotates.

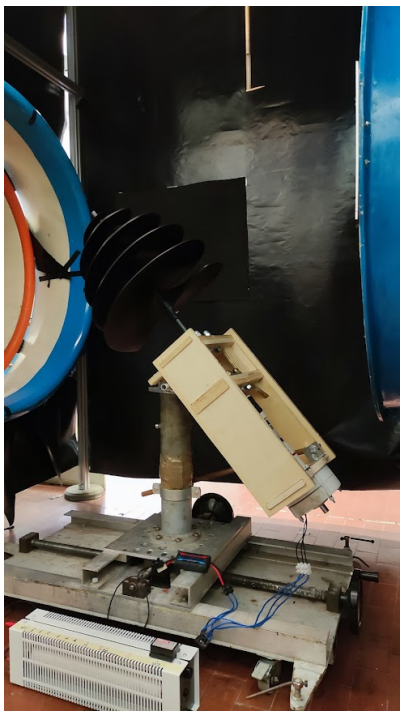

(a) General lay-out of electrical experience in the wind tunnel

(b) Inner of the wooden support box with conventional generator (white color)

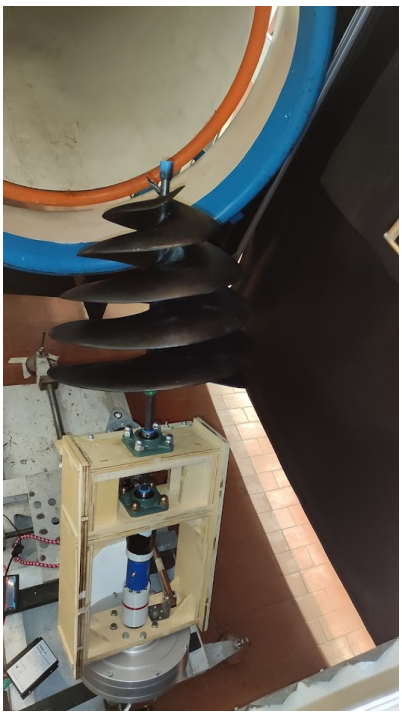

(c) Measurements with coreless stator AFPM generator of 200W (grey color)

Figure 5.9: Electrical set-up

At the bottom of the structure is the generator, which will be driven by the turbine shaft. Three different generators will be used in the different experiments. They are three-phase alternating current permanent magnet generators. Their nominal powers are 100W and 200W. Their use is recommended for low performance wind turbines, and they are on the market for this purpose.

The generator will produce an alternating current output. This is transformed by a diode rectifier circuit into direct current ready to be stored in a battery. The circuit through which the current flows has a digital wattmeter to quantify it.

Finally the electrical energy, which is to be used to charge a battery in the real system, in this case arrives at a rheostat. The rheostat is nothing more than a variable resistor. This rheostat replaces the battery in the real system and thus the resistance of the system can be varied. This device is located a bit far away from the structure because it will be varied manually for each configuration using a sliding actuator. All this configuration is schematized in figure 5.10

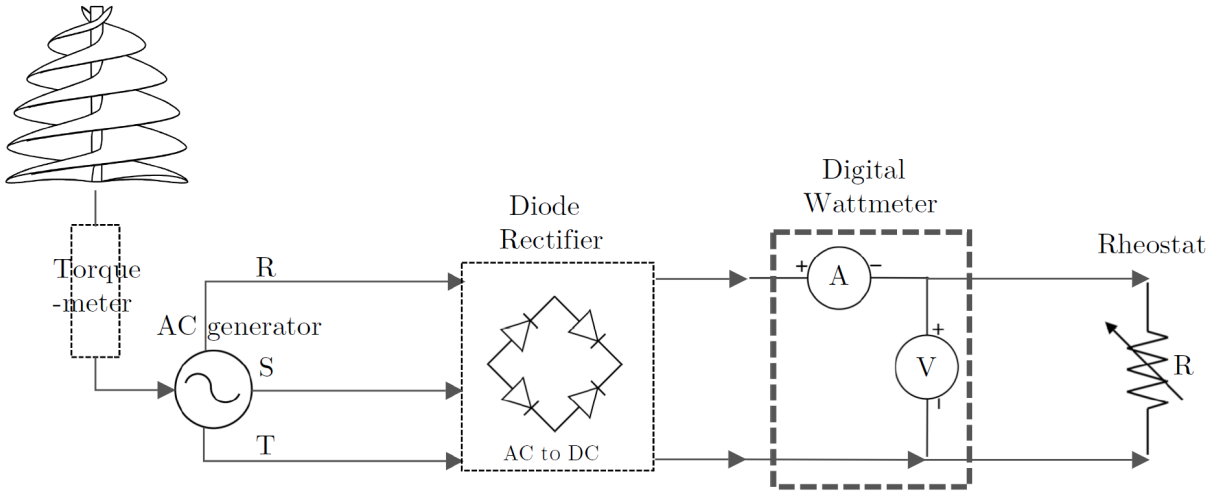

Figure 5.10: Electric diagram of the study

For this electrical experiment, the measuring process is as follows. First, the inclination of the prototype is changed with the help of the inclinometer of a mobile phone, and it is fixed by means of an auxiliary bar connected to the base of the platform. The wind tunnel is switched on and provides speed to the free stream flow. A free stream velocity is set and torque-meter and wattmeter data are taken for 3 different system resistances by varying the rheostat manually.

Once the three resistance configurations have been measured, the wind tunnel speed is increased. Once velocity measurements are finished for one AoI, the inclination of the support is adjusted again and the process is repeated once more for different angles of inclination. With all the data obtained, the graphs in this section are made for analysis.

With all this, different configurations will be made by changing the angle of incidence (10, 20, 30, 40 and 50 deg), and the flow speed (from $8m/s$ to $22m/s$) and for various values of rheostat resistance (32Ω, 20Ω and 10Ω). All this with 3 different generators: 2 conventional PM generator with 100W and 200W of nominal power and 1 coreless stator AFPM generator of 200W.

All this amount of data is processed by reading the thousands of data provided by the sensors for each instant of time, and then transforming and storing them in MatLab structs. In this way it is possible to work with them comfortably, make calculations, and obtain graphs where their characteristics can be observed.

The presentation of the graphs is organised in this section as follows. The calculated parameter is presented in a figure with 3 subfigures. Each subfigure corresponds to the 3 generators used, which from top to bottom are conventional PM generator of 100W (a), of 200W (b) and coreless stator AFPM generator of 200W (c). Inside each subfigure there are 3 graphs with the different rheostat resistances tested, from highest to lowest from left to right (32Ω, 20Ω and 10Ω).

Finally, the coloured lines represent the evolution of the variable studied for each angle. Each colour represents an angle, and this colour is maintained for all cases (as shown in the legend). In this way, a comparison is made of the evolution of the parameters for each variable. All the subfigures have the same scale on the axes to facilitate the comparison of the resistance parameter.

5.2.1 Mechanical Performance

The first parameter that is measured directly from the torque-meter is the **torque**. It quantifies the torque exerted by a motor on the power transmission shaft or, in other words, the tendency of a force to rotate an object around an axis. Since power cannot be generated without rotation, it cannot be generated without angular velocity and torque.

In a vertical axis turbine which rotates around it, this torque parameter oscillates over time. It has a periodic behaviour over time that depends on the frequency at which the structure rotates. To quantify this parameter, the amplitude of the torque evolution in time will be used for each case.

Due to the rotation of the turbine, the value of the torque-meter always oscillates between the same values. The torque amplitude is calculated by estimating the average value of the maximum and minimum obtained in the sinusoidal oscillation and obtaining the difference between them.

This torque amplitude in many other studies is called “torque ripple”. Torque ripple is an effect seen in many electric motor designs, referring to a periodic increase or decrease in torque as the motor shaft rotates. It is measured as the difference in maximum and minimum torque over one complete revolution. In this case not only one revolution is taken but all revolutions, whose values are similar, are taken as the average.

In general terms, as can be seen in figure 5.11, torque amplitude values within a similar range are obtained for each generator. Comparing the three engines used, it can be seen that the torque value is similar between them, being around 0.8 and 1 Nm for almost all cases.

The main differences appear in the conventional PM generator of 200W (5.11b), where for high speeds this torque amplitude increases. For high resistive values (32 and 20Ω) there is an increase in torque at high speeds for high angles of incidence, particularly for 30 and 40 degrees with values above even 1.2Nm. The values in the case of 10Ω are more contained. This is because the system rotates less easily as the resistance is lowered.

Torque amplitude

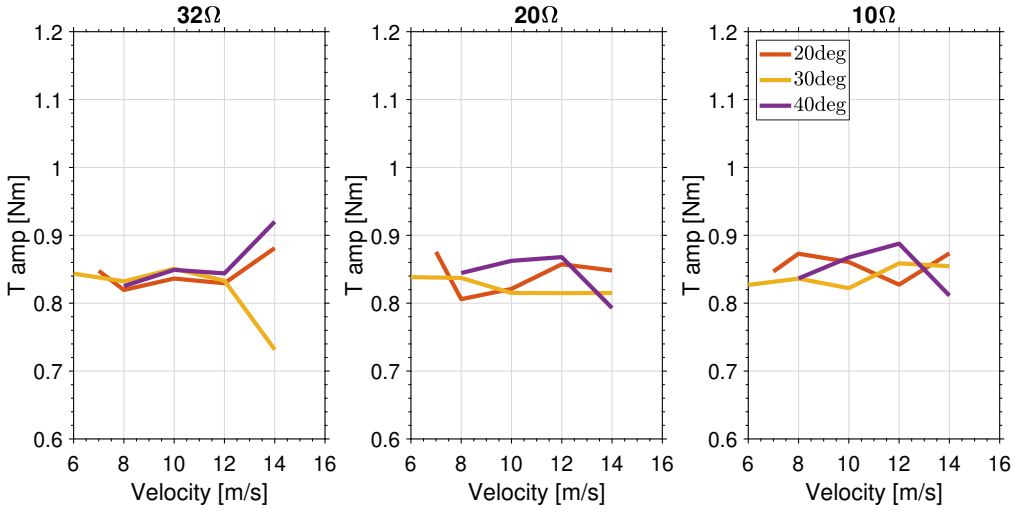

(a) Conventional PM generator of 100W

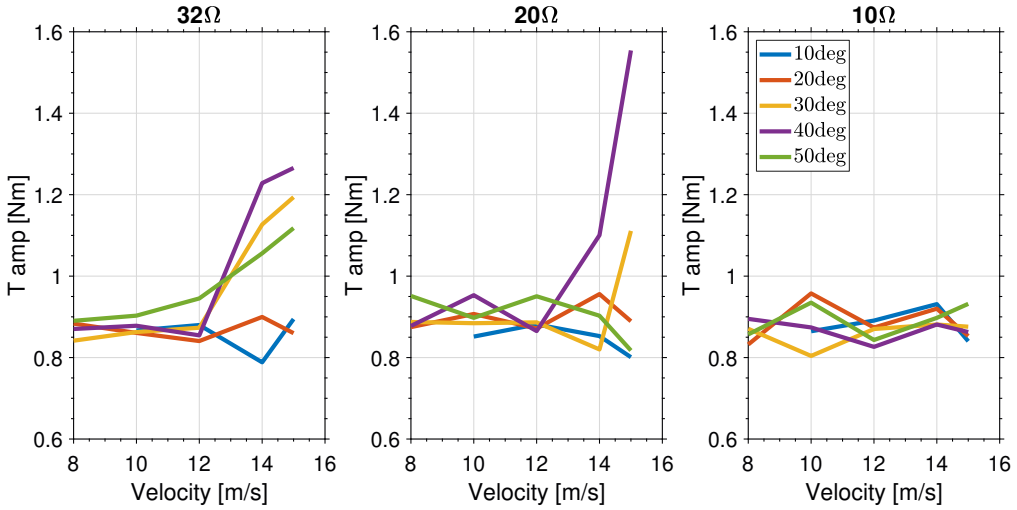

(b) Conventional PM generator of 200W

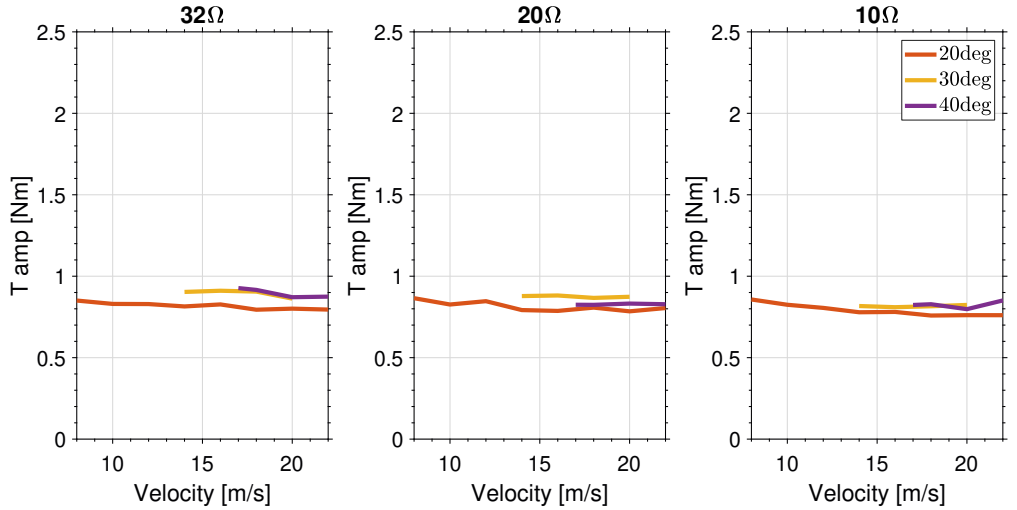

(c) Coreless stator AFPM generator of 200W

Figure 5.11: Maximum torque achieved, evolution with freestream velocity

Frequency and Angular velocity (Ω)

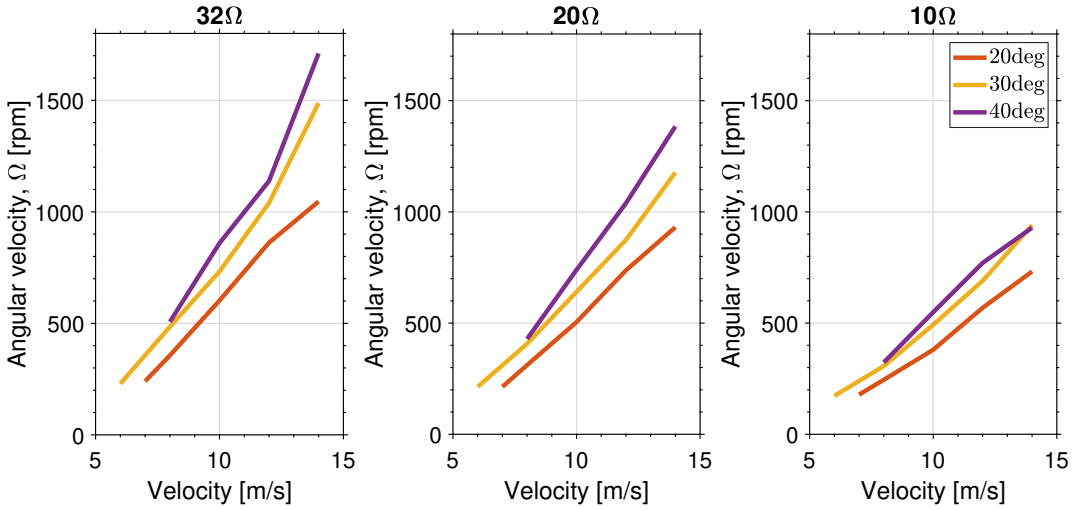

(a) Conventional PM generator of 100W

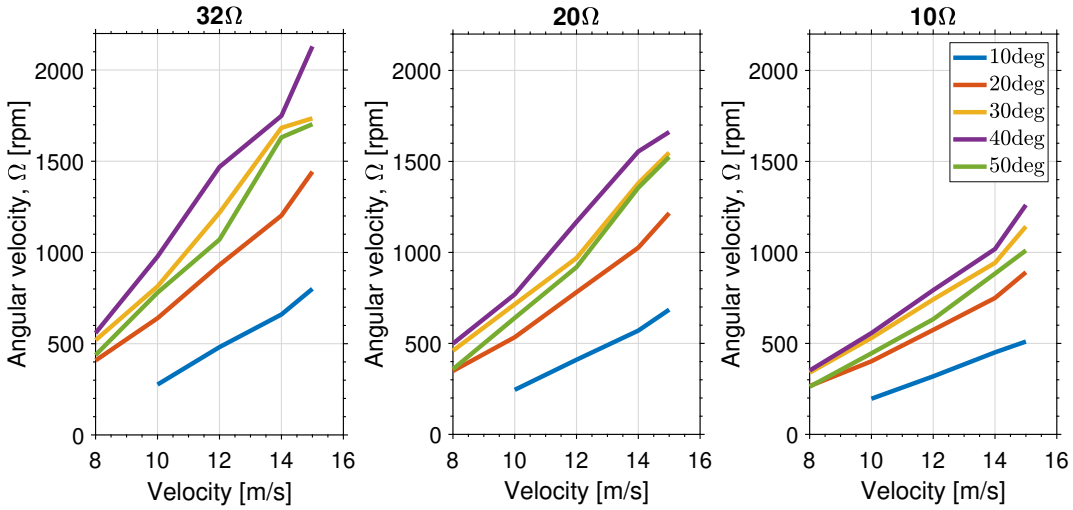

(b) Conventional PM generator of 200W

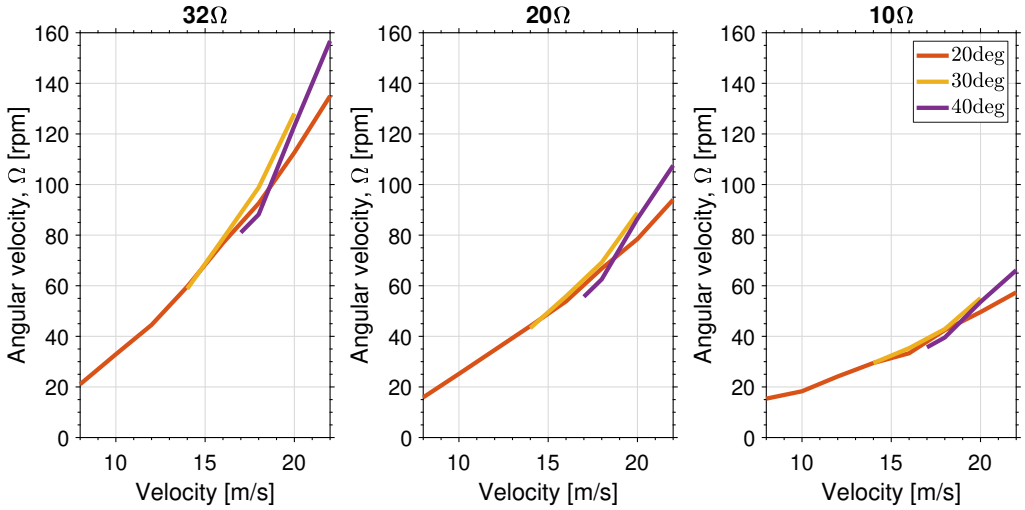

(c) Coreless stator AFPM generator of 200W

Figure 5.12: Angular velocity

Using the torque meter measurements, the rotational frequency characteristic of the structure can be easily derived. With this characteristic frequency the **angular velocity** is calculated. In this case they are presented in the form of angular velocity, which is a more convenient way than in terms of frequency. Figure 5.12 shows the angular velocity in units of revolutions per minute as a function of speed. The evolution of the angular velocity is directly related to the rotational speed.

It is clear that the angular velocity has different values for each engine. The generator with the highest rotational speed is the 200W conventional PM generator (5.12b). It is closely followed by the 100W analogue generator (5.12a).

However, the AFPM coreless stator generator obtains rpm results that are 1 order lower than those of conventional generators. In the wind tunnel experience it was observed that with this generator the rotation of the RoDaVi was not excessive for any of the speeds, and for this reason it was decided to test even higher speeds, up to 22m/s as seen in 5.12c. Even so, although it generated an average torque similar to the other generators, and even a slightly higher maximum torque, the resistance of the generator to the rotation of the shaft is enormous, and the angular velocity reached is so poor.

Therefore, everything seems to indicate that this AFPM coreless stator generator is not very suitable for this study. This fact will also become visible in the mechanical power calculation as well as in the electrical power generation.

Now, the evolution of one of the most important parameters of the study, **mechanical power**, will be discussed. Its evolution is represented in figures 5.13.

As explained in section 3.1, the calculation of the mechanical power generated by the rotation of the shaft of the structure is calculated by multiplying the torque generated by the angular velocity ($P = T \cdot \Omega$). In this way, the objective is to obtain the maximum mechanical power given by the system to the generator for its subsequent transformation into electrical power.

Figures 5.13 shows the results of the mechanical power in W for the 3 generators for the 3 resistances measured. The 200W conventional PM generator presents the best performance, followed by the 100W generator, and finally the AFPM coreless stator generator presents very low mechanical power values, so its performance is not good in comparison with the other 2.

The total maximum values reached by the 200W conventional generator are above 250W (for 32 and 20Ω), while those of the 100W generator exceed 150W (32Ω). Let's remember that the name or label of these generators is given by their nominal power, also called rated power (200W and 100W). This rated power is what the generator demands under normal conditions of use to provide optimum performance, which means that the appliance is designed to withstand that amount of power during long periods of work.

However, the real or actual power may differ from the nominal power, being lower or even higher. Likewise, the generator has also a maximum power rating, which refers to the maximum load it can withstand with a continuous use of 20 minutes.

Looking for the characteristics of the generators at both datasheets of the manufacturer, presented in section 4.3, it can be seen that for both generators the maximum power is exceeded in some cases. So special care must be taken in these situations in order not to

damage them. Even if it is intended to work intensively in the range where it is exceeded, it would be advisable to change the engine for a superior model with a higher rated power.

In any case, in both conventional generators, the optimum cases are those with a high speed, with a high angle of inclination, for high resistances.

In terms of the variation of the resistance by using the rheostat, for both generators, higher values are reached when the resistances are high, in the cases of 32Ω and 20Ω. While the values of 10Ω are always below the nominal power.

In terms of free flow speed, the trend of the mechanical power is always increasing. The more the free stream flow accelerates, the more energy is extracted, and as with the angular velocity, the mechanical power increases.

This growth tendency is greater for higher angles of inclination. For AoI of 10 and 20 degrees, the growth is lower than for higher angles, which even reach a cudruplication of the generated power. The optimum case for both engines corresponds to the 40 degrees AoI for all cases. This is followed by the 30 degree case, and close behind is the 50-degree case. The difference of having a moderate or high pitch at high speeds can be 3 or even 4 times higher, so it is a very important factor.

Therefore better mechanical power values are obtained with high AoI, high speeds, and higher resistances.

Mechanical power (P[W])

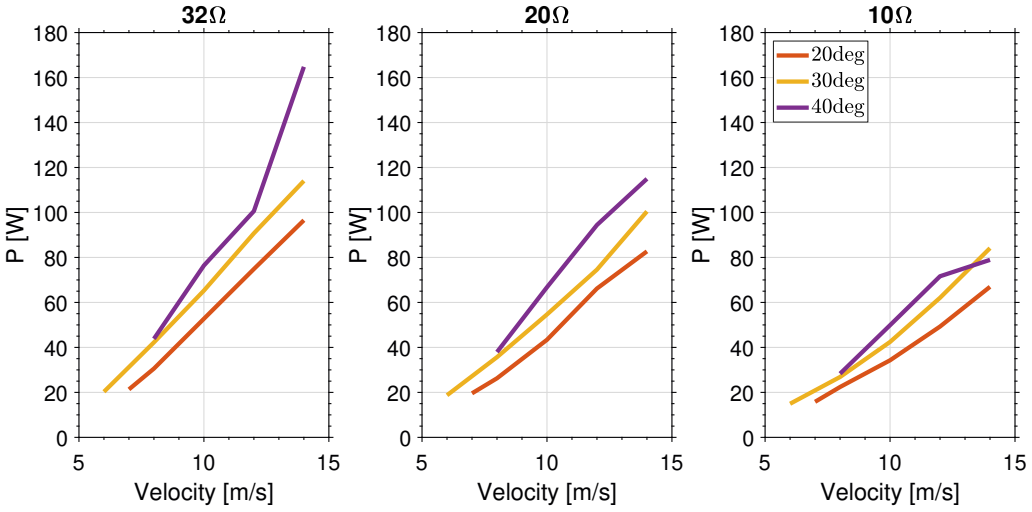

(a) Conventional PM generator of 100W

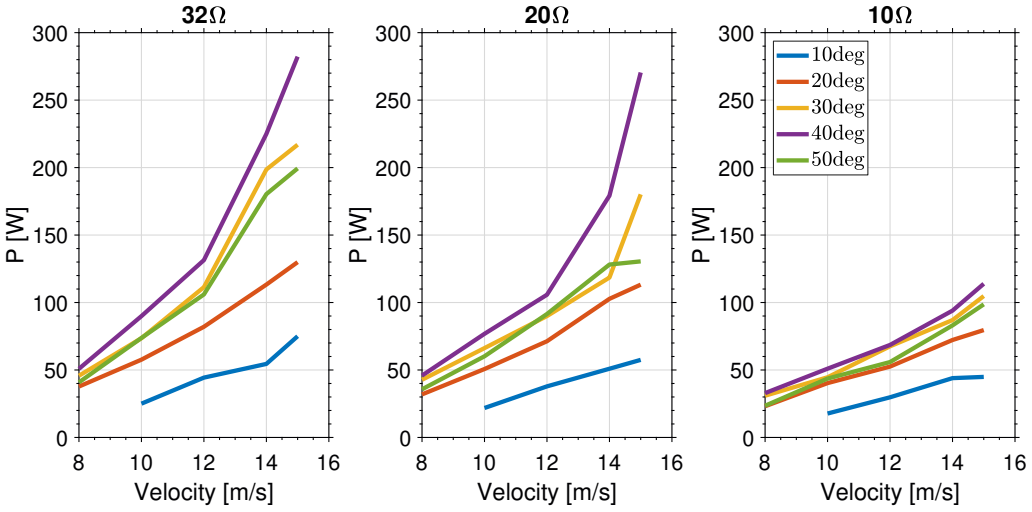

(b) Conventional PM generator of 200W

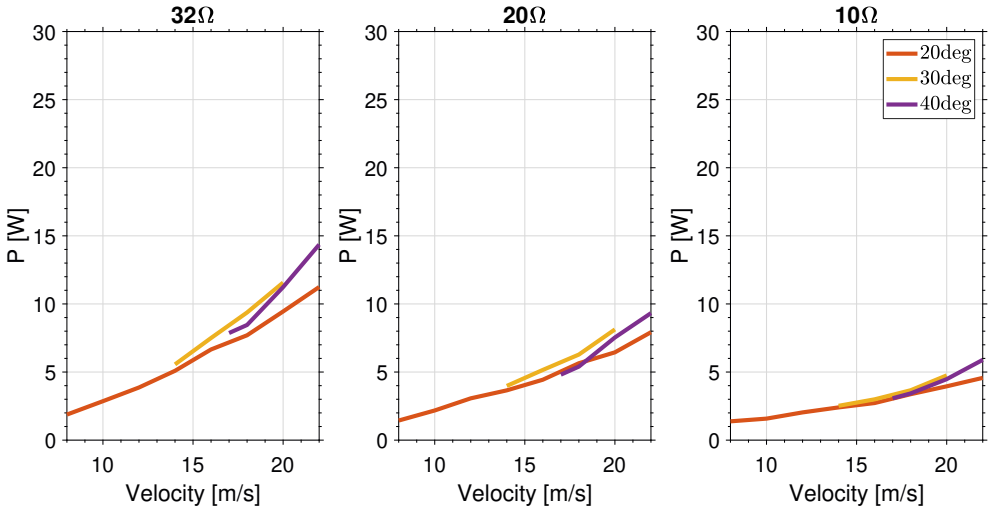

(c) Coreless stator AFPM generator of 200W

Figure 5.13: P evolution with velocity

Tip Speed Ratio (λ)

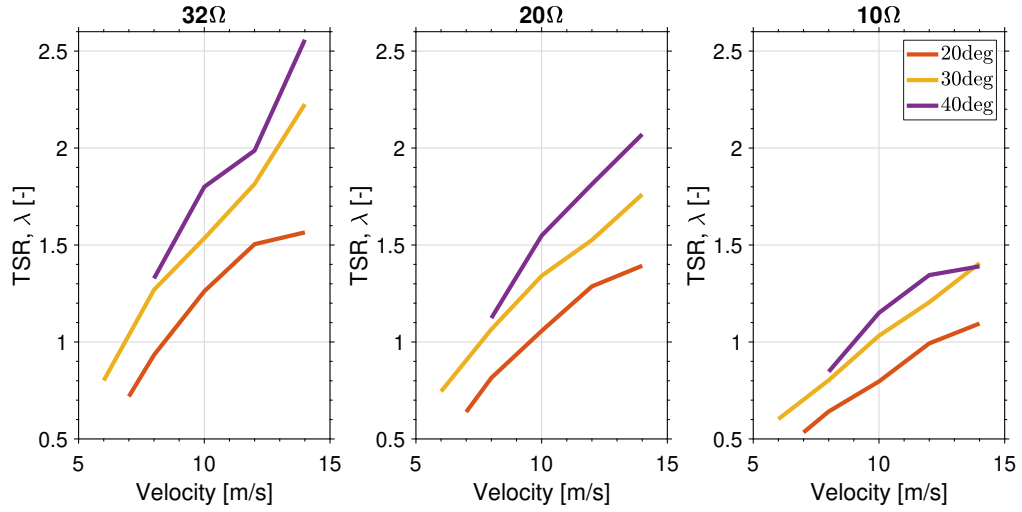

(a) Conventional PM generator of 100W

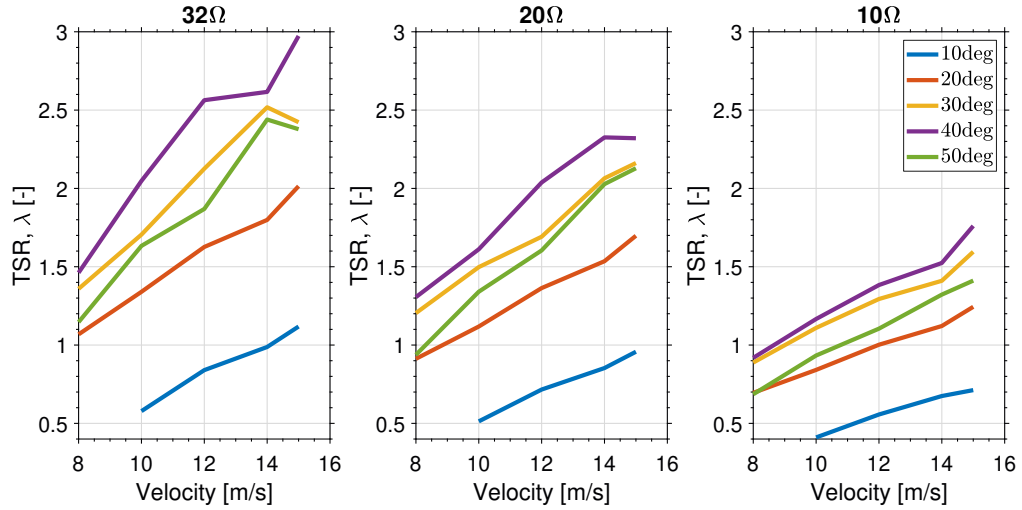

(b) Conventional PM generator of 200W

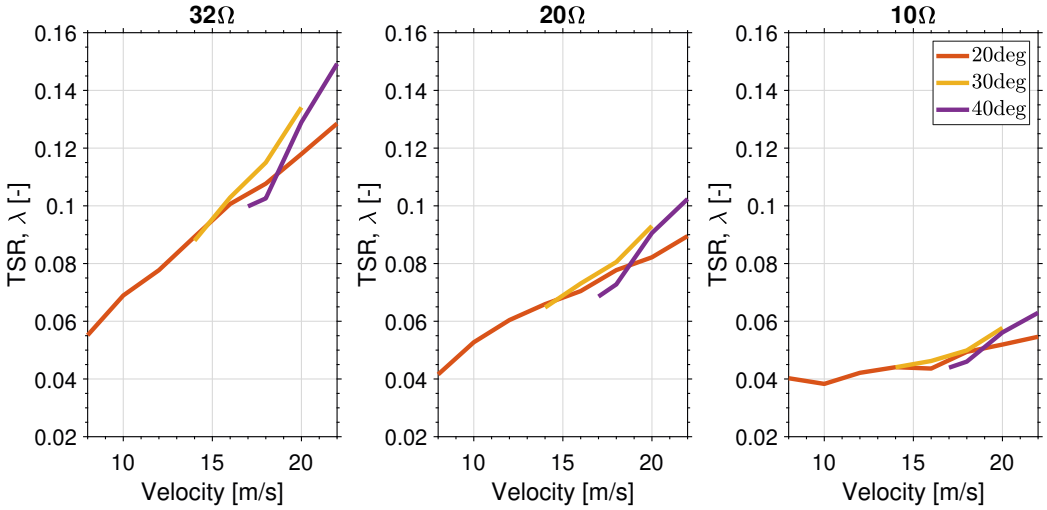

(c) Coreless stator AFPM generator of 200W

Figure 5.14: Tip Speed Ratio evolution with velocity

A characteristic parameter used to classify and compare wind turbines is the **Tip Speed Ratio**, TSR or λ. It is the ratio between the tangential velocity at the blade tip and the free flow velocity, as already discussed in section 3.1.

This non-dimensional parameter will be useful to determine the range of operation of a turbine. In this way, turbines with similar TSR can be compared.

The values in which RoDaVi TSR oscillates with the different engines are between 0.5 and 3. These are typical values for Savonius turbines, American type windmills, Dutch windmills and even Darreius turbines at low speeds. This comparison will be done in the next section 5.2.2 considering also the electrical performance.

A way to compare the better or worst performance of a wind turbine is using C_P parameter. It is very common to find comparisons of turbines of very different construction using a C_P vs TSR graph.

So, the final objective is the calculation of the C_P together with TSR parameter in order to confront them in a graph for comparison with different types of existing turbines. These graphs are presented in next section 5.2.2, at figure 5.17.

After all, the basis of this analysis is whether the turbine can compete under electrical conditions with similar existing models. Thus, the following subsection continues with the electrical power analysis.

5.2.2 Electrical performance

The same way that the torsio-meter is the main sensor in responsible for measuring the mechanical parameters derived from the rotation of the structure connected to a generator, now a wattmeter will make it possible to quantify the electrical current generated thanks to the transformation that takes place inside the engine.

This means that the electrical power coming out of the generator and used to charge the batteries (in this case represented by a rheostat) will now be measured and presented in graphs. Recall that the electrical circuit was presented in figure 5.10. The power generated will determine whether the wind turbine prototype is able to extract enough mechanical energy from the air to be transformed into electrical energy suitable for storage in batteries and consumption.

The first parameter to be measured is the **electrical power**. The wattmeter is placed at the generator output, after the current rectifier. Its display shows the voltage, current and power values. The power values are shown in figure 5.15.

The highest electrical power values are obtained with the conventional 200W PM generator, followed by the 100W generator and finally the worst results are obtained with the coreless stator AFPM generator. In the latter, very high speed values must be reached in order to achieve power values comparable with the other two conventional generators.

Regarding the development with speed, it is important to pay attention to the start of the power measurement. The wattmeter has a threshold power at which it starts measuring. This is a quite low threshold power, but it must be taken into account because there are cases where high speeds must be reached in order to be able to measure.

This is notably observed in the case of the coreless stator motor (5.15c), where it does not start to produce a minimum power output until a speed of 16m/s is reached. In contrast, the other two generators start to produce power from low speeds such as 8m/s, which makes their operating range much wider.

This power generation threshold also depends on the inclination of the structure. It is clearly observed that for the 10deg cases the start of power measurement is very delayed, and that the values obtained are very low.

In the same way as for mechanical power, the optimal cases with the best electrical power results are those with high AoI. The optimum case is again 40 degrees of inclination, followed by 30deg and very close to that of 50deg. Therefore, an optimum of both mechanical and electrical performance is reached at 40 degrees.

Speed also has an influence, as electrical power increases with speed, and with an even greater gradient than mechanical power. With a difference of only 5m/s it is possible to go from 2W to 20W of power as shown in figure 5.15b. It is therefore advisable to work at high wind speeds in order to maximize the electrical power.

Finally, the resistance of the battery, which is replaced by the rheostat, plays an important role in the behaviour of the electrical system. Measurements start with a high resistance of 32Ω, decreasing to 20Ω and 10Ω. At high resistance, a higher voltage is produced than at lower resistances, but the current generated is small. By contrast, as the resistance is decreased, the voltage decreases, but the current increases.

Electrical Power

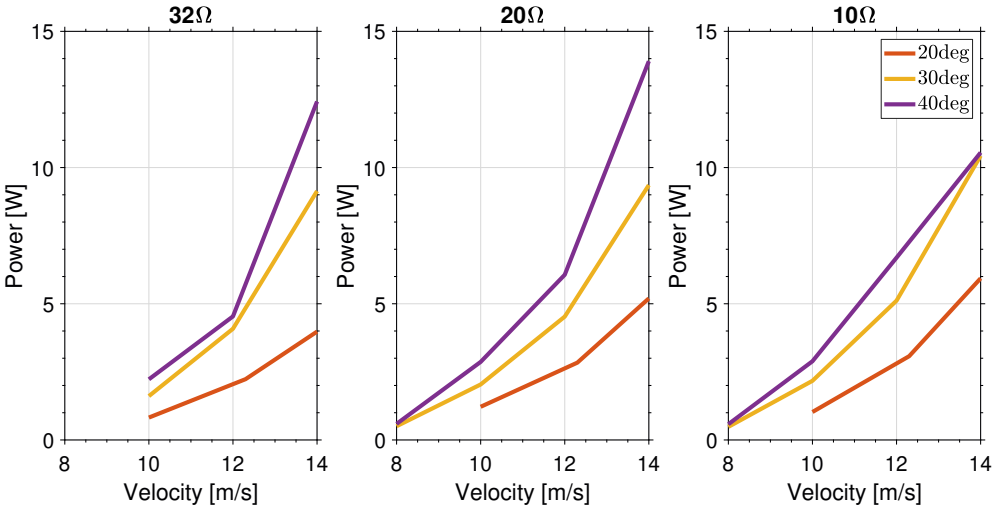

(a) Conventional PM generator of 100W

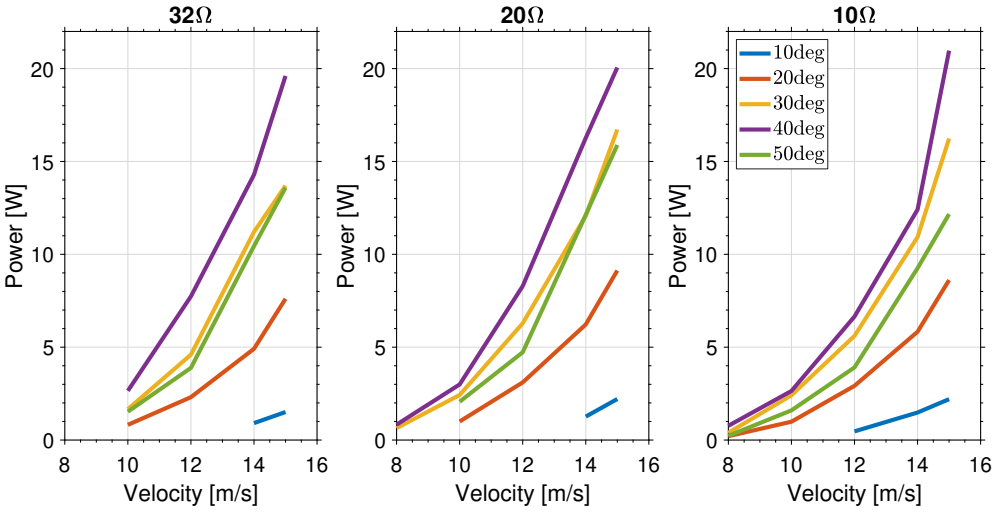

(b) Conventional PM generator of 200W

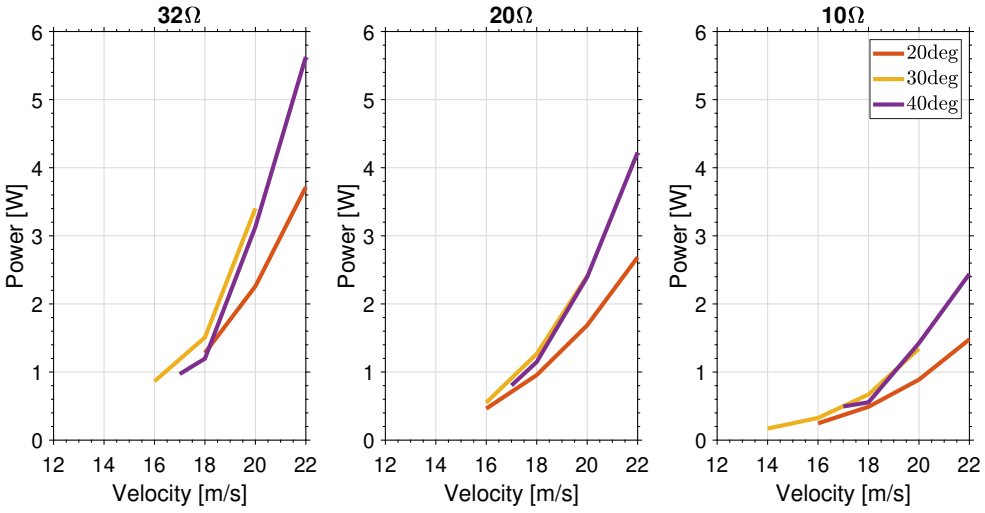

(c) Coreless stator AFPM generator of 200W

Figure 5.15: Measured electrical power evolution with velocity

The power depends on both terms directly ($P_{elec} = V \cdot I$), so a compromise must be found between them. It is not advisable for the current to obtain very small values, because even if the voltage is considerable, the resulting power will be lower.

It is for this reason that in the cases with 20 and 10Ω resistors, higher power values are obtained, since although the voltage produced is slightly lower than in the case of high resistance, the current generated is higher and compensates for this effect.

Due to all this, the configuration in which the greatest electrical power is obtained is with 40 degrees, with a high free stream velocity and a medium electrical circuit resistance, that can maximise the trade-off between voltage and current to achieve the highest possible electrical power.

As it has been introduced previously, another characteristic parameter for the classification of wind turbines is the **power coefficient** or C_P. The power coefficient is a dimensionless parameter used to compare different types of conventional turbines and represents the ratio between the power extracted and the power available in the wind. Its origin and expression have been explained in section 3.1, where Betz's theory was presented.

For its calculation in this subsection, its classical definition is used as set out in equation 3.14. This is the simplest expression to calculate the C_P over a rotor without thickness and with an infinite number of blades (among other configurations).

For each different model of wind turbine, depending on factors such as the number of blades, the pitch angle of the blades, the surface area facing the wind, the tip speed ratio, or the angular speed of the rotor, a analytical expression of C_P can be calculated directly without the necessity to measure the electrical power. However, this is a preliminary study and therefore it is necessary doing all the measurements of the electrical power extracted, and the results obtained are shown in figure 5.16.

As C_P depends directly on the electrical power, so the highest values are found for higher angles and incidence, being the optimal performance at 40 degrees for all the cases studied.

It is observed that the higher the speed, the higher the C_P for all cases as well. However, as the TSR parameter has been calculated by mechanical analysis, this speed dependence will be discussed later.

As for the influence of the circuit resistance, larger C_P values are obtained for the case of 20Ω followed by 32Ω, so it is a trend analogous to that of the electrical power. In a certain way this is to be expected as the coefficient is directly dependent on it.

In terms of values, the two conventional generators perform best. Both are between C_P of 0.02 for low inclination and speed, and 0.12 in the most optimal cases mentioned above. The coreless stator is not a competitor for these motors, offering a C_P of very low values that do not reach 0.01.

The values of C_P at which the Savonius turbine operates are around 0 to 0.15, so that the two conventional generators offer similar performance.

A comparison in terms of electrical power with a similar vertical axis engine, such as the Savonius wind turbine, will be carried out later on. In this way it will be possible to check whether or not the RoDaVi prototype improves on the performance of existing prototypes already in use on the market.

Power coefficient (C_P)

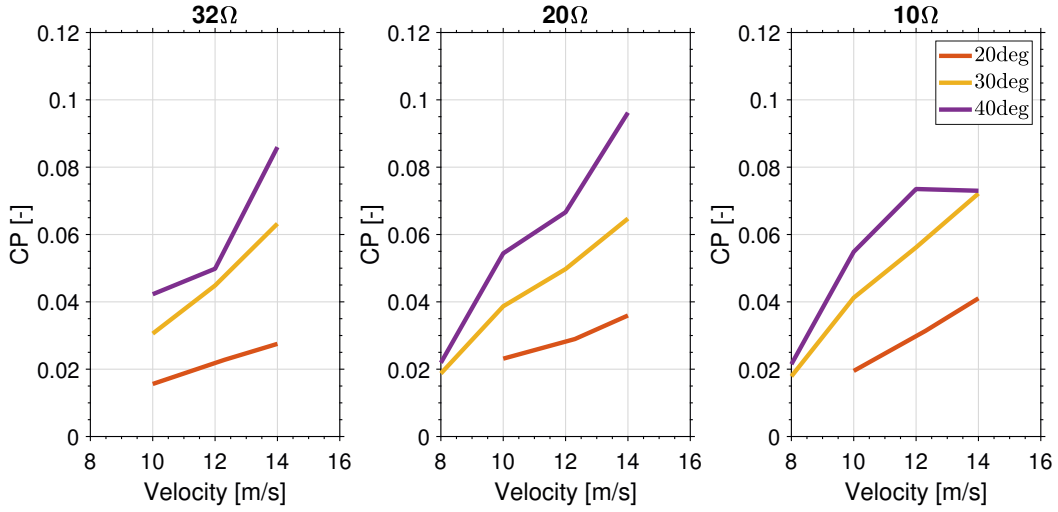

(a) Conventional PM generator of 100W

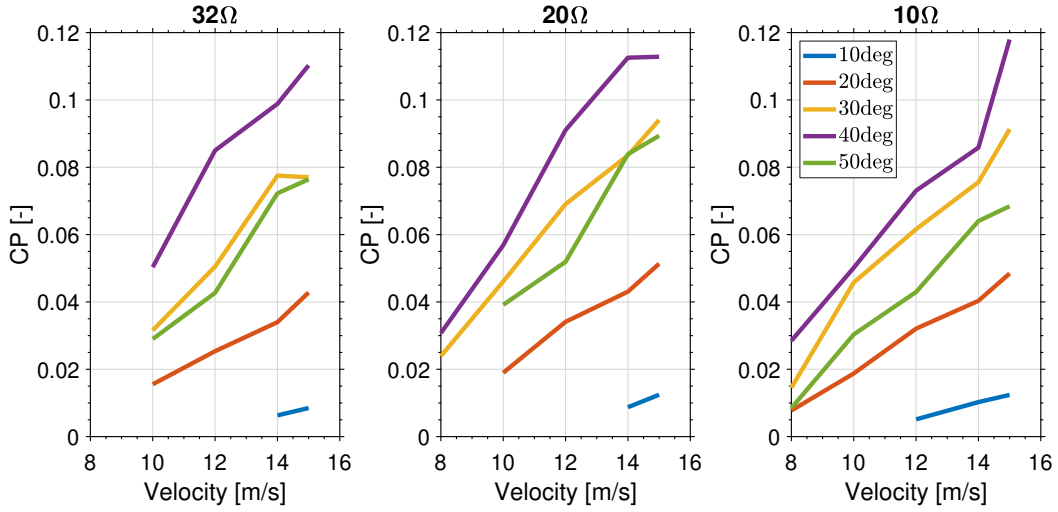

(b) Conventional PM generator of 200W

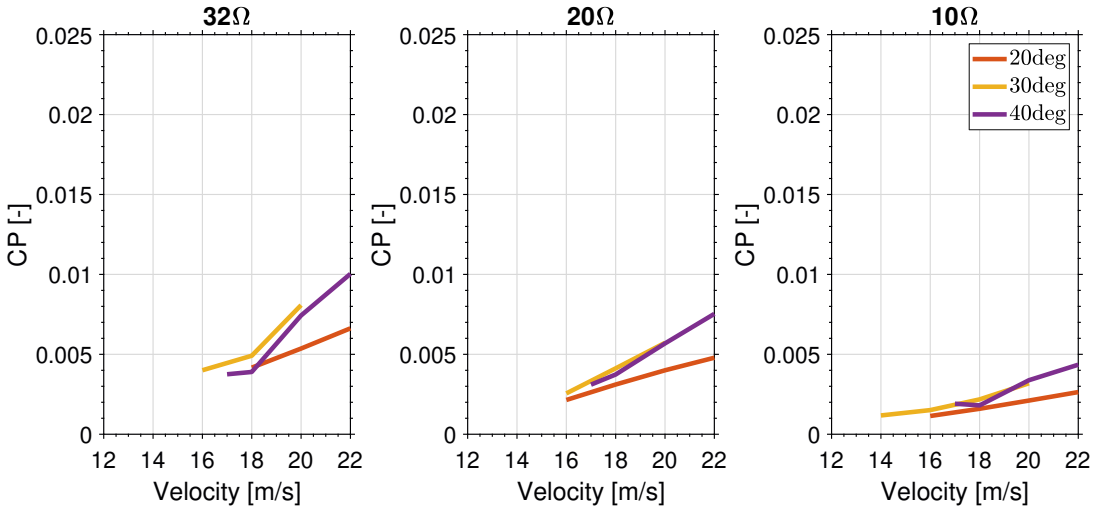

(c) Coreless stator AFPM generator of 200W

Figure 5.16: CP evolution with velocity

CP-TSR Relation

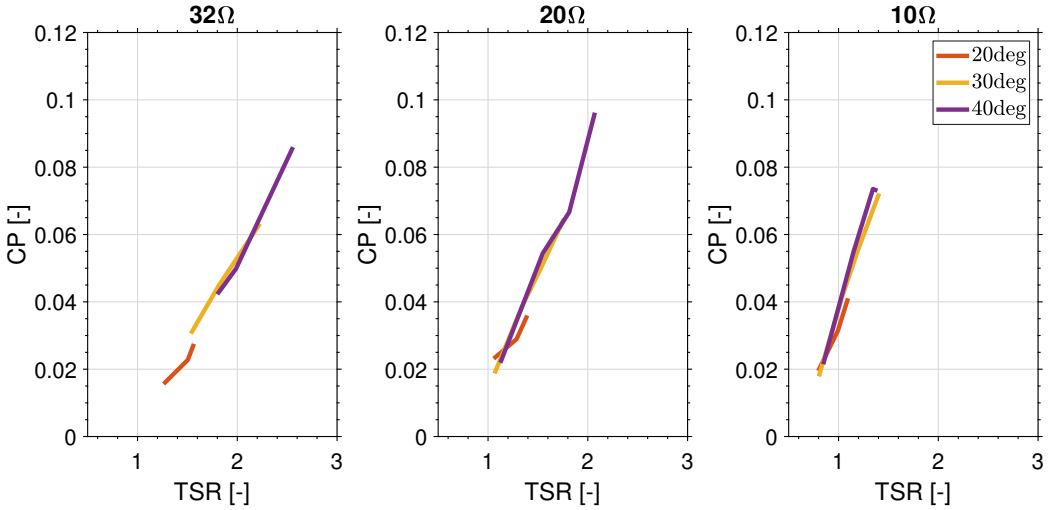

(a) Conventional PM generator of 100W

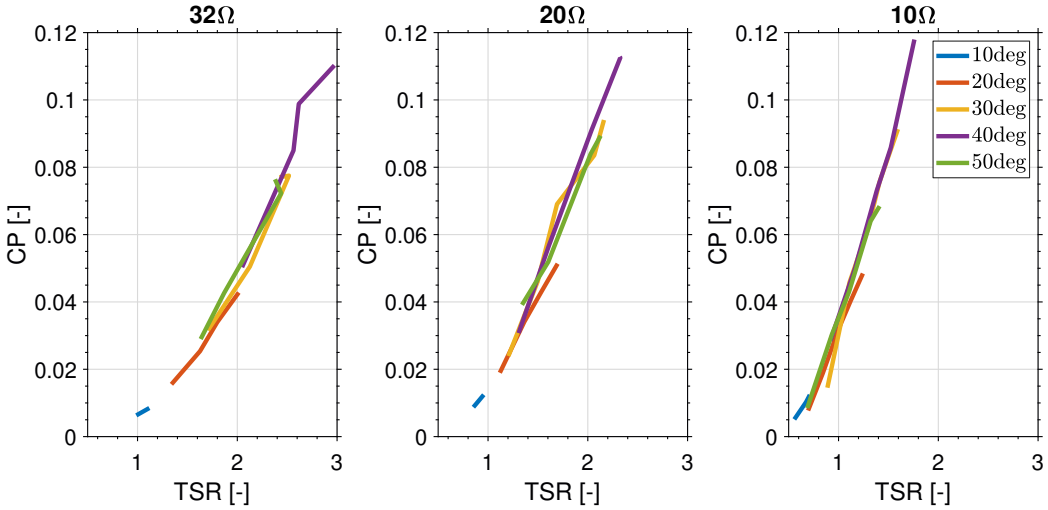

(b) Conventional PM generator of 200W

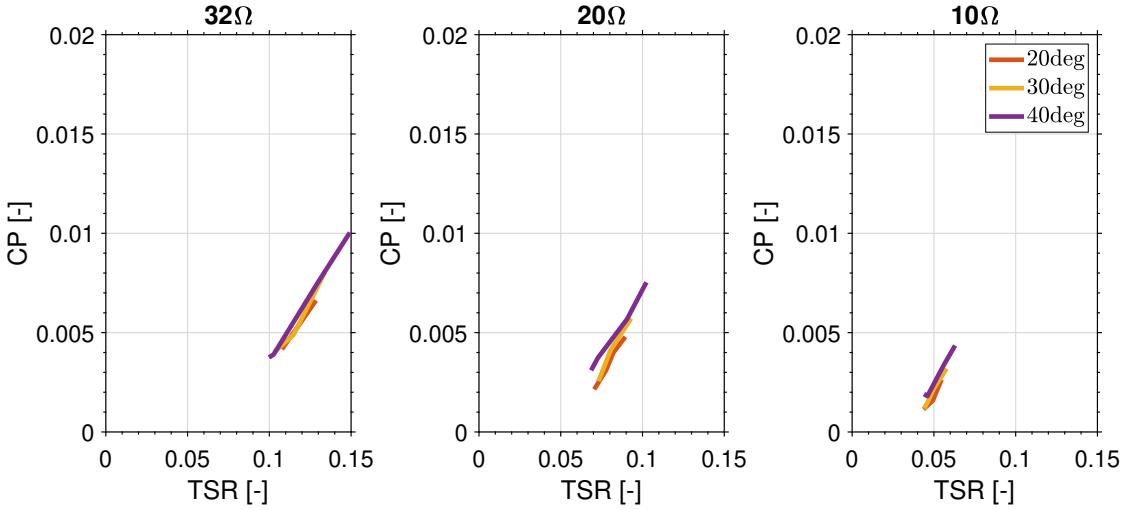

(c) Coreless stator AFPM generator of 200W

Figure 5.17: CP-TSR evolution

Now it is the turn to present the usual relationship between the two dimensionless parameters obtained from the study. This is the **relationship between the power coefficient (C_P) and the Tip Speed Ratio (TSR, λ)**. This will allow to fully characterise the behaviour of the turbine, and to compare it with existing models.

The results are presented in graphs 5.17. As mentioned above, this ratio of parameters makes it possible to characterize the general behaviour of the turbine. This is why it serves to situate the operating range of the turbine and the comparison with other models.

The dimensional dependence of the speed disappears. It can be seen that all cases with different angles fall on the same line which represents the behaviour of the system. With the relationship of C_P with the velocity, different behaviour lines were presented for each degree, but now they fall on the same one.

In essence, this complete curve of all possible operating cases of the model has the form of a concave parabola. In this way, at its maximum, the best performance of the turbine can be identified, where the $C_{P,max}$ and λ_{max} are found.

In the graphs shown, this maximum does not yet appear, so different configurations with the objective of increasing the TSR until reach a decreasing trend of the C_P must been done in order to find the maximum.

Nevertheless, the values reached for conventional engines in figures 5.17a and 5.17b are similar to or even higher than those of the Savonius turbine. Figure 5.18 shows the CP vs TSR graph for this turbine and many others for comparison.

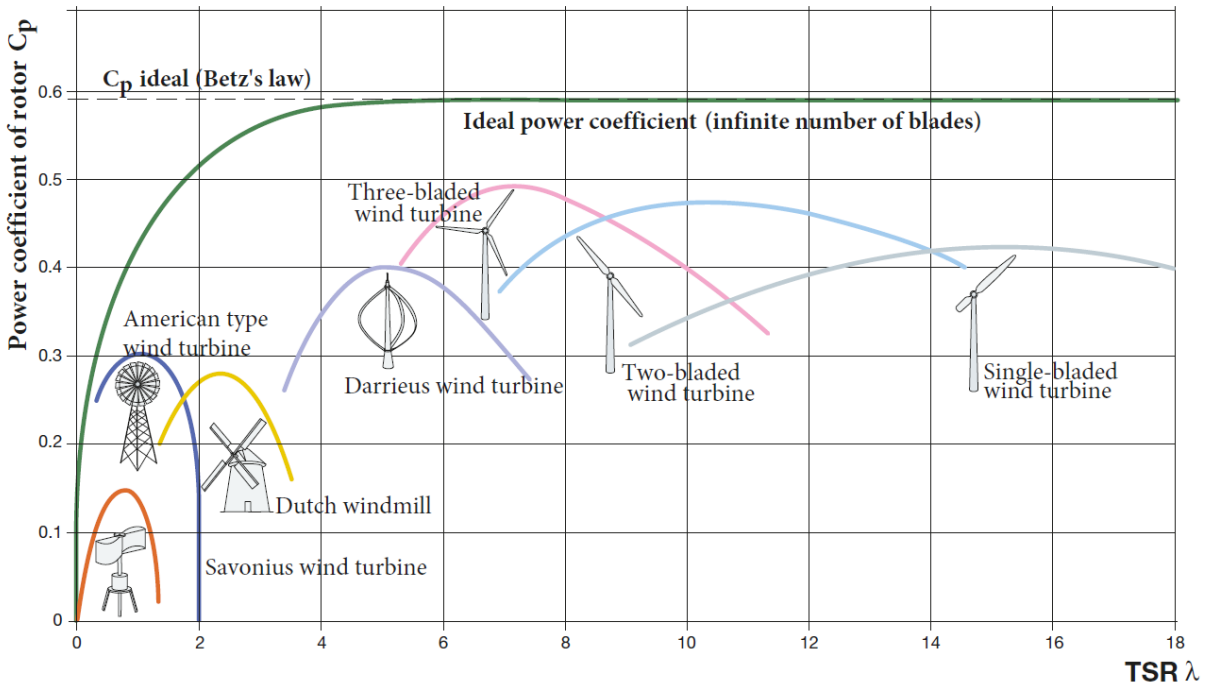

Figure 5.18: Cp vs TSR for different wind turbines designs [12]

Moving on to other issues, the values of the electrical power generated by the generator differ from those of the mechanical power previously obtained by the rotational movement of the shaft. Dividing both values we can obtain the **efficiency of the electrical transformation**.

The evolution of the efficiency can be seen in figure 5.19. Here are presented the efficiency values corresponding to the electrical power measured after rectifying the current from alternating current to alternating current (thanks to diode rectifier). Dividing these values with the mechanical power for the 3 generators, the results of η_{RD} are obtained, whose expression is as follows.

$$P_{cc} = \eta_{RD} \cdot P_M \quad \Rightarrow \quad \eta_{RD} = {}^{P_{cc}}/_{P_M} \tag{5.1}$$

So, in this way the efficiency parameter is telling how much of mechanical power is converted into electrical power.

Looking at figure 5.19 for the different generators, it can be seen that for the conventional generators (5.19a and 5.19b) efficiencies between 3 and 15% are obtained. This low value is due to the fact that the mechanical power described in the previous subsection reaches very high values. These values are around the nominal or rated power and even exceed it, and are approximately 100W or 200W depending on the generator (figure 5.13).

On the other hand, the electrical power values are not so high and, as can be seen in figure 5.19, are respectively around 10 and 20W for the conventional motors, so these electrical efficiency values are to be expected.

Looking at the AFPM coreless stator generator, its efficiency seems to be higher. This is due to two main reasons. The first is that the mechanical power (figure 5.13c) that it receives from the wind is much lower compared to the previous two, not even close to its nominal power of 200W.

For this reason, despite the fact that the electrical power generated (figure 5.15c) is lower than that of the previous two, its efficiency is higher. In other words, even if it has a higher efficiency, the effective available power is lower

The second reason is that, as can be clearly seen in subfigure 5.15c, the generator is working at higher speeds than the others, due to its inability to produce power at low speeds as seen above. If the comparison is made for the same speed for all 3 cases (e.g. 15-16 m/s) it can be seen that the efficiency of this engine does not exceed that of the other 2.

Therefore, to think that the efficiency of this engine is higher than that of the others is wrong, it simply works in another higher speed range, in which the other 2 conventional generators would exceed the efficiency values of the coreless stator generator.

Electrical efficiencies

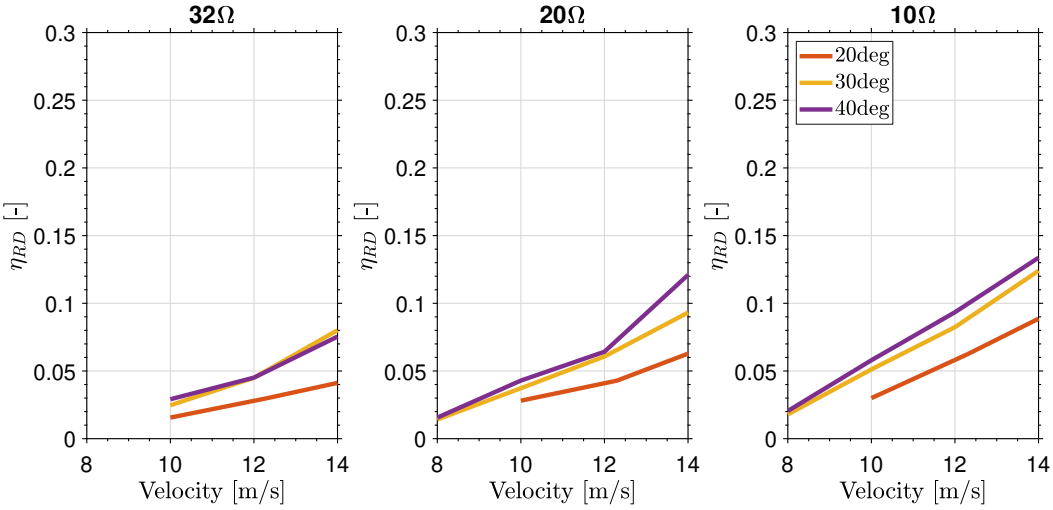

(a) Conventional PM generator of 100W

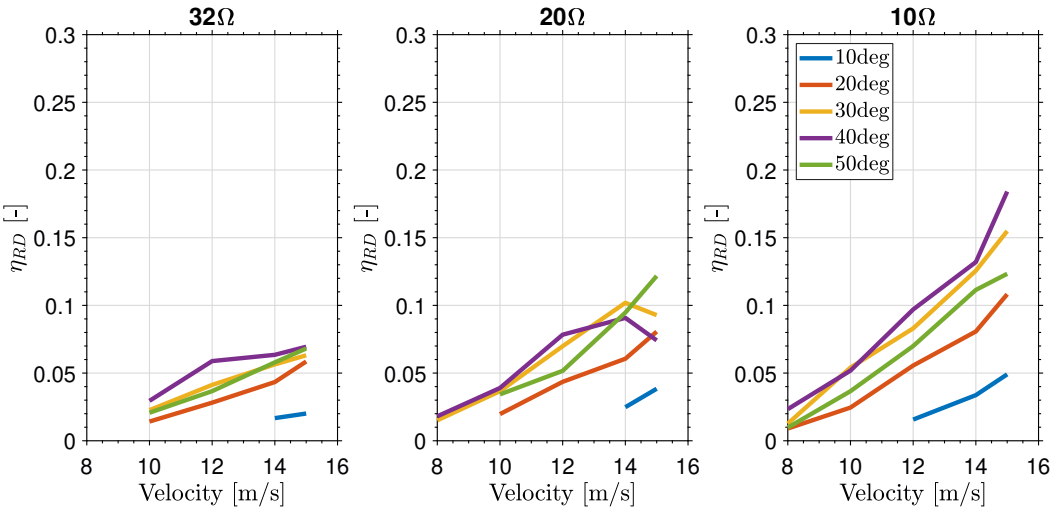

(b) Conventional PM generator of 200W

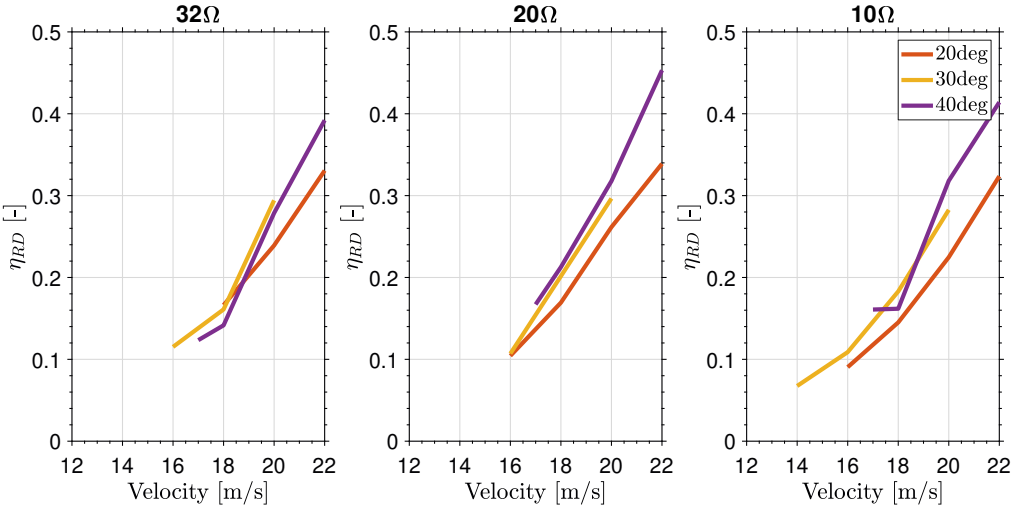

(c) Coreless stator AFPM generator of 200W

Figure 5.19: Electrical power direct current efficiency evolution with velocity (η_{RD})

In terms of trends for the three cases it can be clearly seen that the efficiency increases with increasing speed, as more electrical energy is produced. This increase also occurs with the angle of inclination of the prototype, obtaining better values at the same inclinations as before.

These speeds were achieved with this generator and not with the other two due to the impossibility of generating power at low speeds. The speed of the other 2 conventional generators was also not increased because their angular velocity reached very high values.

Meanwhile, it can also be seen that the efficiency values are higher the less electrical resistance the system has. In the case of 10Ω, the electrical efficiency values are maximised for all cases.

In addition to this analysis, figure 5.20 shows the power measured immediately at the output of the three-phase generator and the electrical efficiency considering this power (η_G). It has been decided to measure this three-phase power only for the case of the most optimal engine, the 200 W conventional generator.

With the help of a multimeter the three-phase power is measured directly at the output of the generator. The measurement is made between two three-phase branches and the electrical power is calculated. In the same way the efficiency expression is obtained.

$$P_{3F} = \eta_G \cdot P_M \quad \Rightarrow \quad \eta_G = {}^{P_{3F}}/_{P_M} \tag{5.2}$$

The evolution is very similar to the previous one, obtaining very close values. Thus analysis of the results is analogous, as it presents the same characteristics and trends as the direct current.

It can therefore be said that the loss of power in the transformation between alternating and direct current is minimal, as the values measured are practically the same.

As for the efficiency comparison with the Savonius, in the literature studies it appears with an average efficiency ranging from 10% to 17% in electricity generation. The average efficiency of the RoDaVi turbine is lower, not exceeding the 10% but is close to that of the Savonius.

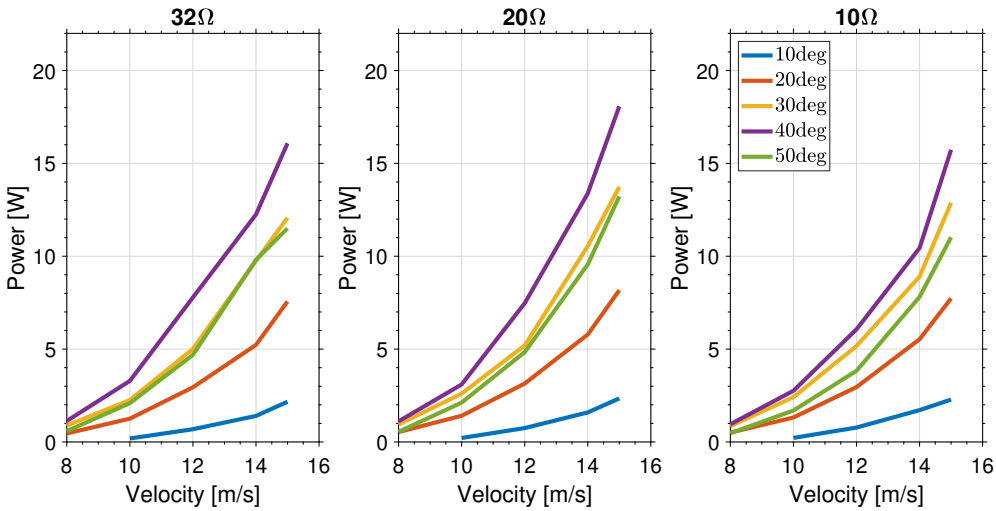

(a) 3-phase electrical power of conventional PM generator 200W

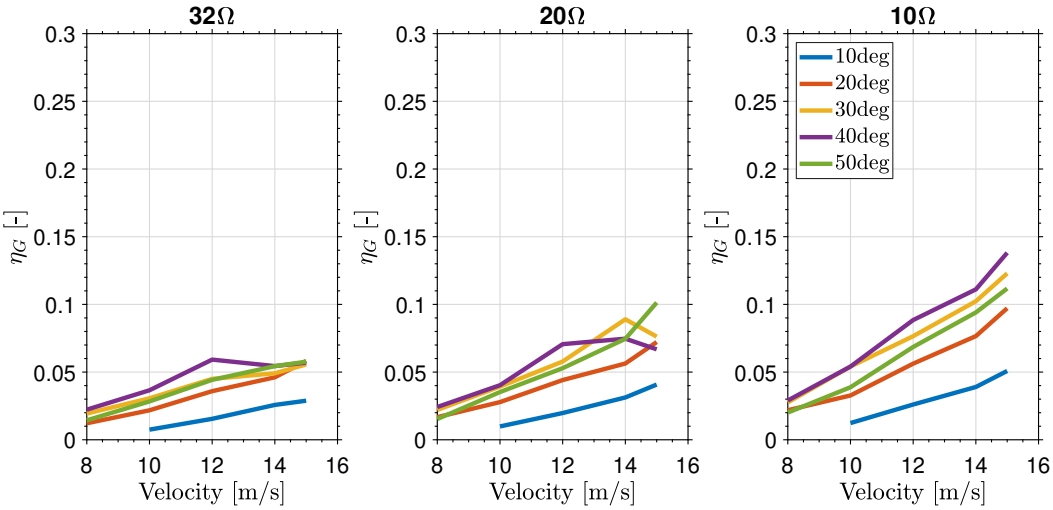

(b) η_G for the conventional PM generator of 200W

Figure 5.20: Measured three-phase electrical power evolution with velocity and efficiency (η_{3F})

Savonius comparison with 2 engines

As mentioned above, this prototype has a TSR within the range of the Savonius wind turbines.

It has already been compared in terms of operating range, C_P, TSR, and efficiency. All of this is based on values provided by the literature. But it will also be compared with laboratory measurements.

For this purpose, a pre-built Savonius turbine is used. Savounius is coupled to a structure similar to a wooden table, and the conventional generator is directly coupled to it.

The construction of the model has a very simple structure built in laboratory, in which it is impossible to fit a torque meter. For this reason the angular velocity, and therefore the TSR, cannot be calculated.

However, it will be possible to make measurements in the electrical circuit, so a comparison will be made based on the production of electrical energy, which, in the end, is the main function of the two turbines.

In this way, the comparison of the electrical power generated by the Savonius will be carried out for its optimum case, which is 0 degrees, and with the two conventional generators of 100W and 200W. It should be remembered that these generators have been the ones with which the best performance has been obtained with the RoDaVi.

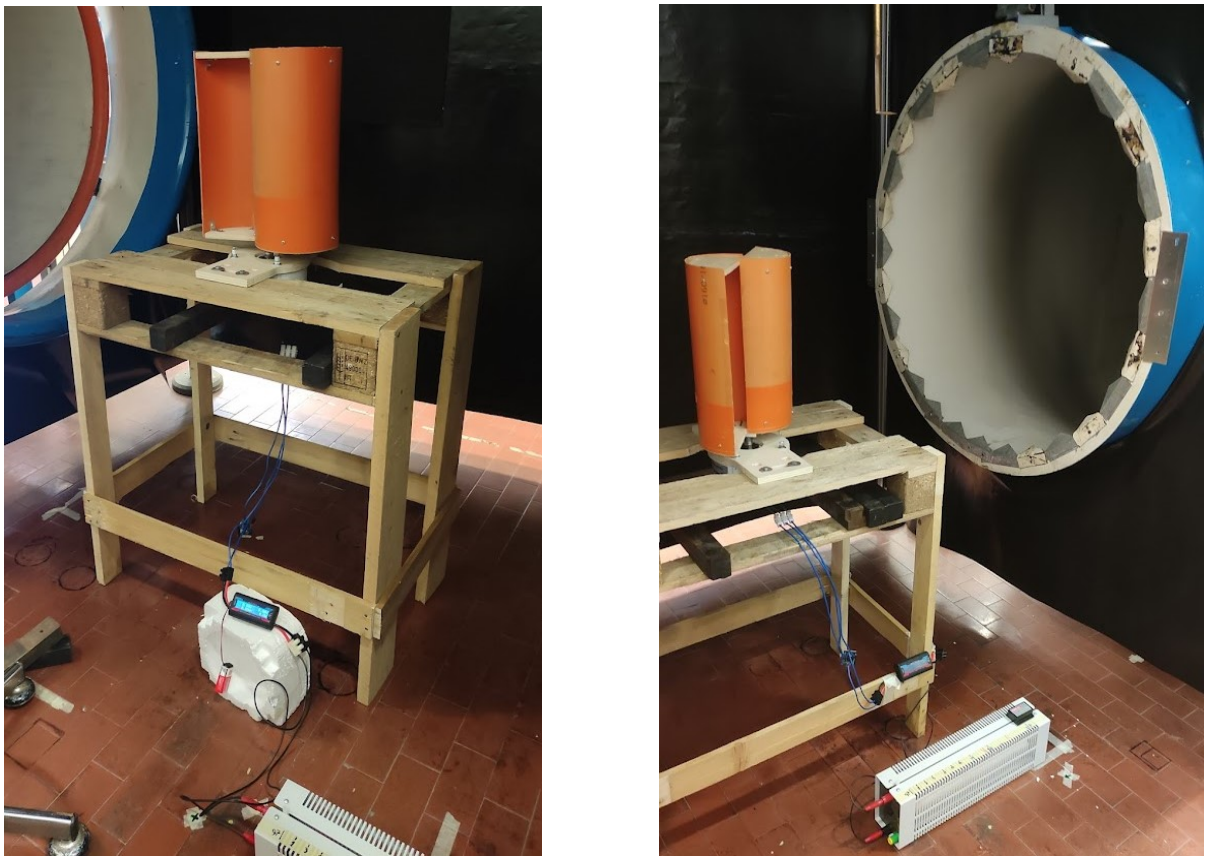

Figure 5.21: Savonius electrical set-up

The Savonius results are represented by a black line in figure 5.22. As can be seen, the electrical power generated for inclination angles of 30 degrees or more is higher than that generated by the Savonius in its optimum case. Savonius case only exceeds the 10 and 20 degree inclination. In some high speed cases, the RoDaVi is even twice the power generated by the Savonius turbine.

Therefore, it can be confirmed that this wind turbine can compete in the electricity sector, as the electrical power it generates is higher than that of similar ones in the same range of application.

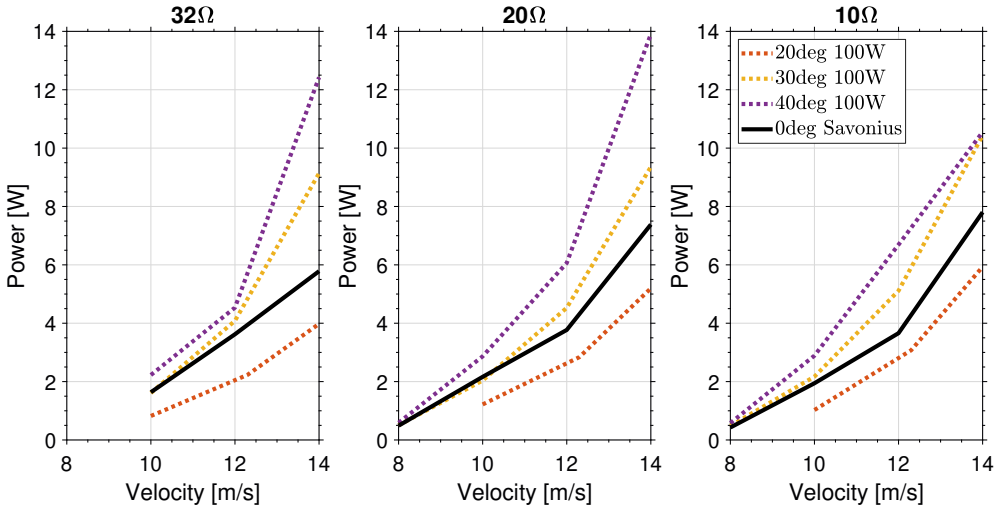

(a) Conventional PM generator of 100W

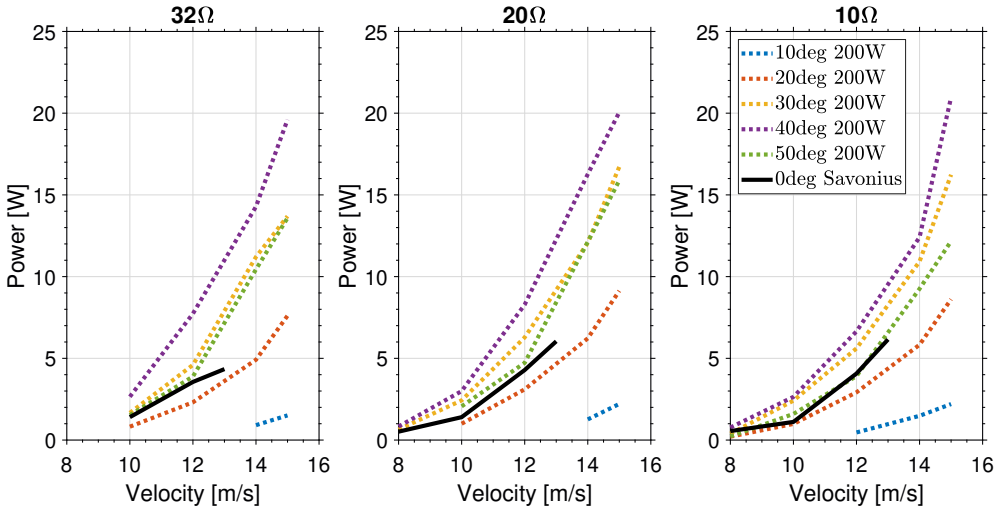

(b) Conventional PM generator of 200W

Figure 5.22: Savonius comparison

5.2.3 Conclusions of electrical and mechanical study

As a conclusion of the study, it could be said that the optimal configurations for the production of electrical energy with the RoDaVi turbine have been found, as well as different points to improve for its future development.

With regard to the mechanical study, it has been found that the performance of conventional permanent magnet generators is better than that of the coreless stator AFPM generator. The power generated by the conventional is an order of magnitude higher than the coreless.

Therefore, conventional generators are more suitable for implementing a turbine with these characteristics. However, the coreless stator AFPM generator should not be directly discarded. This generator can reach higher free flow speeds without having too high an angular velocity, so it is interesting to find out what happens at higher TSRs with this generator.

In the same time, conventional generators are limited to increase their free flow speed because they exceed 2000rpm and this can lead to structural failures.

On the other hand, it would be interesting to have conventional generators with a higher nominal power, since in their optimal operation both generators have exceeded it.

As for general trends, the higher the speed, the better the performance, but always without exceeding structural limits that could lead to the failure of the structure.

As for the inclination, the turbine has a great performance for high AoI, reaching its optimum inclination at 40 degrees.

The calculation of the C_P has made possible to compare the RoDaVi turbine with others on the market, thanks to the study of the evolution of the C_P with the TSR.

It should also be noted that the optimal configuration of maximum $C_{P,max}$ and λ_{max} in the CP vs. TSR curve has not been reached, but the performance of the measurements that have been made make it compete with existing turbines such as the Savonius.

On the other hand, the TSR parameter also has been used to classify the turbine and compare it with others of similar performance.

As for the electrical study, power ratings of 20W have been obtained. These values have been obtained with the 200W conventional PM generator, being higher than those of the 100W generator, which reaffirms that if better performance is desired, generators with higher nominal power are needed.

The growth trends are analogous to those of the mechanical study, with the optimum again being found for high speeds and an inclination of 40 degrees.

The efficiency analysis shows how well mechanical energy is converted into electrical energy. Values higher than 10% efficiency have been obtained, which are close to those of Savonius (between 10 and 17%).

The trends indicate that at higher speeds the efficiency improves. Limitations are also seen in the generators, which are only capable of providing up to 24V, so the values are consistent.

It is also observed that there are practically no losses in the transformation from alternating to direct current in the 200W generator.

Finally, the comparison with the Savonius of electrical parameters indicates that the turbine improves its performance for high slopes (30, 40, 50 degrees), so that the RoDaVi turbine could be a competitor in the field of low TSR turbines.

5.3 Flow field measurements using PIV

In the following section, an analysis of the flow field behind the turbine will be carried out using Particle Images Velocimetry or PIV technology. Determining the free-flow disturbances and consequences due the flow-structure interaction is a key factor in the positioning of a wind turbine.

The importance of this analysis lies in the placement of various wind turbines on a surface. The wake they leave behind can have negative effects on downstream turbines. RoDaVi turbine is intended for installation on rooftops, so this analysis will determine which distribution of turbines is appropriate.

PIV technology will be in charge of identifying and characterizing the behaviour of the flow behind the turbine. In this preliminary analysis, the velocity parameters, their components and the vorticity produced will be studied.

PIV technology is based on the displacement of particles introduced into the fluid under study. In this case, the particles introduced into the air are soap bubbles, which are introduced into the wind tunnel and supposed to follow the fluid flow. (section 4.4). Directly, by studying the movement of these particles in the images obtained using the PIVlab software, instantaneous velocity measurements can be obtained.

By using a laser and a high power photocamera, 2 measurement configurations will be made. This elements and their working principles of PIV technology has been described in section 4.4. In order to obtain good data acquisition, it must be completely dark. The lights in the wind tunnel facility are turned off, and black plastic is placed around the entire open section of the tunnel to prevent any light from entering and disturbing the results.

In the first configuration the laser is positioned at the top of the wind tunnel and the camera captures a vertical plane, as it is observed in the figure 5.23a. In the second measurement the position of the laser and the camera are exchanged. Now the laser is placed on one side of the wind tunnel and the camera on top (figure 5.23b).

Therefore 2 planes are measured, one vertical and one horizontal, which are presented in the following subsections 5.3.1 and 5.3.2 respectively. The variation of the parameters in these planes will allow to observe the influence of the wake left by the turbine.

For these 2 measurements, different configurations are made. Due to the computational cost, time and laboratory resources involved in carrying out all the electrical analysis simulations for both planes, a smaller number of cases are selected.

Simulations are carried out at 10, 20, 30 and 40 degrees of turbine inclination for low speed and high speed. The optimum electrical behaviour occurs at 40 degrees, which is why it was decided to go as far as this AoI.

As for the speeds, measuring the entire range used in the previous study is not viable. In the case of the vertical plane, a low speed of 10m/s and a speed of 14m/s are measured. While for the horizontal it is measured for 7 and 10m/s.

On the other hand, the laser beam is emitting radiation only in one plane by placing a lens on its radiating focus. From the vertical plane, the measuring plane is placed parallel

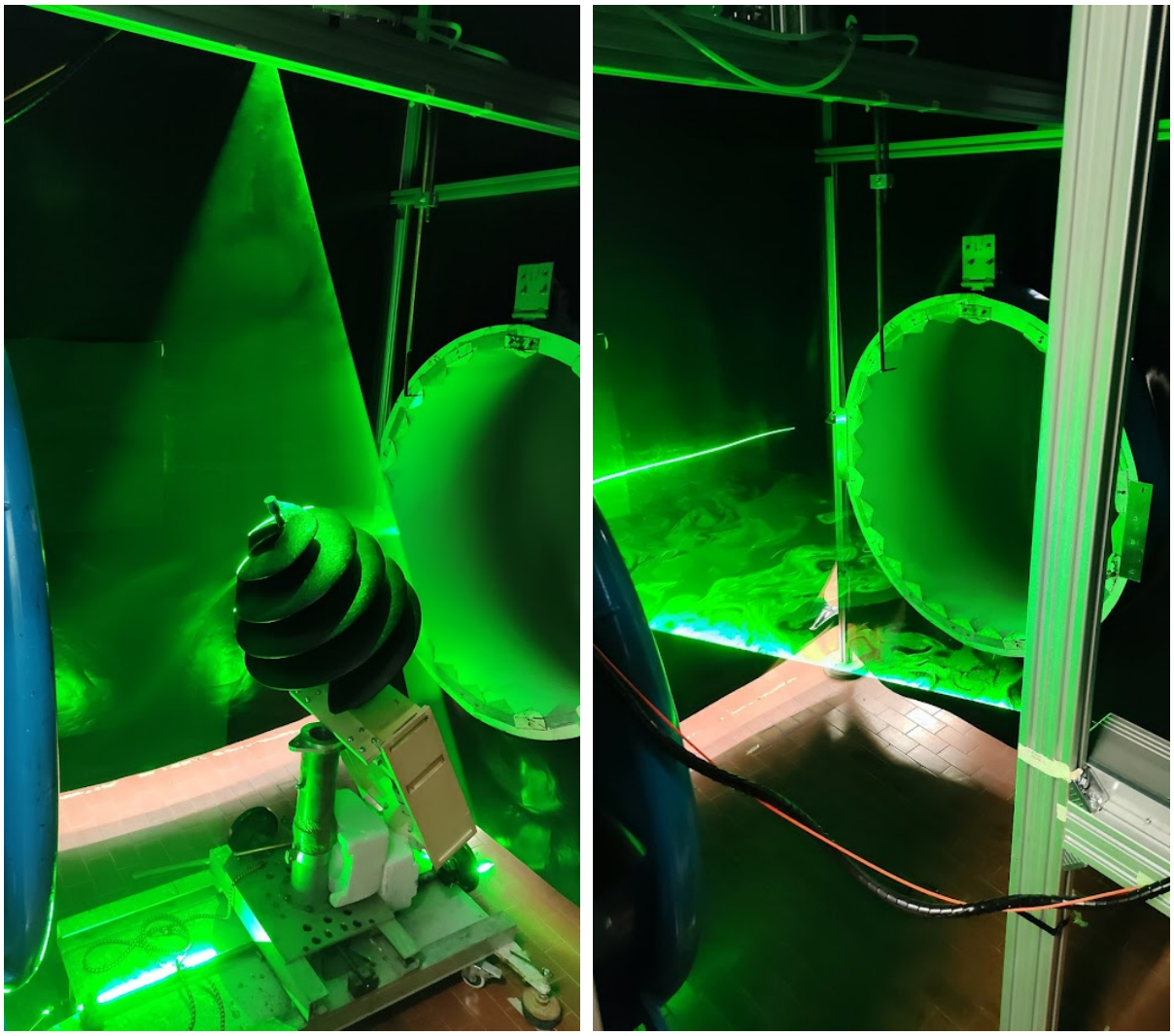

(a) Vertical plane with complete set-up and turbine mounted

(b) Horizontal plane configuration (turbine added later as in (a))

Figure 5.23: PIV measurements configuration

to the freestream flow, measuring a plane slightly offset from the centre of the turbine in order to measure the influence of all turbine channels.

The horizontal plane is placed approximately at the height of the middle channel of the turbine. It would be convenient to make several horizontal planes to observe completely the different vortices and recirculation zones that are created downstream of each of the channels, but this would be too costly in terms of resources and time.

The first phase consists of data acquisition with the high-precision photocamera. 5000 images are acquired for each case with a frequency of 2000Hz, so each scan is 2.5s.

As it is seen in the set-up, the camera is placed a few metres away from the structure. From this position the captured region is not too large. For this reason, it is necessary to choose which part of the flow field to study. So, the region immediately downstream of the turbine is selected, which will be the area where the most relevant effects will occur.

Also the bubbles have a direct impact only in a limited area. This means that the height of the tube that introduces the bubbles must be correctly adjusted so that they hit the structure. However, due to the size of the prototype, they do not hit all regions of the prototype equally.

Once the setup is in the right position and under the right conditions, measurements are taken.

As an example of the acquisition of the images, some of the frames obtained with the camera are shown in figures 5.24 and 5.25. Figure 5.24 shows the vertical plane and figure 5.25 the horizontal plane. All cases correspond to 20 degrees and 10m/s. It is known that this case rotates at 640rpm, or about 10.67rev/s (or 67 rad/s).

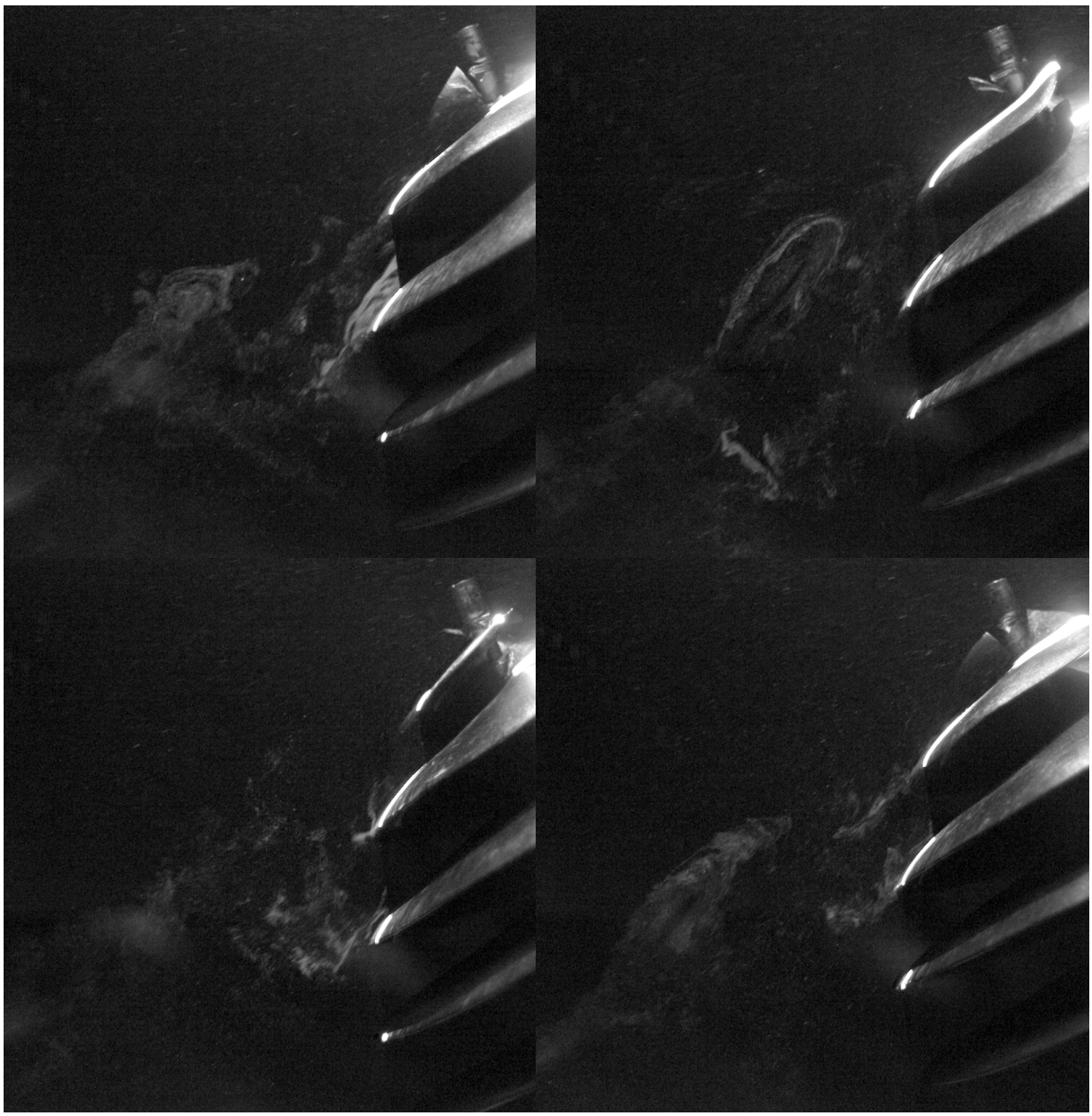

Figure 5.24: Image acquisition, representation of one revolution for **vertical plane** with 20 degree and 10m/s configuration

The camera has measured with an acquisition rate of 2000Hz, so 2000 pictures per second are taken of the turbine. In one second, the turbine makes 10.67 revolutions, or in other words, every 187 frames it makes one complete turn.

To present the images of figures 5.24 and 5.25 , only one revolution is taken, and 4 equidistant snapshots are taken (at every 47 frames). In this way, the fourth image (bottom-right corner) will return to the positioning of the first image (top-left corner).

In this way, a small sample of 4 of the 5000 images is presented to visualize how the micro bubbles move and how the camera has been adjusted to measure them. A priori, the first trends in flow behaviour can already be seen. The PIVlab analysis will try to critically characterise this behaviour, thanks to the use of all the images and specific software.

Figure 5.25: Image acquisition, representation of one revolution for **horizontal plane** with 20 degree and 10m/s configuration

A priori, the first trends in flow behaviour can already be seen. The PIVlab analysis will try to analyse this behaviour in a critical way, thanks to the use of all the images and specific software.

Once measured, work begins with the PIVlab software to obtain the results necessary to perform the critical analysis of the results.

Each measurement is stored on a hard disk and then processed using PIVlab software. The images are loaded and a region of interest (ROI) is defined, where the calculations are performed. In this region, unnecessary parts of the acquisition are discarded where reflections exist or have not been measured correctly. This is why the figures to be presented do not have exactly the same dimensions and are not perfectly square. The size scale has been respected to make it easier to see the non-deformed results.

In PIVlab settings, a mask is applied on the structure, as the results in this area are not measured correctly in the laser plane. This is because the structure produces a shadow that the laser cannot illuminate. Thus, in this shadow region, the particles of the plane to be studied are not illuminated, so the area where the structure and its shadow are located must be discarded.

This area is represented in the images in black. The shape of the turbine can be seen (both vertical and horizontal). Due to the different inclinations, the shape and inclination of the mask can be seen to change in each case.

Contrast adjustments are made in the software to visualise the particles correctly. Velocity field of all the measured frames is calculated using the PIV algorithm developed in the programme based on Fast Fourier Transform (FFT) windows. This process takes about 6 hours for each case of 5000 images. Once the calculation is finished, the case is validated with the post-processing settings and the average of all the frames is calculated.

Before obtaining the results, an image of a graduated ruler with the camera's focus settings is loaded and the case is calibrated. In this way, length values are assigned to the measured pixels and the results are obtained in real units.

Once the simulation is calibrated with the graduated image, the parameters to be studied are plotted and the mask and parameters are exported to MatLab. Working with the data, the graphs in figures 5.26 to 5.41 are obtained.

5.3.1 Vertical Plane

Velocity magnitude

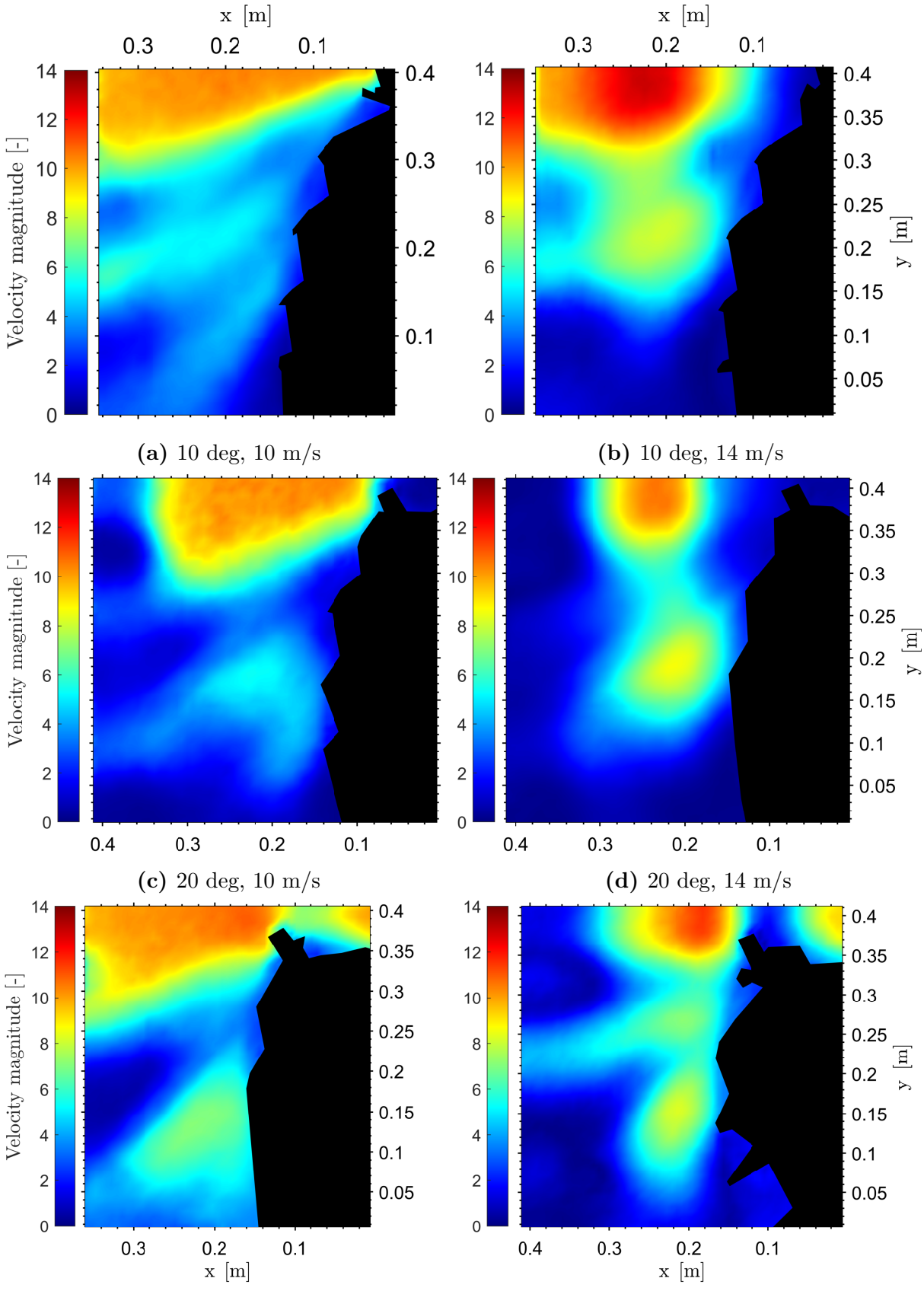

(a) 10 deg, 10 m/s

(b) 10 deg, 14 m/s

(c) 20 deg, 10 m/s

(d) 20 deg, 14 m/s

(e) 30 deg, 10 m/s

(f) 30 deg, 14 m/s

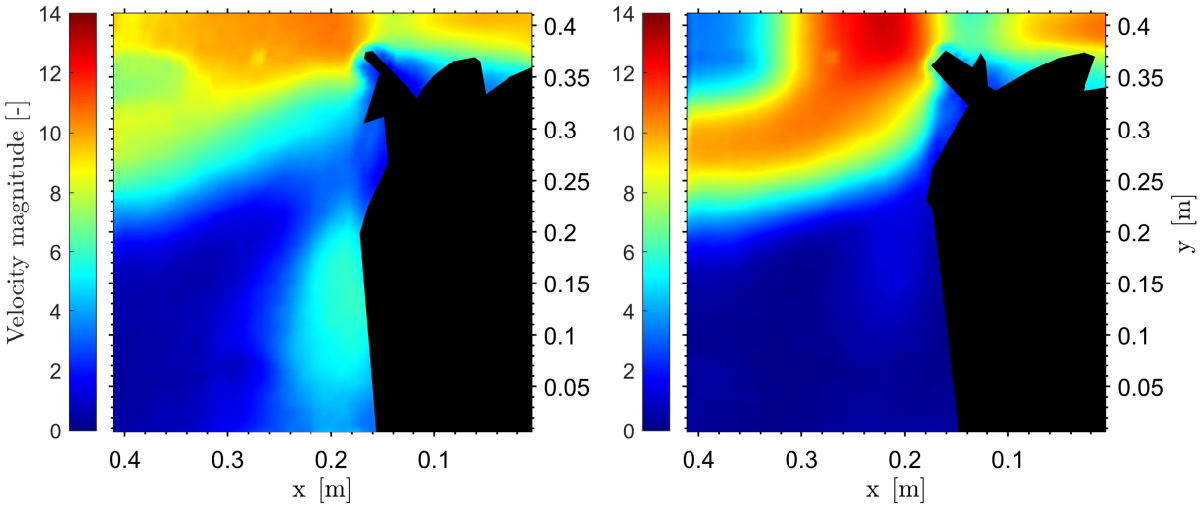

(g) 40 deg, 10 m/s **(h)** 40 deg, 14 m/s

Figure 5.26: Velocity magnitude

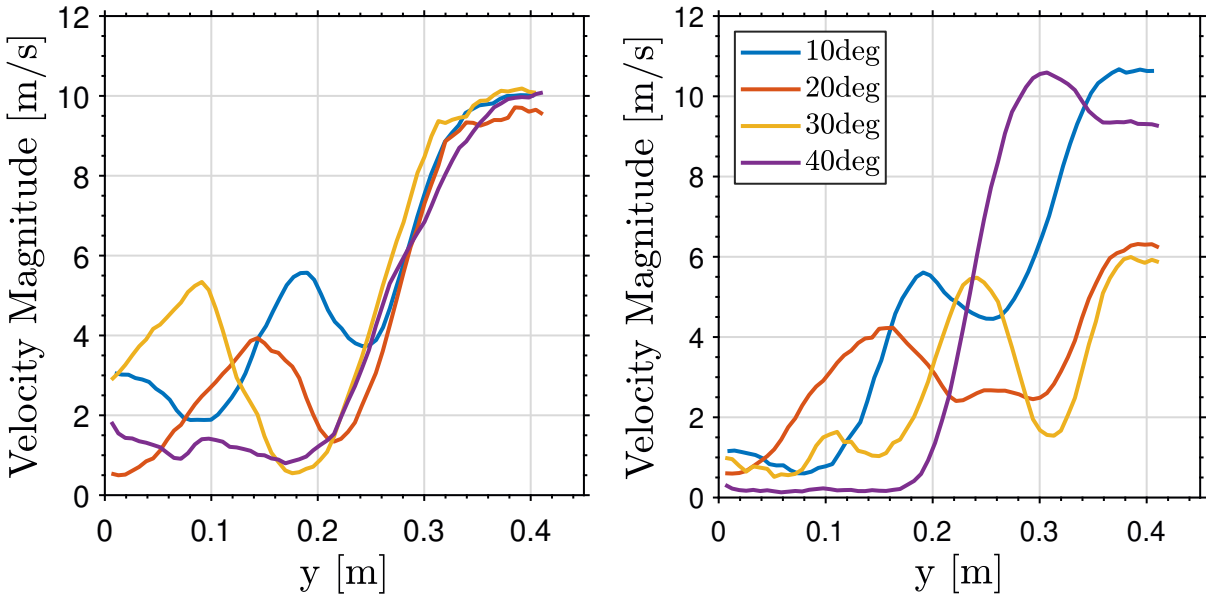

(a) 10 m/s **(b)** 14 m/s

Figure 5.27: Velocity magnitude profiles for x=0.3m

The first results correspond to the vertical plane. Figure 5.26 presents the **velocity magnitude** for the average of all instantaneous simulations. As in all graphs, each column represents a different velocity and each row a different AoI. All colourbars have the same upper and lower limits (0m/s and 14m/s), and on the axes are the scaled dimensions taking as origin the lower right corner. The X-axis grows from right to left and the Y-axis from bottom to top. This reference system has been taken as the air flow comes from right to left.

Observing the evolution of the velocity magnitude it can be seen that after the turbine there is a decrease in velocity. This is normal, as the turbine absorbs kinetic energy carried by the air for its rotational movement.

Furthermore, looking at the top of the turbine, it can be seen that the free-flow velocity is maintained. In the case of 10 degrees and low velocity (5.26a) it can be seen how the free-flow velocity is recovered starting from the top. Along the X coordinate the free flow velocity zone continues to grow. The different velocity depressions tangential to the three upper exit channels of the turbine can also be observed.

For the high speed case (5.26b) there is still a free flow velocity region in the upper turbine zone. It reaches a point where this region ceases to have any influence as the flow starts to decelerate, which is why the blue tone colours of low velocities reappear.

This fact becomes visible for higher inclinations, as can be seen in the images of the successive rows. For 20 degrees the high velocity zone corresponding to the free flow speed becomes smaller and smaller. For the case of 10m/s (5.26c) this effect is already apparent, but it becomes even more noticeable for the case of 14m/s (5.26b). It is the same trend for higher inclinations of the prototype.

For these higher inclination angles, in the middle part of the turbine, where the velocity is lower, higher velocity zones appear. This higher velocities zones correspond to vorticities created at the outlet of the different turbine channels.

The vorticity zones have the turbine inclination direction, because they emerge with this accelerated velocity from inside the structure, tangential to the trailing edge of the turbine, that is, downwards. These zones are quite clearly observed in the case of 30 degrees and 14m/s (5.26f), where 3 high velocity zones are observed, the upper one being the one that follows the free flow velocity, and the other two at the exit of the turbine cavities.

Finally, in the case of the 40 degree turbine, the upper part follows the same trends as the previous cases. However, there is not much variation in speed in the lower part, especially for the high speed case (5.26h), where recirculation zones do not seem to appear.

The reality is that they do exist, but when the model is tilted, the bubbles mainly affect the upper part of the model, not allowing the behaviour of the lower part of the turbine to be clearly observed. Another factor to take into account is the impact of the bubbles, which, at high speeds, tend to rise in altitude and pass over the prototype.

The graphs in figure 5.27 show the velocity magnitude for a profile of the colour chart. A vertical line has been selected within the graph, located at $x = 0.3m$ metres in all cases.

In this way the velocity magnitude values of all cases are plotted for this distance and can be compared one with each other. The direction of the Y-axis that in the coloured figures goes from bottom to top, now goes from left to right, so the values of the lower

part of the turbine will appear on the left, and those of the upper part on the right.

Two subfigures have been plotted with the low speed and the high speed to make it easier to differentiate the cases. Each angle has its own colour (as in the previous section) and the minimum and maximum limits of the graphs are preserved.

As can be seen in figure 5.27, looking at low velocities (5.27a), it can be seen that for the upper part of the turbine, or in other words, for high values of Y, all cases have free stream velocity. As seen in the previous colour images, this area is not altered by the presence of the turbine and the free stream velocity is maintained.

Compared to the high velocity case (5.27b), it can be seen that the maximum velocity is no longer reached at this point ($y = 0.3m$), instead the velocity after the structure far downstream is lower.

Looking at the evolution in the lower part of the turbine, the previous mentioned increments in speed can be seen. In subfigure 5.27b it can be seen that the peaks appear closer to zero as the degree of inclination increases. For the case of 30 degrees, it can be seen how different peaks are captured, corresponding to the 3 outlets of the turbine channels.

The last peak appears for 10 degrees approximately at $y = 0.2m$, for 20 at $y = 0.15m$, and for 30 at $y = 0.1m$. For the case of 40 degrees they do not appear due to the low density of bubbles arriving for the reasons mentioned above.

Figure 5.28 shows the graph of the evolution of the **u-component** of velocity, in other words, the vector projection of the velocity in the X-direction. As can be seen, the evolution is very similar to that of the velocity magnitude.

This is due to the fact that the flow leaves the wind tunnel in this direction. Because of this, the largest component of the velocity magnitude is this u-component. Therefore, the trend analysis of this parameter is analogous to the previous one, as the same behaviour is obtained.

The areas where the results differ slightly are at the outlets of the channels that make up the turbine. In these areas the u component is lower than the velocity magnitude. This is due to the fact that the geometry of the turbine directs the flow downwards, so the flow is no longer parallel to the X-direction and starts to move in the Y-direction. This is why the u component becomes less important in these areas, as the vertical component or v starts to predominate.

In figure 5.29 the $x = 0.3m$ profile is represented again to study the linear evolution of this parameter in Y and the evolution is analogous to that of the velocity component.

U velocity component

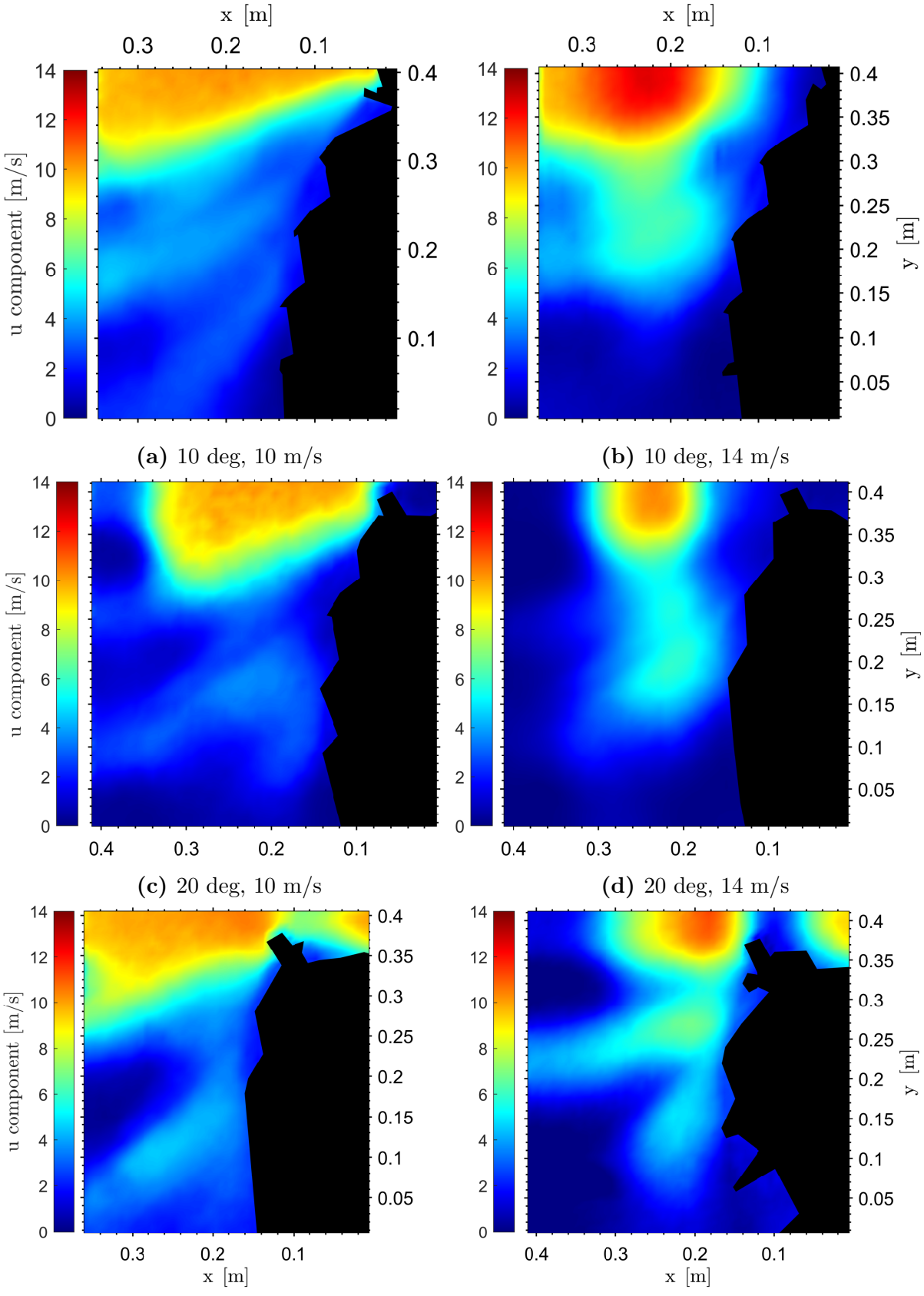

(a) 10 deg, 10 m/s

(b) 10 deg, 14 m/s

(c) 20 deg, 10 m/s

(d) 20 deg, 14 m/s

(e) 30 deg, 10 m/s

(f) 30 deg, 14 m/s

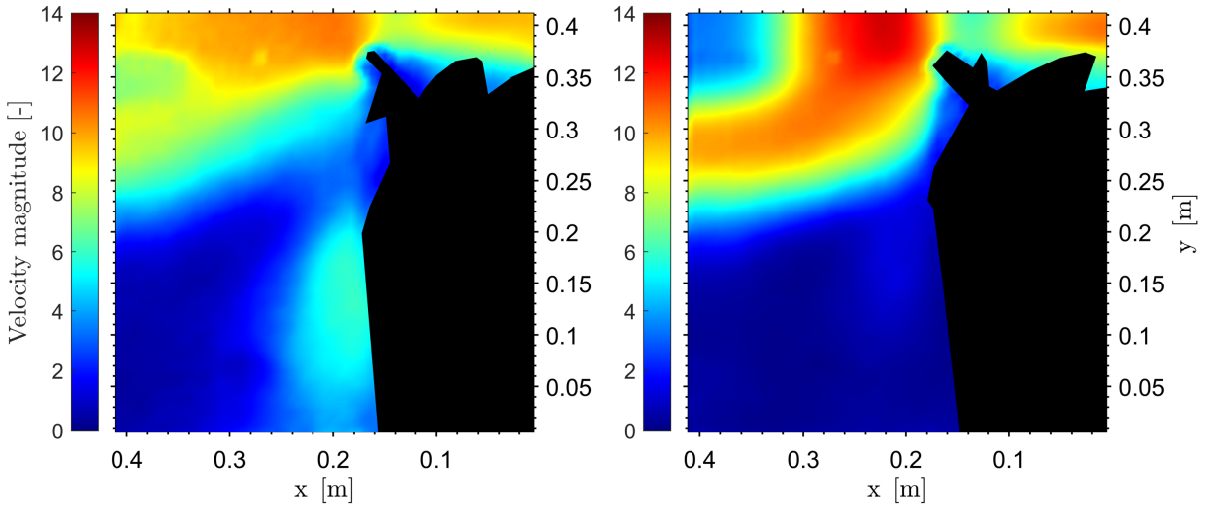

(g) 40 deg, 10 m/s **(h)** 40 deg, 14 m/s

Figure 5.28: u velocity component

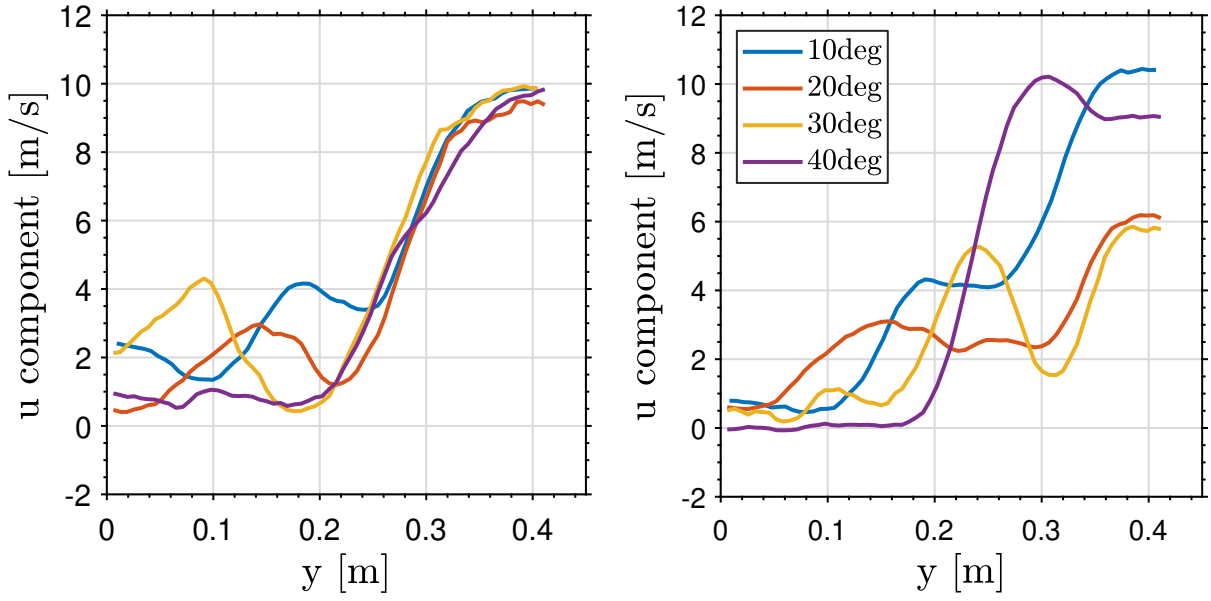

(a) 10 m/s **(b)** 14 m/s

Figure 5.29: U component profiles for x=0.3m

V velocity component

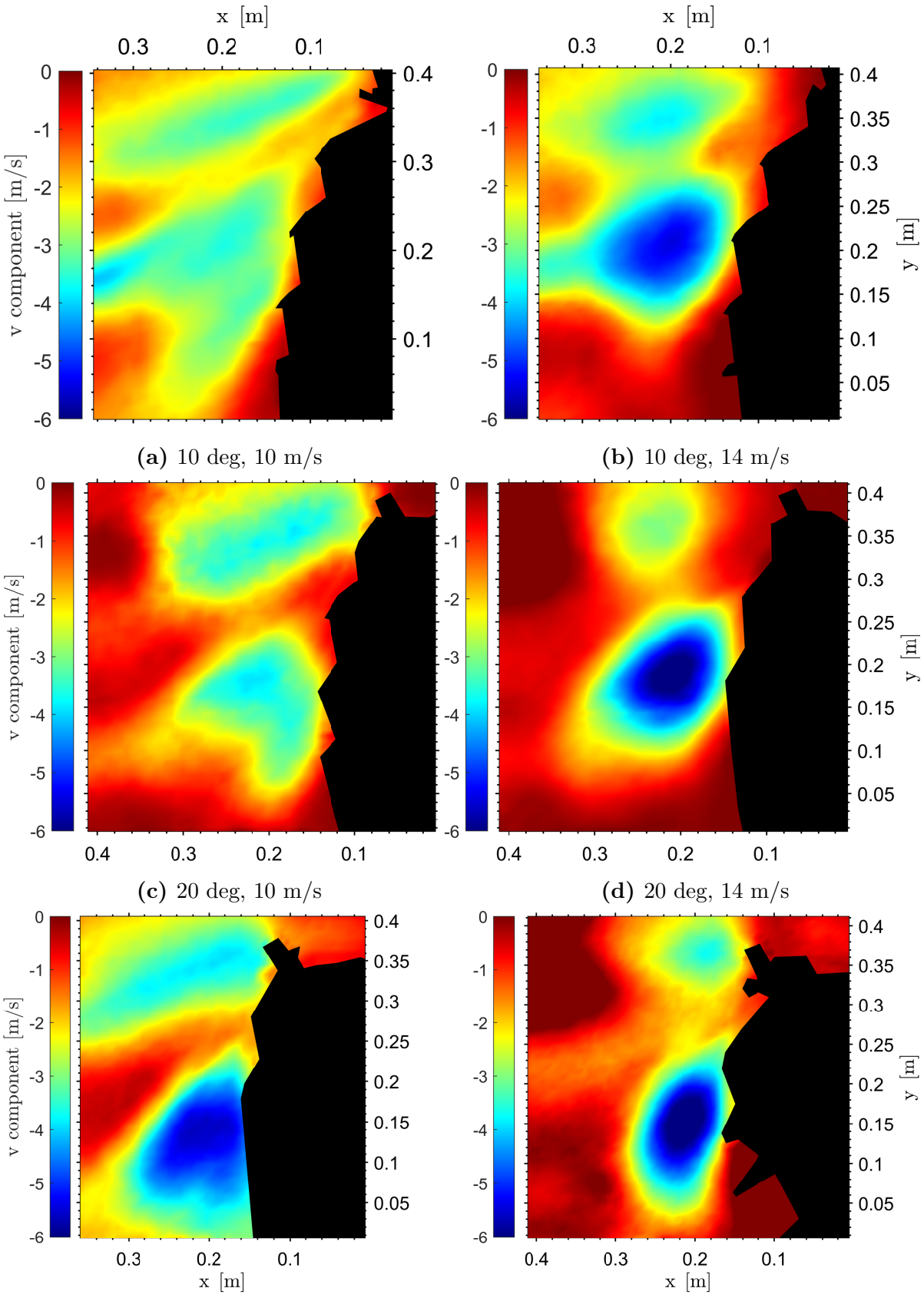

(a) 10 deg, 10 m/s

(b) 10 deg, 14 m/s

(c) 20 deg, 10 m/s

(d) 20 deg, 14 m/s

(e) 30 deg, 10 m/s

(f) 30 deg, 14 m/s

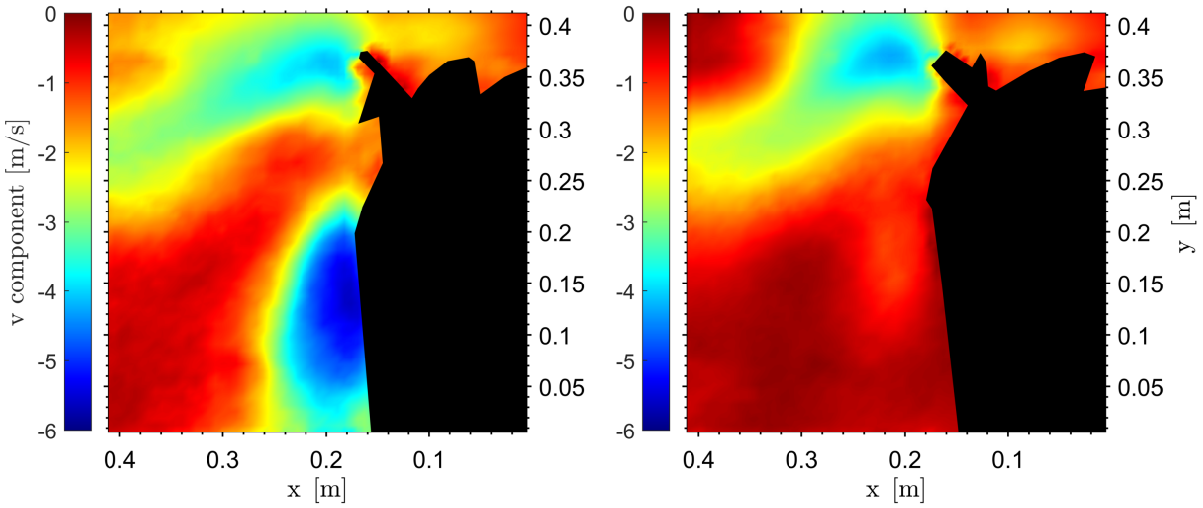

(g) 40 deg, 10 m/s **(h)** 40 deg, 14 m/s

Figure 5.30: v velocity component

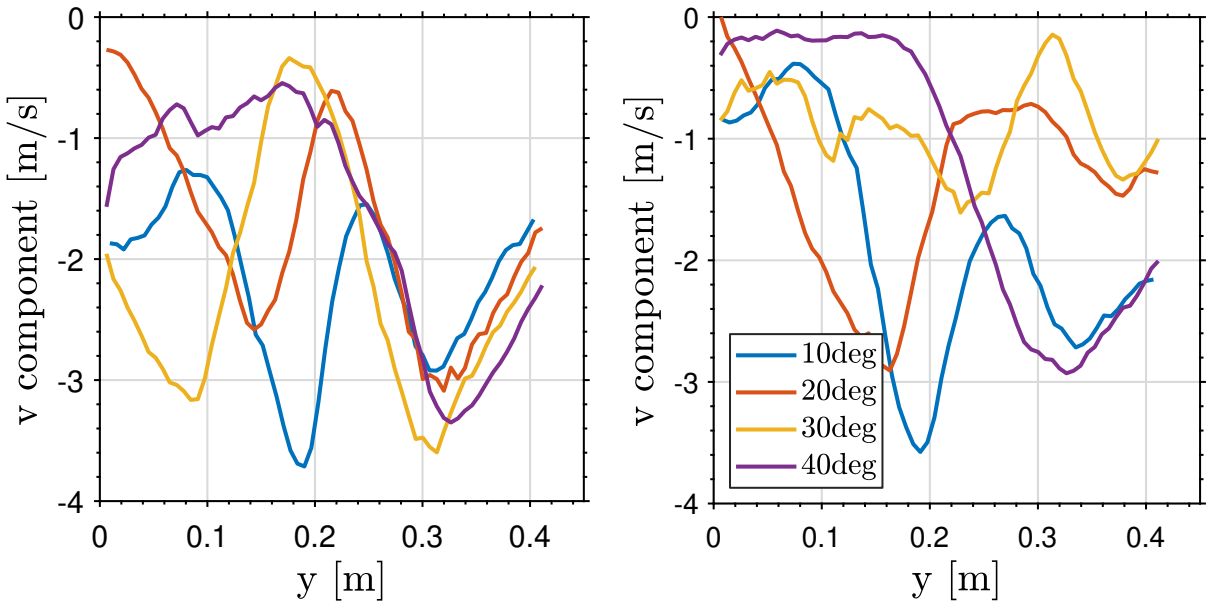

(a) 10 m/s **(b)** 14 m/s

Figure 5.31: V component profiles for x=0.3m

Figure 5.30 shows the graphs of the **v-component** of the velocity in the flow field, which is the vertical projection of the velocity. It can be seen that the values of the v-component have a negative value. This means that the direction of the velocity vectors is opposite to the growth of the y-axis, that is to say, the direction of the v-component is downwards. This is expected, due to the channelling of the flow in the turbine. As the turbine is inclined, it expels the flow in a downward direction from its channels.

The highest values of v-component in absolute value will be represented in blue, up to a maximum value of about 6m/s, which is less than half of the maximum speed tested. Meanwhile, red tones indicate that its value is 0 or close to it. This means that when the map is reddish in colour, the v-component has little influence. It is observed that this colour is quite present, so that in these areas the predominant component is the u-component. This explains the similarities between the velocity magnitude and the u-component.

However, the v-component also has a significant influence. The highest values of this v-component occur immediately after the exit of the wind turbine channels. These coincide with the high values of the velocity magnitude parameter.

Therefore, at the exit of the turbine, there are acceleration zones that lead to areas with high velocities with possible vorticity.

As for figure 5.31, the minima of the graphs correspond to the peaks observed earlier in the velocity magnitude.

In figure 5.32, the **vorticity** plots are shown. The presence of vorticity in a fluid always implies the rotation of fluid particles, whether or not accompanied by some transverse deformation. Therefore this vorticity will appear in regions where a change of velocity direction occurs.

There are negative and positive values of vorticity. There is little spatial difference between them. This is because in areas where recirculation vortices occur there is a contrast between positive and negative values of vorticity.

The negative values are those with the highest intensity in absolute value. The negative value is given in the areas where the rotation is clockwise, and the positive value when it is counterclockwise.

By studying the mean, it is not possible to clearly discover the transient character of the simulation. In other words, it is only possible to observe where the recirculation vortices are located, which coincide in the areas where there are greater velocity gradients.

For a proper study of the transient phenomenon of vorticity, it would be necessary to study each instantaneous snapshot and observe its evolution in a video. In this way, the creation and destruction of vortices that occurs in a revolution of the structure, and its evolution over time, would be perfectly observed. This comparison will be made by means of a video in the presentation.

However, the appearance of the vortices will be observed in the horizontal plane from another perspective, which will allow them to be better visualised.

Finally, figure 5.33 shows the evolution of the vorticity in the x=0.3m plane.

Vorticity

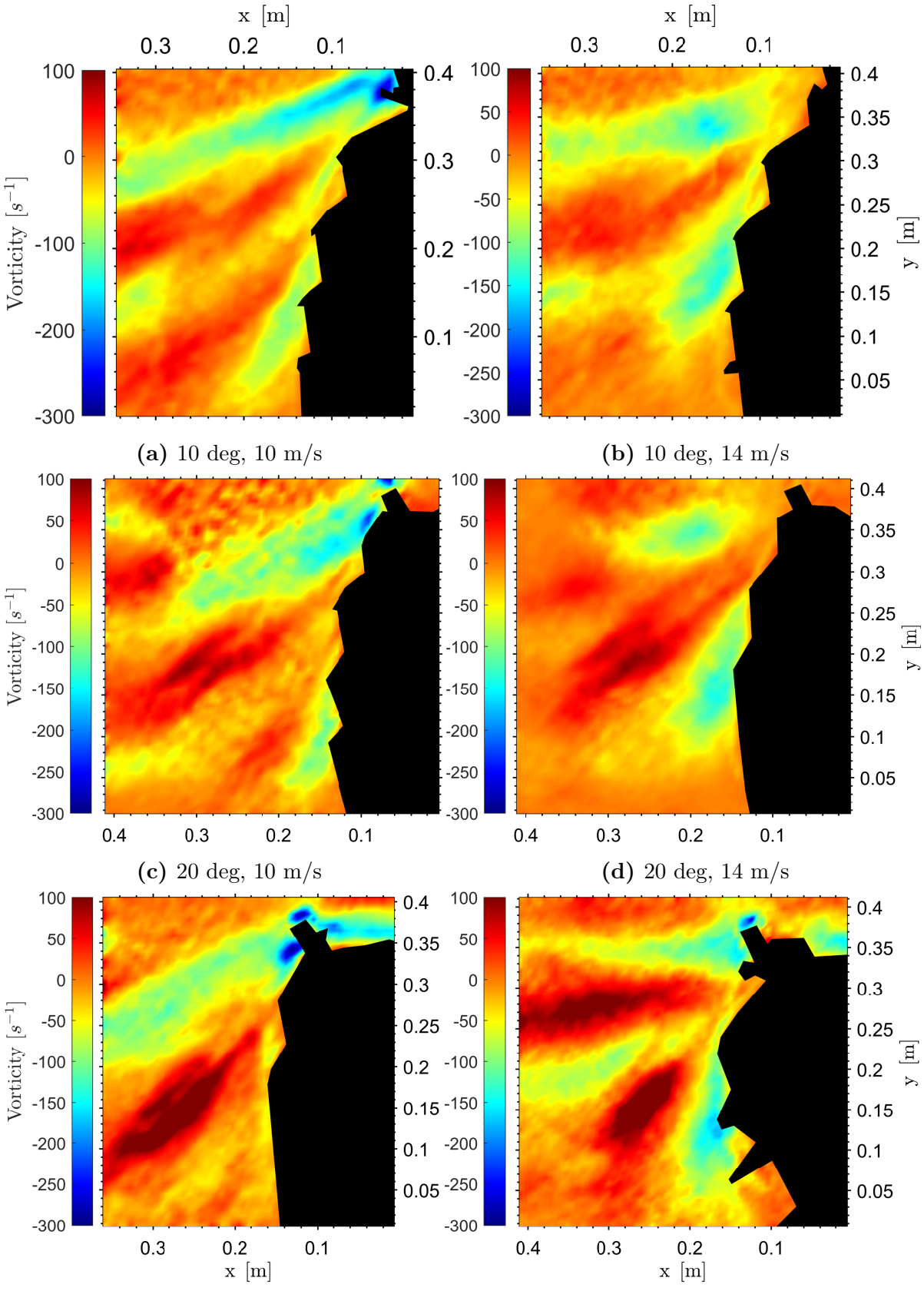

(a) 10 deg, 10 m/s

(b) 10 deg, 14 m/s

(c) 20 deg, 10 m/s

(d) 20 deg, 14 m/s

(e) 30 deg, 10 m/s

(f) 30 deg, 14 m/s

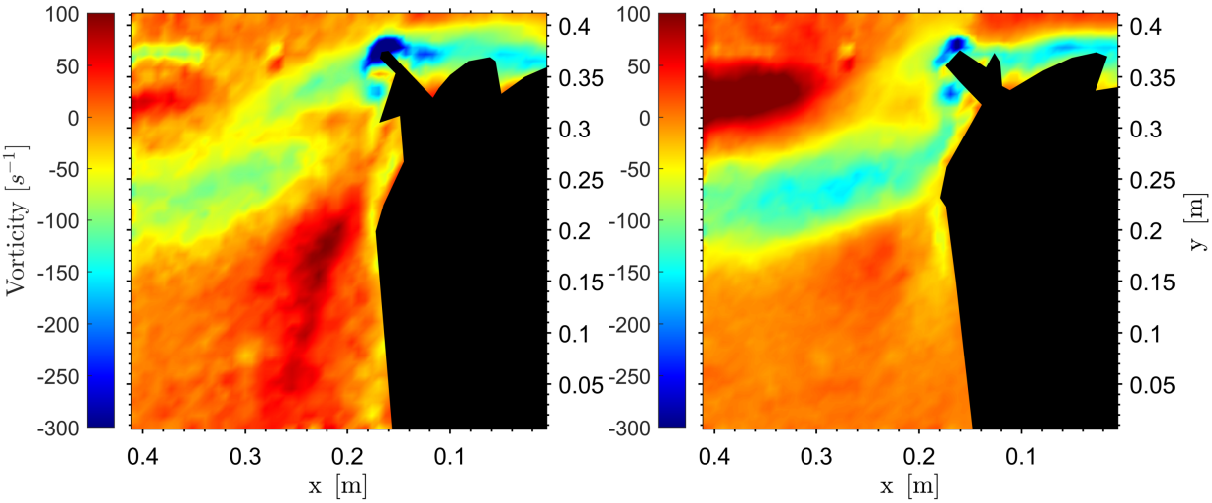

(g) 40 deg, 10 m/s **(h)** 40 deg, 14 m/s

Figure 5.32: Vorticity

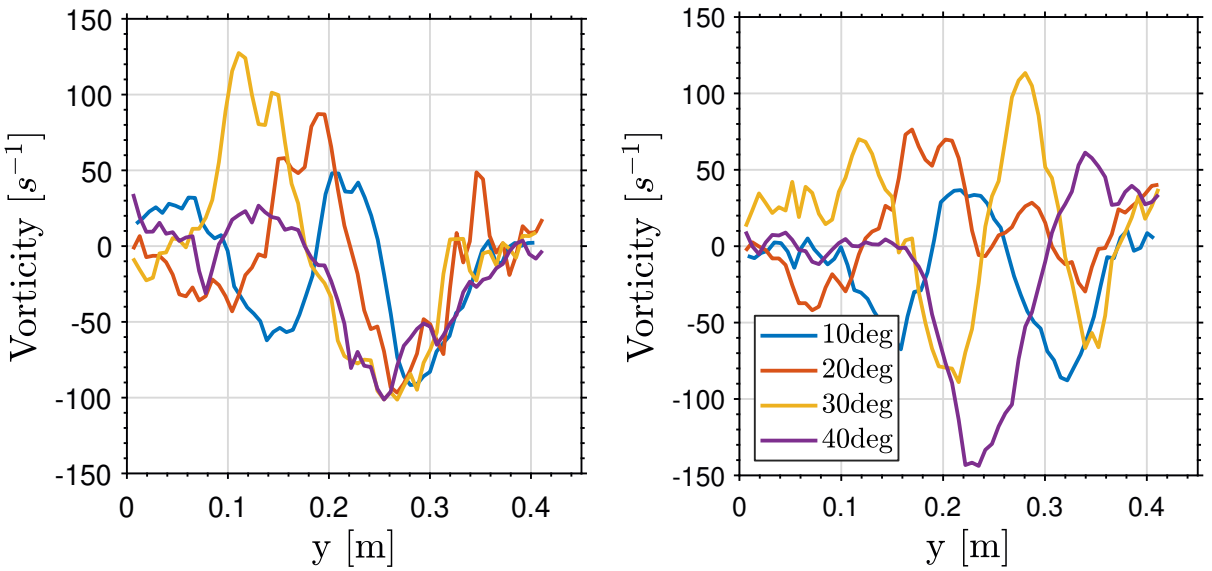

(a) 10 m/s **(b)** 14 m/s

Figure 5.33: Vorticity profiles for x=0.3m

5.3.2 Horizontal Plane

The study of the horizontal plane is identical to that of the vertical plane. The mean parameters of velocity magnitude, u-component, v-component and vorticity are also presented for different angles and 2 velocities. The study of this plane will show how the flow behaves from another perspective.

In this study it has been chosen to change the values of the velocity. The lowest velocity is 7m/s and the highest is 10m/s. This decision has been made to keep the bubbles as low as possible and to study a mid-plane of the turbine. Therefore, the laser now points to a low mid-horizontal plane where structure width dimension is almost complete.

The spatial limitations of the camera imply that only a small region behind the turbine can be studied. The images show the turbine in black colour and the flow behind it. That is why the criterion for the axes remains the same as before. The origin is in the lower right corner. Now the Y-axis indicates the back of the turbine and grows as the flow moves further downstream. And the X-axis grows from the turbine to the outside left direction.

The main flow is coming from the bottom to the top of the figures, following the growth direction of Y-axis.

The turbine, which is represented with its black mask, has a circular shape, which corresponds to its top view. It rotates in a clockwise direction. The shape changes between cases of different inclination.

The figures 5.34 show the **velocity magnitude**. It can be seen that on the left part of the graph, outside the turbine, the free flow velocity is again reached. Downstream of the turbine, at the rear, the above mentioned decrease in velocity is clearly visible.

There is a zone within these low velocities where the velocities are slightly higher. This is the area in which the flow in the channel under study is accelerated, forming a wake. With the magnitude of the velocity it is only possible to determine the position but not the characteristics of this zone. This is why its components and vorticity will be studied.

For this experiment, the evolution has also been plotted on a plane for all cases. In this plane, the intersection corresponding to $x = 0.25m$ has been selected, and the evolution is plotted for all cases in figure 5.35.

The trend described above is observed. In the outside zone on the left-hand side, the free flow velocity is obtained for all cases, both low and high velocity. Remember that the high velocity is 10m/s and is in agreement with the study of the vertical plane, where this behaviour was always the case for 10 m/s and not for very high velocities (such as 14 m/s).

Regarding the evolution of the velocity, it is possible to observe those high and low velocity paths or tracks where the vortex streets will be located. Their size can be seen, but not their characteristics, which will be seen with the following parameters to be studied. Their position varies according to the angle of inclination.

Velocity magnitude

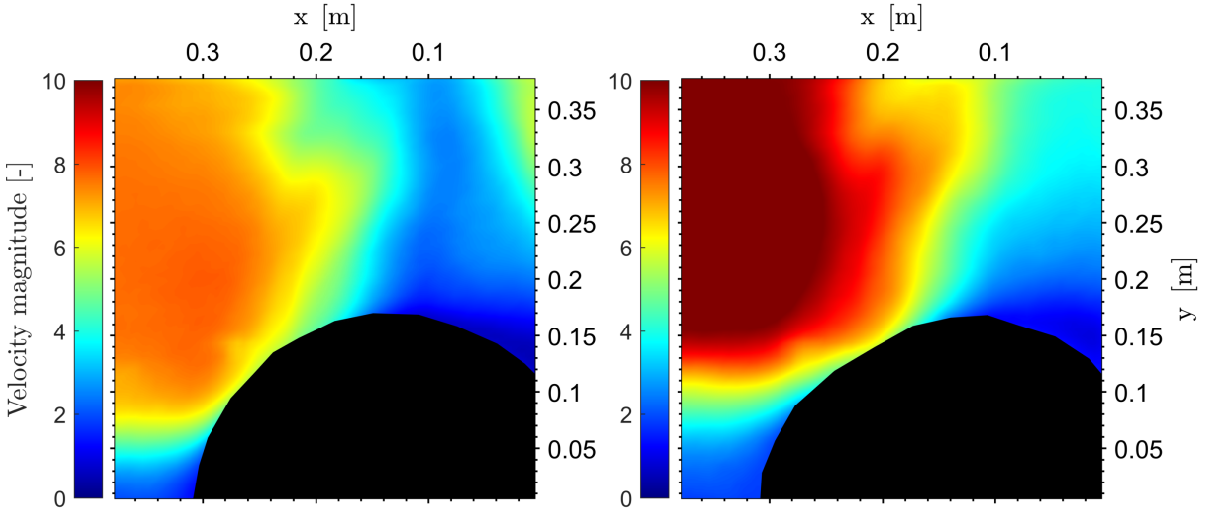

(a) 10 deg, 7 m/s

(b) 10 deg, 10 m/s

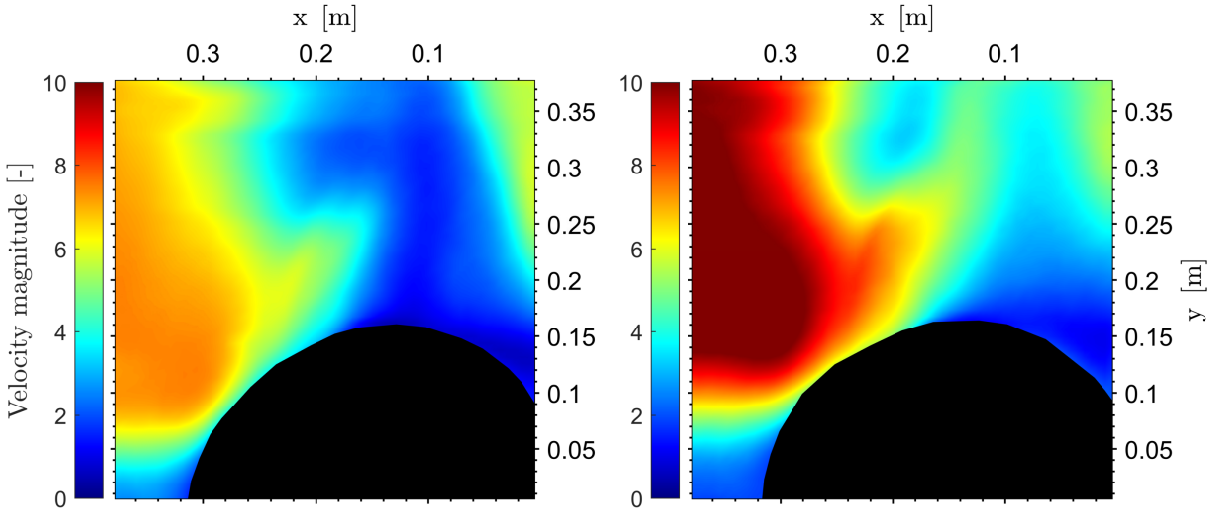

(c) 20 deg, 7 m/s

(d) 20 deg, 10 m/s

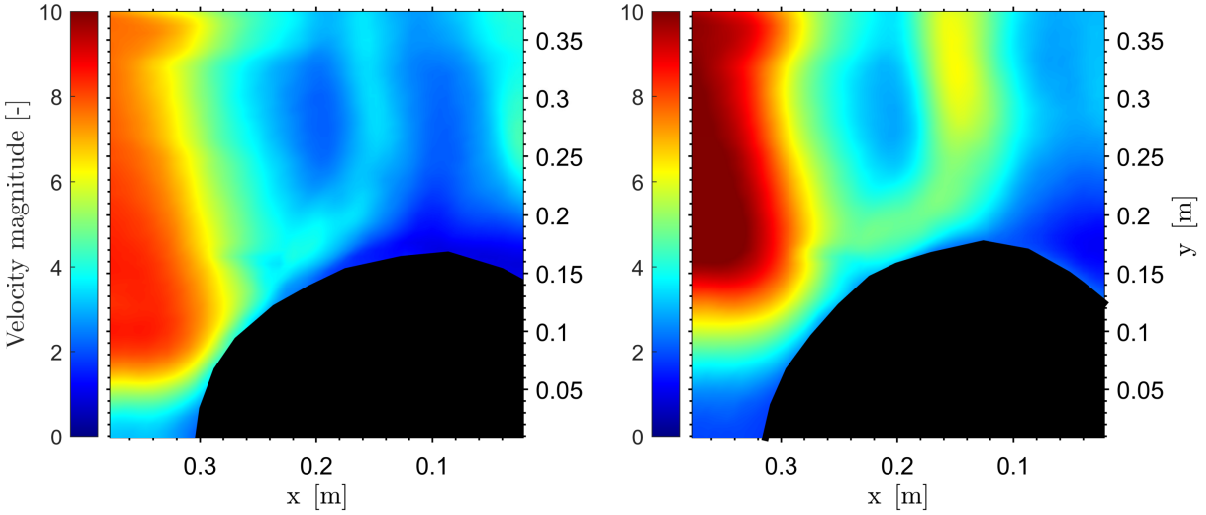

(e) 30 deg, 7 m/s

(f) 30 deg, 10 m/s

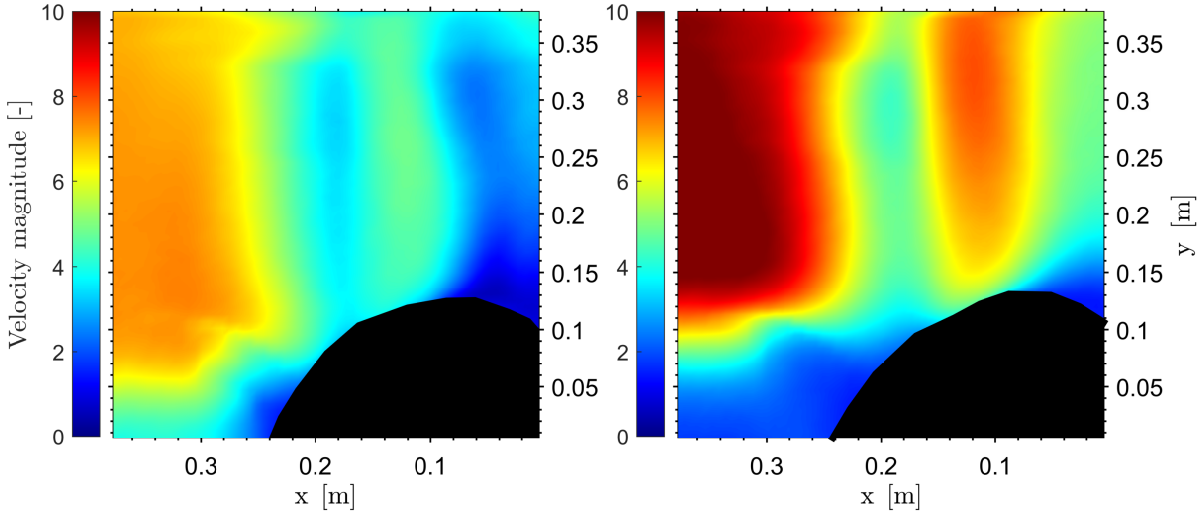

(g) 40 deg, 10 m/s **(h)** 40 deg, 15 m/s

Figure 5.34: Velocity magnitude

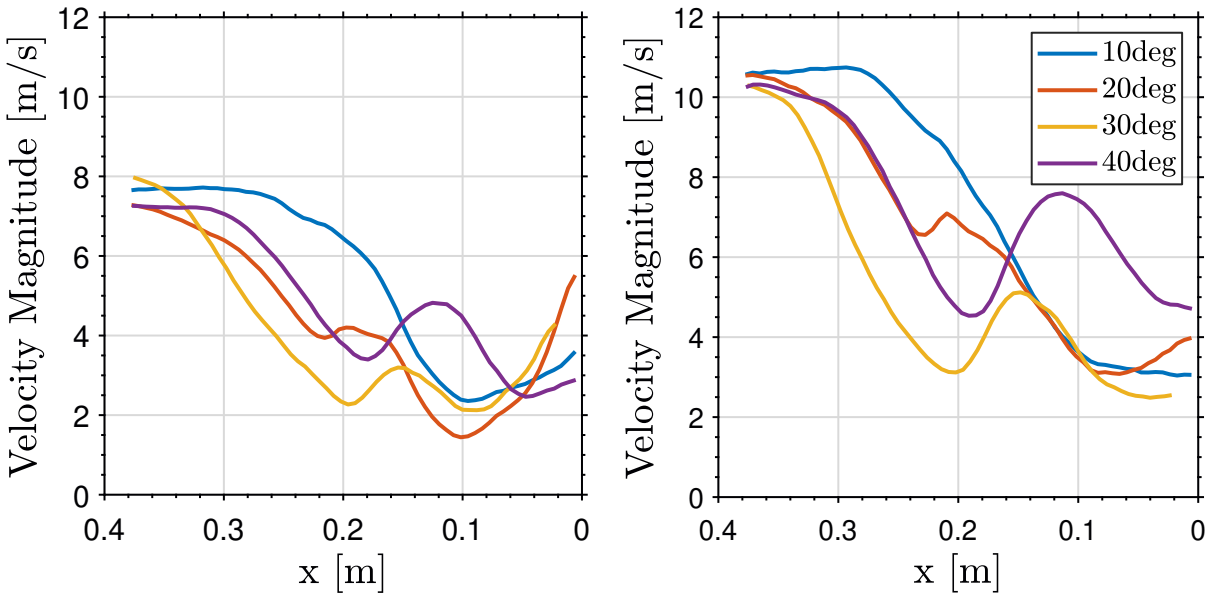

(a) 7 m/s **(b)** 10 m/s

Figure 5.35: Velocity magnitude profiles for y=0.25m

U velocity component

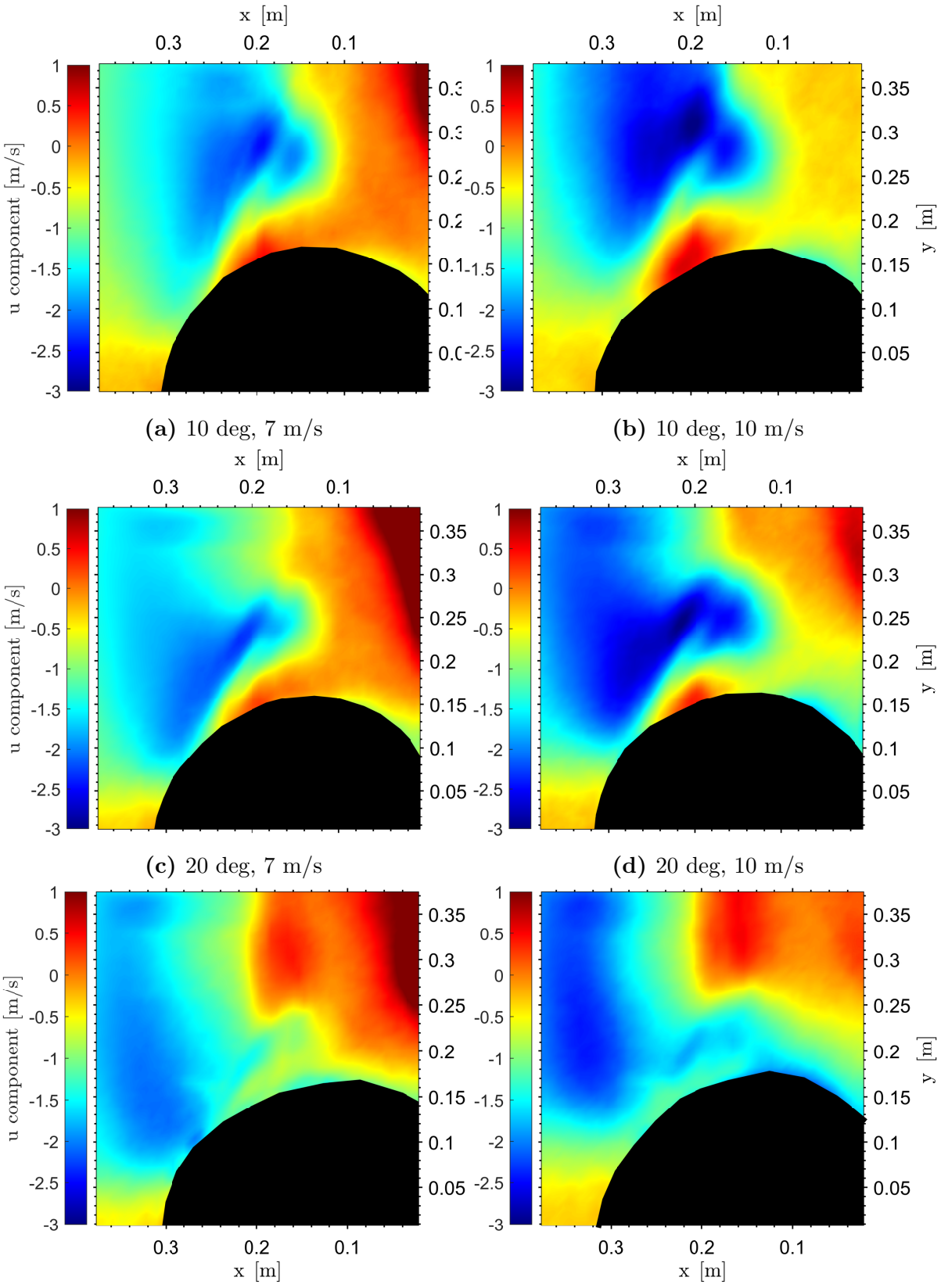

(a) 10 deg, 7 m/s

(b) 10 deg, 10 m/s

(c) 20 deg, 7 m/s

(d) 20 deg, 10 m/s

(e) 30 deg, 7 m/s

(f) 30 deg, 10 m/s

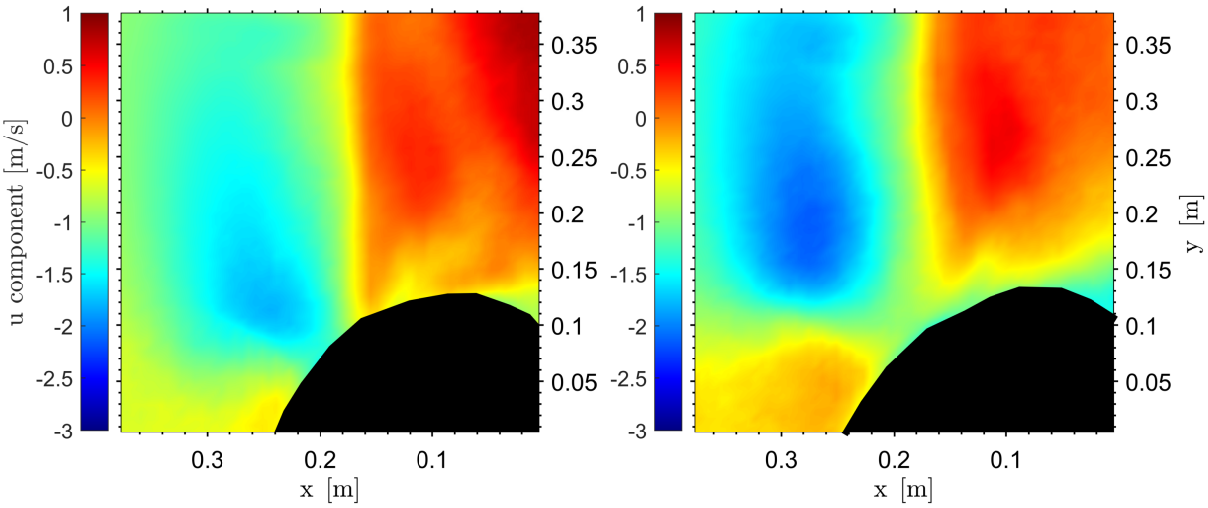

(g) 40 deg, 7 m/s **(h)** 40 deg, 10 m/s

Figure 5.36: u velocity component

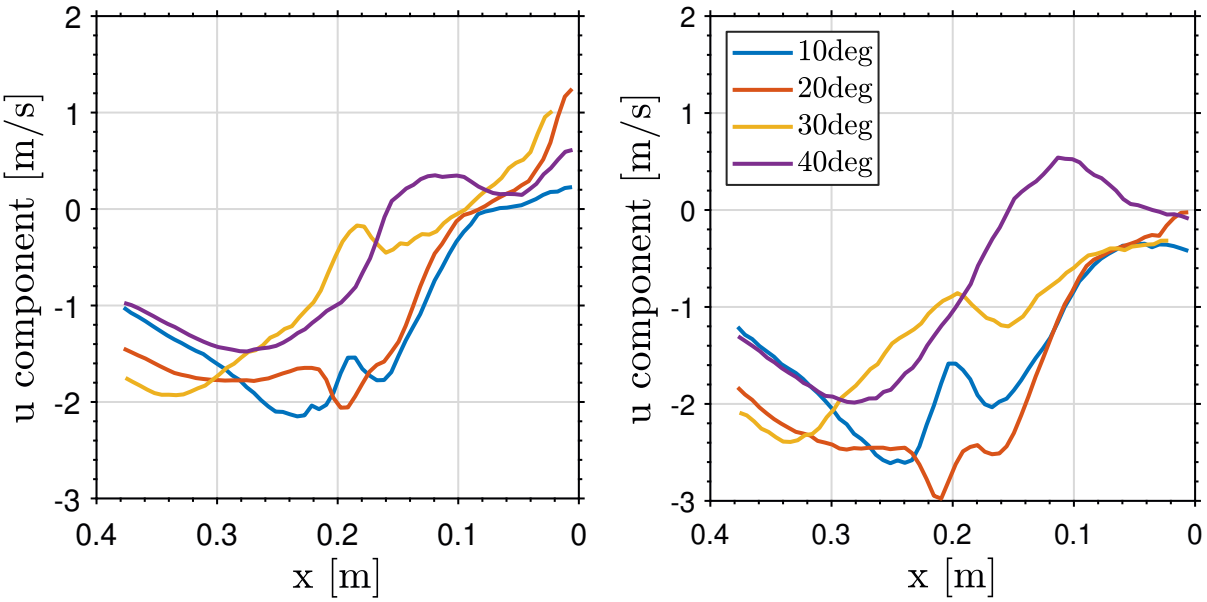

(a) 7 m/s **(b)** 10 m/s

Figure 5.37: U component profiles for y=0.25m

Figure 5.36 shows the horizontal component of the velocity or **u-component**. It can be seen that there are both positive and negative values of this velocity parameter. Therefore, the u component will have 2 directions.

Observing the graph, it can be seen that there are a series of counter-rotating vortices behind the turbines that change the direction of the u-component. This happens for all cases studied.

Where the u-component is smaller (more negative) there are large velocity gradients, which are found where the turbine wake is located. In this area many vortices are formed behind the turbine. Their approximate shape can be seen in the pictures in figure 5.36. It can be seen how several vortices appear, going in different directions.

The paths or streets left by these vortices have a curved shape in a clockwise direction, just like the direction of rotation of the turbine. For larger angles, these vortices can be seen to have a straighter shape, as they cover a larger part of the fluid field.

The position of the streets formed can be seen in graph 5.37, where the peaks are observed near positions of $y = 0.2m$ in the plane of $x = 0.25m$ studied.

The **v-component** can be seen in figure 5.38. Its analysis is analogous to that of the velocity magnitude, something that already occurred in the vertical case between the u-component and the velocity magnitude.

This is because this direction coincides with the direction of flow and is the component that has the most weight within the velocity magnitude. The analysis in figure 5.39 is also analogous to the previous one.

V velocity component

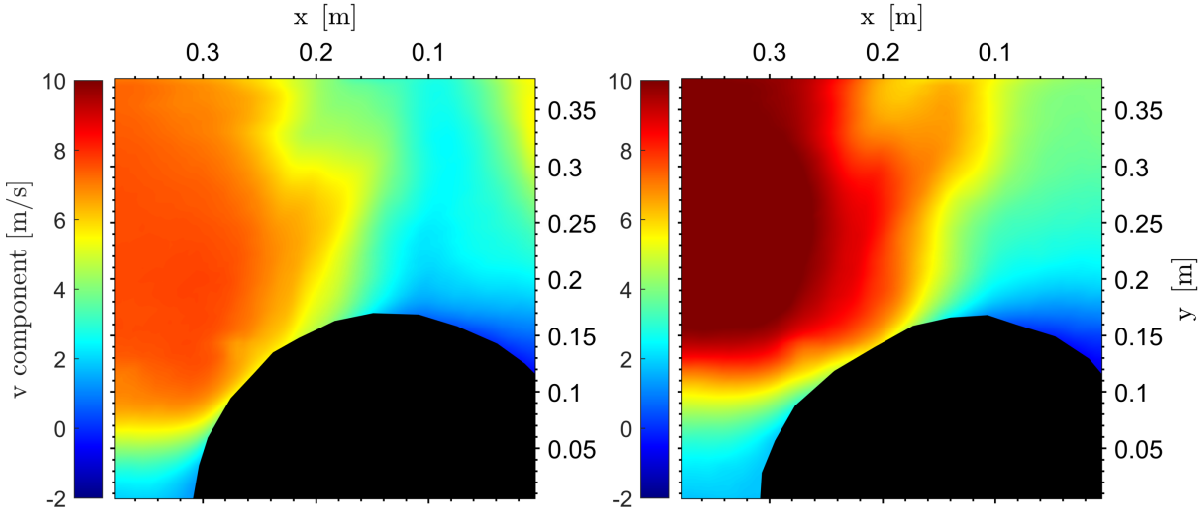

(a) 10 deg, 7 m/s

(b) 10 deg, 10 m/s

(c) 20 deg, 7 m/s

(d) 20 deg, 10 m/s

(e) 30 deg, 7 m/s

(f) 30 deg, 10 m/s

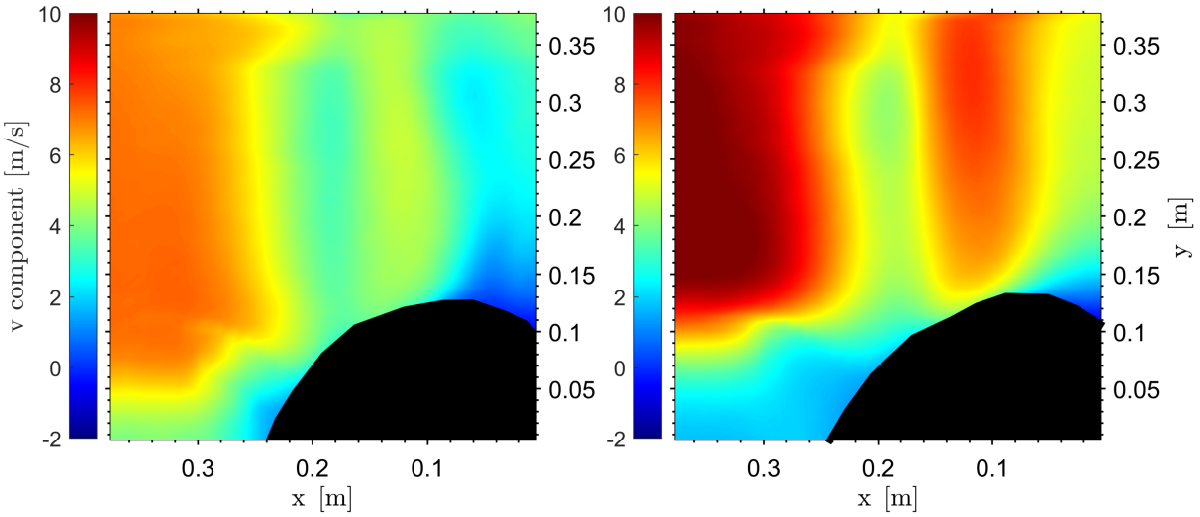

(g) 40 deg, 7 m/s **(h)** 40 deg, 10 m/s

Figure 5.38: v velocity component

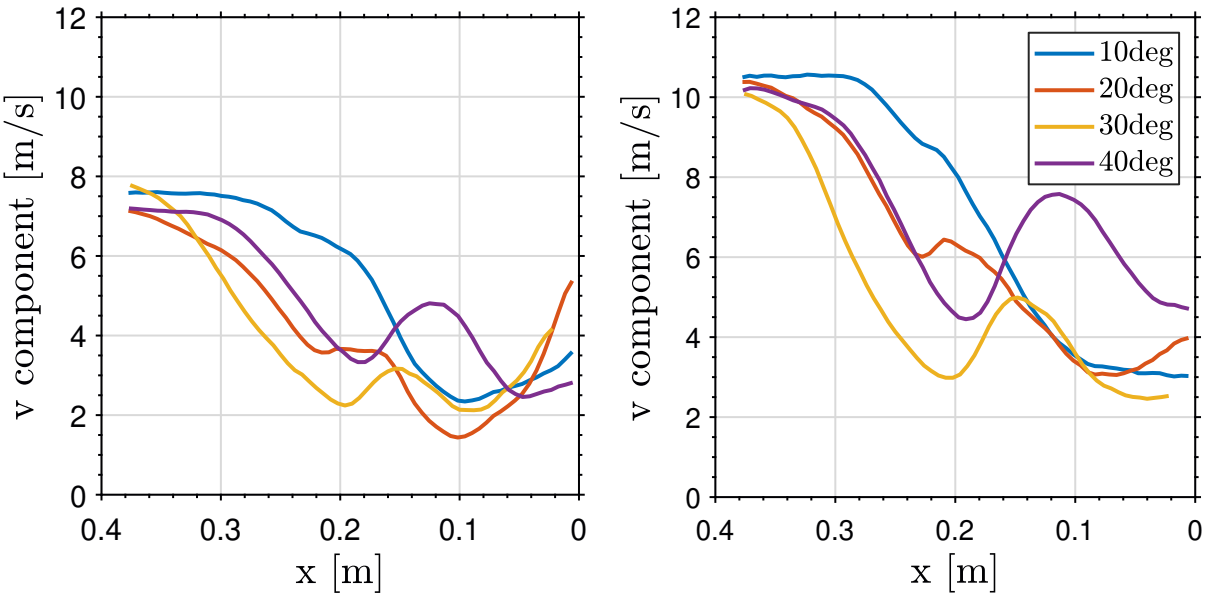

(a) 7 m/s **(b)** 10 m/s

Figure 5.39: V component profiles for y=0.25m

Vorticity

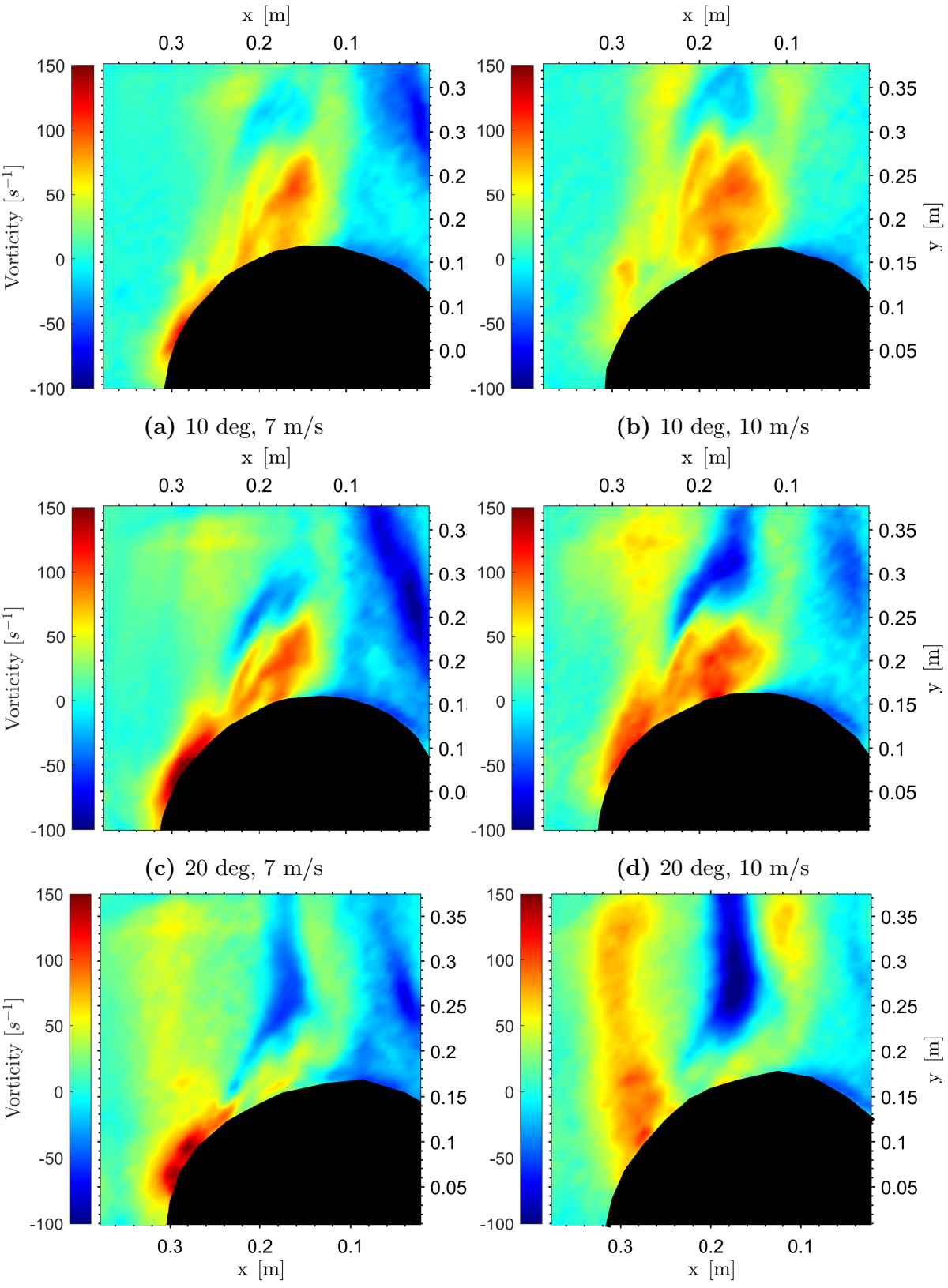

(a) 10 deg, 7 m/s

(b) 10 deg, 10 m/s

(c) 20 deg, 7 m/s

(d) 20 deg, 10 m/s

(e) 30 deg, 7 m/s

(f) 30 deg, 10 m/s

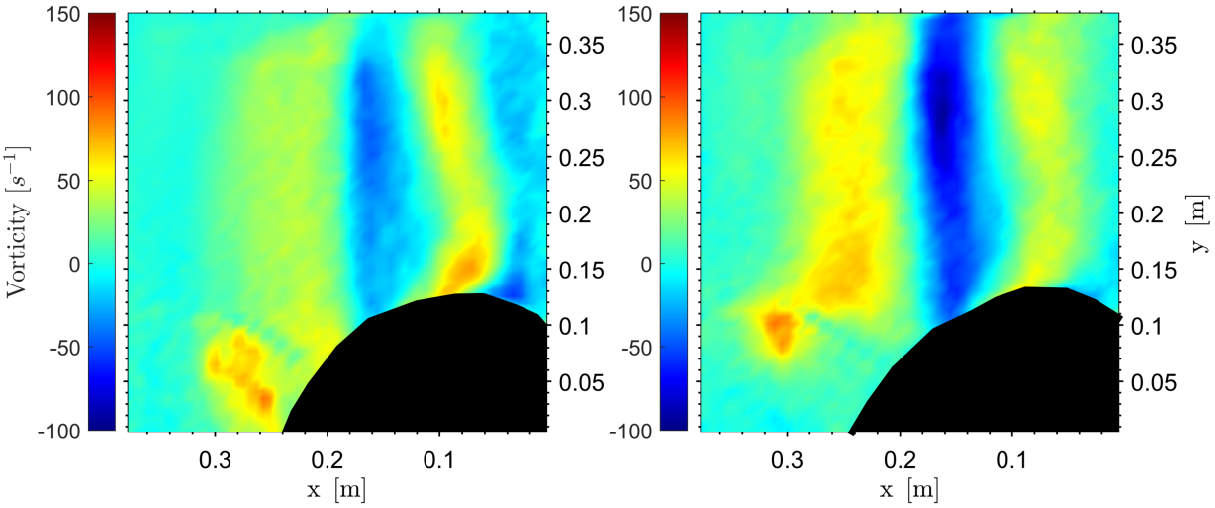

(g) 40 deg, 7 m/s **(h)** 40 deg, 10 m/s

Figure 5.40: Vorticity

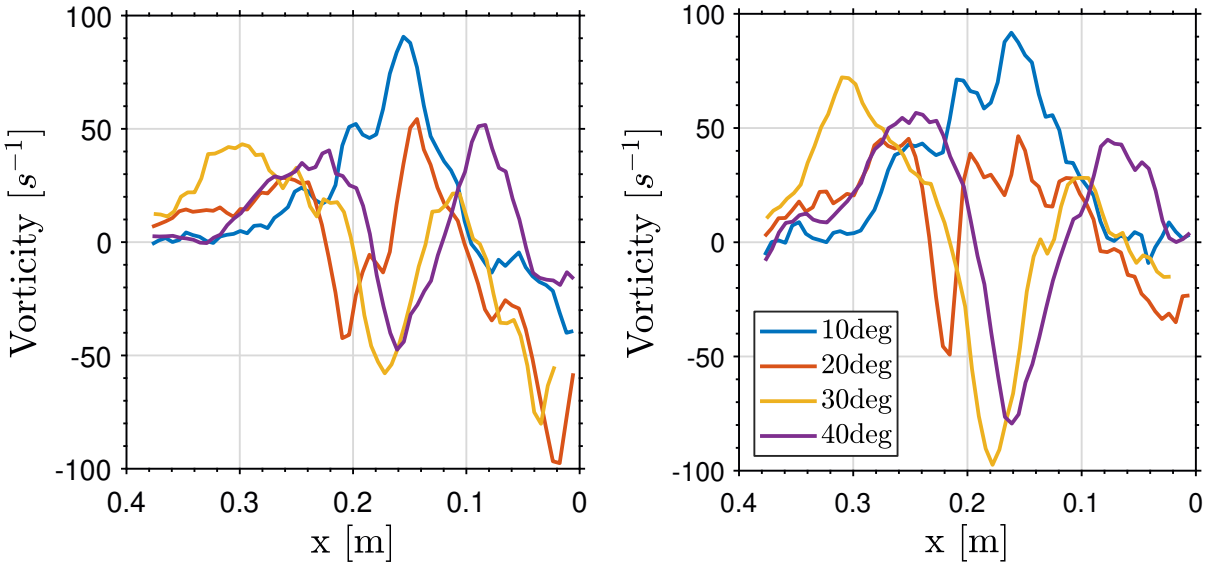

(a) 7 m/s **(b)** 10 m/s

Figure 5.41: Vorticity profiles for y=0.25m

Figure 5.40 shows the evolution of **vorticity** downstream of the prototype. Positive and negative values are obtained. The positive values correspond to counterclockwise vortices and the negative values to clockwise vortices.

In the drawing, the positive vortices are shown in orange and the negative ones in blue. Both have opposite direction of rotation and appear close to each other. Thus, 2 counter-rotating vortices are facing each other.

Since it is a plot of the mean, its entire area of influence can be seen. At an instant the vortices do not necessarily have to be in the whole coloured area, because they move with time depending on the angular velocity of rotation of the structure.

The shape of the wake is curved and goes in the direction of the rotation of the turbine. It is also noticeable that as the wake moves away from the structure, it gets bigger and bigger.

The positive vortices, which are of greater intensity than the negative ones, appear just outside the turbine channel. When interacting with the fluid, the negative vortex pair is formed and continues in space. For the 40-degree case, the negative vortex is predominant.

Figure 5.41 shows for a cut at y=0.25m how the position of the wake and the size of the vortices generated evolves, whether positive or negative.

5.3.3 Conclusions of fluid field analysis

As conclusions of this study, it can be extracted that the PIV technology has good qualities to observe the behaviour of the flow behind the RoDaVi turbine.

From the study of the vertical plane, it can be extracted how the vortices have the nature to exit from each channel that conforms the turbine, so that several are formed at different heights. Their direction of exit is tangential to the shape of the channel, and vorticity zones are formed in a downward direction. The size of the vortices and their zone of influence are also visible.

Regarding horizontal plane, the vorticity streets can be observed. Different counter-rotating vortices are identified, which appear together and propagate beyond the studied field.

The most intense ones appear just at the exit of the turbine. They move following the counter-clockwise rotation of the turbine. In the areas far from the turbine, where free flow predominates, there is no vorticity, so the turbine only disturbs the flow downstream of it.

As there are several vortices at different heights, it would be appropriate to study various horizontal planes at the same time, and correlate them with each other, in order to determine the behaviour of vorticity in a three-dimensional way.

Regarding the placement of a set of turbines, it is observed that after a turbine the decrease in speed is very large, and there are vorticities that can induce oscillating movements in the turbine. For this reason, placing the turbines immediately behind each other is not a good option.

It is observed that for a height higher than the turbine altitude dimension, and for a lateral distance of less than half the turbine diameter, the free flow remains undisturbed. Therefore, the placement of another turbine in this area would not lead to any loss of speed. Thus, the possibility of placing different turbines laterally separated, or at different heights, is considered.

However, the field of influence of the wake behind the turbine could not be fully studied due to the limited dimensions of the wind tunnel, the area of capture of the photocamera and the laser radiation.

For future studies, the next step could be to carry out a CFD study to validate the PIV study. In the CFD study, different RoDaVi turbines would be used, and the influence between them would be studied, taking into account both their horizontal and vertical separation. In this way, not only will it be studied whether they interfere with each other, but also whether the acceleration of the flow in their vicinity would improve their performance even more.

6 CONCLUSIONS

This master's degree thesis has achieved the objectives set at the beginning of the project. The study of a newly designed wind turbine has been carried out through experimental experiences in the laboratory over the last few months. In these conclusions, the scope of the project will be explained in summarized way, highlighting the most important results achieved.

The 3 types of experiments carried out have provided critical results on the viability of the RoDaVi and its main characteristics and improvements with respect to similar turbines.

Firstly, in the aerodynamic study with the smaller scale turbines, the needs and limitations of the system are made known. By studying the evolution of the aerodynamic coefficients with respect to the variables of inclination and wind speed, it is determined that it is necessary to operate at large inclinations and high speeds in order to achieve optimum performance of the system. Furthermore, by studying the frequency, the turning behaviour of the prototype begins to be known.

The second study carried out has revealed the electrical behaviour of a turbine on a scale of 1:3. The main objective was to produce electrical power levels capable of charging a battery. Moreover, in comparison with turbines with similar characteristics already existing and in use today, their performance has also been improved.

In this experiment, it has been determined that conventional permanent magnet generators are suitable for this type of installation. The use of coreless stator generators has been discarded due to their low performance.

In terms of mechanical behaviour, mechanical power values above the nominal power of conventional generators used are obtained. The mechanical power generation is closely related to the angular speed. From 1000 rpm the generators operate close to their rated power (100 and 200W).

This behaviour occurs at high gradients, from 30 degrees and further. The high angular velocity is generated at high free flow velocities, its trend always increasing and with a higher slope for these high velocities.

In terms of electrical performance, the turbine is at its optimal for cases with an inclination of 40 degrees and speeds as high as possible, producing more than 20W of electrical power for the motor with a nominal mechanical power of 200W.

The power coefficient (C_P) and Tip Speed Ratio (TSR) have been calculated in order to compare and characterise the turbine with existing turbines. The TSR values approximate the behaviour of the similar Savonius vertical axis turbine. The TSR values measured are between 0.5 and 3, and the C_P values obtained range from 0 to 0.12.

Comparing the C_P of the two turbines, the RoDaVi beats the Savonius values. In terms of efficiency, the Savonius theoretically has an average efficiency of between 10 and 17%, while the RoDaVi is closer to 10%.

By building a Savonius in the lab of similar size, the electrical energy production is compared. The RoDaVi model produces more electrical power than the Savonius in inclinations of the 30, 40 and 50 degrees for the full range of speeds and resistances.

Therefore, the objective of demonstrating that the RoDaVi turbine is useful for electricity production and can be a potential competitor to existing turbines, such as the Savonius, is fulfilled.

The latest study carried out using PIV technology allows the fluid field to be measured, in order to see the main characteristics of the flow disturb due to the fluid-structural interaction.

By studying a vertical and a horizontal plane for different cases, it is observed that the body leaves behind it a velocity field lower than that of the free flow, as it transforms kinetic energy into electrical energy.

In this area behind the body, vorticities appear for each of the outlets of the channels that make up the turbine. The vertical plane shows the magnitude of these vortices and their downward direction with the inclination of the turbine.

The horizontal plane shows how the vorticity moves downstream of the turbine. A wake is created in which the vortices follow the clockwise rotational movement of the turbine.

In this way, a vorticity street is created for each configuration, making it impossible to place one turbine behind the other because the wake generated would not be favourable to performance.

With all this, it can be considered that the objectives presented at the beginning of the work have been achieved, and the knowledge and skills acquired during the master's degree studies have been expanded.

Future works

On the other hand, as future work that could be applied to this study to further develop the RoDaVi turbine with more time or as a continuation of this project, several options are proposed:

- Use of engines with better performance, i.e. with higher power ratings. This would allow higher speeds to be achieved in the wind tunnel. With higher power engines, it is expected to obtain better results and complete the evolution curve of CP vs TSR.
- Use of a gear system or multiplier wheel to try to maximize the transformation of mechanical energy into electrical energy, thus increasing the revolutions per minute that the generator would receive. In this way the efficiency will also be increased.
- Carrying out tests with various models of different sizes, in order to extrapolate the data measured in the wind tunnel to a turbine that is the size of the real prototype (using similitude theory). In this way a deeper analysis of the capabilities of the real

RoDaVi wind turbine can be pursued without the need to move to a larger wind tunnel infrastructure.

- Measuring more horizontal planes in the PIV study. It would be possible to have 2 lasers measuring at the same time and combining the 2 planes to obtain a complete 3D flow configuration. In this case it is impossible to correlate both planes as it is difficult to square each instantaneous measurement. So it would be convenient to measure simultaneously with 2 lasers to correlate the data.
- Adjustment of a larger camera acquisition field, so that the study area behind the turbine is larger. Also to adjust the bubble injection system, so as to be able to impact more regions and observe the complete fluid field.
- Study of the placement of wind turbines. The next step now that it is known how the flow behaves could be to do a CFD study to validate the PIV study. In the CFD study, several RoDaVi turbines would be used, and the influence between them would be studied. Not only if they interfere with each other, but also if the acceleration of the flow in their vicinity would improve their performance even more.
- Taking into account that the installation is on top of a building. The air gradient on the roofs of buildings is different from that of free flow, as there is a ground effect and the flow is also curved at the corners that form the roof of the building. It would therefore be interesting to take this effect of building height into account in the CFD study.
- Real installation of the turbine on a roof to validate the results obtained. In this way, new unknowns and variables of the problem will also emerge, such as the height of the building or the height of the turbine shaft.

Bibliography

[1] La importancia de las energías renovables: Acciona: Business as unusual. URL https://www.acciona.com/es/energias-renovables/?_adin=0896444253.

[2] Renewable energy generation. URL https://ourworldindata.org/grapher/modern-renewable-energy-consumption?country=~OWID_WRL.

[3] Statistical review of world energy: Energy economics: Home, . URL https://www.bp.com/en/global/corporate/energy-economics/statistical-review-of-world-energy.html.

[4] Types of wind turbines: their advantages and disadvantages, . URL https://kohilowind.com/kohilo-university/202-types-of-wind-turbines-their-advantages-disadvantages/.

[5] T.F. Ishugah, Y. Li, R.Z. Wang, and J.K. Kiplagat. Advances in wind energy resource exploitation in urban environment: A review. *Renewable and Sustainable Energy Reviews*, 37:613–626, 2014. doi: 10.1016/j.rser.2014.05.053.

[6] LuvSide. Horizontal axis wind turbines: Advantages and disadvantages, Mar 2020. URL https://www.luvside.de/en/hawt-advantage-disadvantage/#:~:text=High%20Efficiency&text=Currently%2C%20horizontal%20axis%20wind%20turbines,received%20wind%20power%20into%20electricity.

[7] Types of wind turbines. URL https://energyeducation.ca/encyclopedia/Types_of_wind_turbines.

[8] Francesco Castellani, Davide Astolfi, Mauro Peppoloni, Francesco Natili, Daniele Buttà, and Alexander Hirschl. Experimental vibration analysis of a small scale vertical wind energy system for residential use. *Machines*, 7(2):35, 2019. doi: 10.3390/machines7020035.

[9] Gilbert morris 'gm15' f1c class free flight flapper airfoil. URL http://airfoiltools.com/airfoil/details?airfoil=gm15sm-il.

[10] Adinel Gavrus, Manuel Buisson, Moussa Ndoye, and Francesco Minio-Paluello. Études des performances aérodynamiques et énergétiques d'un rotor éolien hélicoïdal à l'axe verticale RoDaVi par analyses théoriques, mesures expérimentales en soufflerie et modélisation numérique CFD. Congrès Français de Mécanique, 2019. URL https://hal.archives-ouvertes.fr/hal-02429008. Poster.

[11] A Betz. Introduction to the theory of flow machines.(1966)(dg randall, trans.) oxford.

[12] Asea Brown Boveri and S ABB. Cuaderno de aplicaciones técnicas n. 12 plantas eólicas. *Barcelona: ABB*, 2012.

[13] Giampaolo Romano. *Laboratorio di Aerodinamica,*.

[14] Pitot-static tube. URL `https://www.sciencedirect.com/topics/engineering/pitot-static-tube`.

[15] TecQuipment. *AFA3 Three-Component Balance Handbook*.

[16] Standard products, Jun 2022. URL `https://ncte.com/en/standard-products/`.

[17] Zbigniew Czyż, Paweł Karpiński, and Wit Stryczniewicz. Measurement of the flow field generated by multicopter propellers. *Sensors*, 20(19):5537, 2020. doi: 10.3390/s20195537.

[18] Fastcam mini ax - photron. URL `https://photron.com/es/fastcam-mini-ax/`.

[19] Micro bubble generator bg-1000. URL `https://tsi.com/product-accessories/micro-bubble-generator-bg-1000/`.

A | Workplace conditions and budget

A.1 Workplace conditions

During the execution of any project or work, safety, hygiene and health conditions must be complied with. These conditions are regulated by the Spanish Ministry of Labour according to the Real Decreto 486/1997 of 14 April 1997, which establishes the minimum safety and health provisions in workplaces.

It must be ensured that the conditions are met wherever the work is carried out. By way of summary, the main characteristics required for an optimal studio or office in terms of safety, hygiene and ergonomics are presented in the following sections.

Environment

The workplace must be large enough to accommodate all the necessary elements and to allow minimum mobility for the worker.

Companies must adopt safety measures that include evacuation routes and exits in the event of an emergency. The constructor of the facilities must design an emergency plan that the company must make known to the workers either by means of plans or periodically established drills.

In addition, there must be adequate fire protection, with reviews of the material by competent bodies.

It should be emphasised that order, cleanliness and maintenance of the workplace must be maintained. At all times, the work area must be kept in suitable hygienic conditions and the passageways must be free of obstacles so that they can be used without difficulty at all times.

Ergonomics

During the execution of the project, work will be carried out with display screens. The use of these screens in the work environment is included in the legislation of the RD 488/1997 and some minimum requirements are established regarding the ergonomics of the worker.

Thus, the workplace must be adapted to the physical and psychological characteristics of the worker or user who will do most of the work in front of a computer.

Workstation design is directly related to posture problems. If we take into account that work with display screens is characterised by prolonged static postures, it can be deduced that the effects of these postures are aggravated when the design of the workstation is incorrect. Some of the recommendations to be adopted to avoid these problems that damage the employee's health are:

- **Seat:** A seat adjustable in height and inclination is recommended in order to find the correct position to suit each user. Its backrest should support the entire lumbar area. The use of chairs with wheels is recommended so as not to restrict the movement of the worker, as long as there is no involuntary movement.
- **Table:**. A table of sufficient size to accommodate all work material with a non-reflective surface must be available. It shall allow for repositioning and adjustment of the flexible positioning of the display.
- **Screen:** The screen image shall be stable and free of flicker phenomena. The brightness and contrast shall be easily adjustable by the user. The display shall also be adjustable and tiltable at will. The distance between the screen and the user's eyes should not be less than 40 cm, the optimum distance being 45 to 75 cm. The screen shall be positioned so that its useful area can be seen within the user's field of vision.
- **Keyboard:** The keyboard should be inclined and, where possible, independent of the display, so as to allow the worker to adopt a comfortable posture, which does not cause fatigue to the arms and hands. There shall be sufficient space in front of the keyboard for the user to rest his or her arms and hands. arms and hands. The symbols on the keys shall be sufficiently prominent and legible from the normal working position. from the normal working position.
- **Personal protective equipment:** It is advisable to use screen protectors or goggles specifically for working with screens, as they radiate light that is harmful to the eyes. The shields consist of a polarised glass, supported by a frame, which is superimposed on the screen glass. Specific glasses for reading screens have a filter that protects against the blue light that is most harmful to vision. This protects users' eyesight, as well as improving the performance of the screen in terms of contrast and clarity.

Installations

The **electrical installation** must be projected, put into operation and maintained by an appropriate company. This installation must avoid contact with people, fire and explosions, complying with the provisions on voltages and safety in the Low and High Voltage Regulations in force. As established for activities with equipment that includes display screens, the following must be fulfilled: comply with the requirements of the directive on electromagnetic emissions (minimum radiation levels), guarantee adequate maintenance of the cables and provide sufficient cable length. The aim is to facilitate access and maintenance of the cables in order to speed up repair work without interrupting work activities.

With regard to environmental conditions, RD 488/1997 establishes thermohygrometric conditions whereby an adequate temperature must be maintained within established limits between 23 and 26°C in summer and between 20 and 24°C in winter. The humidity of the

air must always be maintained between 45% and 65%. In addition, equipment installed at the workstation shall not produce additional heat which could cause discomfort to workers.

With regard to the ventilation of the workplace, an effective renewal of the air in the workplace must be ensured.

Likewise, all the installations are subject to periodic maintenance, so that their operating conditions always meet the specifications and are in optimal conditions.

Lighting.

The lighting must be adapted to the working conditions, ensuring adequate visibility with minimum lighting levels that do not pose any risk to the safety or health of workers. It can be natural or artificial, although natural lighting is the most advisable. However, given that the intensity of natural lighting varies throughout the day and depends on weather conditions, seasons or geographical location, it must be adequately complemented with artificial lighting.

Lighting levels should be distributed as evenly as possible, with levels and contrasts of luminance appropriate to the visual requirements of the task, without direct or indirect glare caused by objects close to the work areas, and without lighting systems that impede the correct visualisation of the environment or pose a risk of accident.

With regard to the location of the workstation and the screen, the standard gives indications on the most appropriate placement of the workstation to avoid reflections and glare. It is recommended that the screen be placed perpendicular to the windows, and never in front of them or with its back to them, as both cases would cause reflections and/or glare. These measures can be complemented with the use of curtains, blinds or local screens that allow adequate use of natural light.

Noise

The noise level at the workplace should be as low as possible. possible. To achieve this, equipment with minimum noise emission should be used and the room acoustics should be optimised.

The directive states that for difficult and complex tasks requiring special concentration the equivalent sound level should not exceed 55dB(A).

A.2 Budget

This section will deal with the costs generated by carrying out this Final Master Project. As a guideline, a calculation of all the factors that involve a cost when carrying out a project such as this one will be offered. The breakdown will include the human cost used (both author and tutor), the infrastructures required, the documents acquired, the cost of the electronic equipment and the software licences used, among other elements.

Labour

The cost incurred by labour corresponds to the time invested by the student who completes the degree studies and the engineer who tutors him/her. It is considered that the engineer receives a salary in accordance with his work, while the student receives a salary as a junior engineer.

The time dedicated by the tutor consists of meetings, hours of consultation of doubts, revision of the work and management of the project procedures, while the hours dedicated by the student correspond to the 23 credits assigned, which would be 690h.

CONCEPT	UNITS	PRICE UNITY	AMOUNT
Engineer meetings	12 h	30.82 €/h	369.84 €
Engineer supervision	24 h	30.82 €/h	739.68 €
Student	690 h	13.70 €/h	9453 €
		Subtotal	10562.52 €

Infrastructure and material

A certain amount of workspace and specific tools need to be purchased or rented in order to carry out a project. Thus, a suitable working environment with the characteristics set out in the last section will be needed.

The main infrastructure used is the wind tunnel. The operation of the wind tunnel costs about 196.08€/day, which, assuming an 8-hour working day, is 24.51€/hour. This price also includes the work of the technicians, electricity, and access to all the elements found in the laboratory.

On the other hand, the construction of all the turbines used is estimated at around 1000€. This includes design, 3D printing, gluing, accessories, construction of the specific support and transport.

As for the equipment used to carry out the calculations, a standard laptop with a good processor with 4 CPU cores, about 8GB of RAM memory and sufficient storage, whose market value is currently around 700 euros, will be considered.

CONCEPT	UNITS	PRICE UNITY	AMOUNT
Wind tunnel	120 h	24.51 €/h	2941.2 €
Turbines	3	-	1000 €
Laptop	1	700 €	700 €
		Subtotal	4641.2€

Software licences

Finally, the costs associated with the programmes used to carry out the project have yet to be included. The program used for data processing and obtaining the graphs is MATLAB, with an annual licence cost of 840 €. Microsoft Excel and Power Point have also been used, with a personal licence for Microsoft products costing 69 €/year. Finally, the programme used for writing the report is LaTeX, which is freely available.

CONCEPT	UNITS	PRICE UNITY	AMOUNT
MATLAB	1 year	840 €/año	840 €
Microsoft Office	1 year	69 €/h	69 €
LaTeX		0 €	0 €
		Subtotal	909€

Total cost

Adding all the subtotals referring to the different expenses incurred in carrying out the project plus the regressive taxes that must be declared in an invoice, and which correspond to the 22% VAT rate in Italy, gives the total estimated value of the budget.

CATEGORY	**SUBTOTAL**
Labour	10562.52 €
Infrastructure and material	4641.2 €
Software	909 €
TOTAL without VAT	16112.72 €
VAT (22 %)	3544.8 €

TOTAL COST ‖ 19657.52 €

The total cost of the project is:

NINETEEN THOUSAND, SIX HUNDRED FIFTY-SEVEN EUROS AND FIFTY-TWO HUNDREDTHS CENTS